A Continuum Theory with Long-Range Forces for Solids

by

Markus Zimmermann

Submitted to the Department of Mechanical Engineering
in partial fulfillment of the requirements for the degree of

Doctor of Philosophy in Mechanical Engineering

at the

MASSACHUSETTS INSTITUTE OF TECHNOLOGY

February 2005

Author .....
Department of Mechanical Engineering
January 28, 2005

Certified by .....
Rohan Abeyaratne
Professor and Department Head
Thesis Supervisor

Accepted by .....
Lallit Anand
Professor and Graduate Officer

A Continuum Theory with

Long-Range Forces for Solids

by

Markus Zimmermann

Submitted to the Department of Mechanical Engineering
on January 28, 2005, in partial fulfillment of the
requirements for the degree of
Doctor of Philosophy in Mechanical Engineering

Abstract

A non-local integral-type continuum theory, introduced by Silling [61] as *peridynamic* theory, is analyzed. The theory differs from classical (local) continuum theories in that it involves long-range forces that act between continuum particles. In contrast to existing non-local theories, surface tractions are excluded. As consequence, the theory is applicable off and on defects and interfaces: cracks and phase boundaries are a natural part of the body, and do not require special treatment. Furthermore, as the model loses "local stiffness", the resistance to the formation of discontinuities is reduced.

The theory can be viewed in two ways: It is a *multi-scale model* in that it can be applied simultaneously on the atomistic level *and* on the macroscopic level with a smooth interface between the two regimes. Alternatively, it can be used as a purely phenomenological *macroscopic model* that still works off and on defects. Forces of microscopic range may represent the interaction of an underlying microstructure such as discrete particles. Forces of macroscopic range are not necessarily physical and are justified by their effective behavior.

A meshless numerical approximation technique is implemented for the macroscopic model and used to simulate brittle fracture. If the internal length of the simulated peridynamic body is small compared to its macroscopic dimensions, then the simulation results agree well with linear elastic fracture mechanics. In contrast to classical fracture mechanics, however, the crack path does not need to be known in advance.

Thesis Supervisor: Rohan Abeyaratne
Title: Professor and Department Head

Acknowledgements

I would like to express my deep gratitude to Professor Rohan Abeyaratne for his guidance through my years at MIT. I am grateful for our discussions, his helpful advice and his support.

I also would like to give thanks to the members of my thesis committee, Professor Nicolas Hadjiconstantinou and Professor David Parks, for important ideas and critical discussions.

I am grateful to Sandia National Laboratories for supporting my research. I thank Doctor Stewart Silling for discussions and helpful comments.

I am indebted to Professor Yves Leroy who hosted my stay at the Ecole Polytechnique. The stay was made possible by the Embassy of France and the Chateaubriand Fellowship. I thank Professor Lev Truskinvosky for our discussions and the insights he gave me.

I would like to thank Michael Demkowicz and Vadim Roytershteyn for numerous inspiring discussions during my time at MIT. Many thanks to Michael Demkowicz and Olaf Weckner for reviewing the thesis and their helpful comments.

Contents

List of symbols

$\mathbf{1}$	unity tensor of second order
$\boldsymbol{b}$	external body force
$\boldsymbol{b}_{int}$	body force due to particle interaction on Ω
$\boldsymbol{b}_{tot}$	total force
$\boldsymbol{b}_{*}$	prescribed external force on Ω_b
$\boldsymbol{\mathcal{C}}$	classical stiffness tensor of fourth order
$\boldsymbol{C}$	non-local stiffness tensor of second order
$\boldsymbol{C} = \boldsymbol{F}^T\boldsymbol{F}$	right Cauchy-Green tensor
C	stiffness distribution; in section 5.2 only: $C = \bar{C}$
$\bar{C}$	normalized stiffness distribution
$\boldsymbol{\varepsilon}$	linear strain tensor
$\varepsilon = \frac{\partial u}{\partial x}$	strain in 1d
$\varepsilon_{nl} = r/\xi - 1$	link strain
$\eta = r - \xi$	change of distance in 1d
$\boldsymbol{E}$	Lagrangian strain
E	total kinetic energy
E	Young's modulus
$\boldsymbol{e}_i$	unit vector in coordinate direction
$\boldsymbol{e}_r = \boldsymbol{r}/r$	unit vector pointing from $\boldsymbol{y}$ to $\boldsymbol{y}'$
$\boldsymbol{e}_\xi = \boldsymbol{\xi}/\xi$	unit vector pointing from $\boldsymbol{x}$ to $\boldsymbol{x}'$
$\boldsymbol{F} = \frac{\partial \boldsymbol{y}}{\partial \boldsymbol{x}}$	deformation gradient
$\boldsymbol{f}$	interaction force between particles

$2\gamma_s$	surface energy
h	characteristic distance of discretization points
h_0	horizon (i.e. radius of support) of $\boldsymbol{f}$ in the reference configuration
h_c	cutoff radius
$\boldsymbol{I}_{\text{sym}}$	symmetric identity tensor of fourth order
$\boldsymbol{k}$	wave vector
k	wave number
λ	Lamé constant
λ	normalized internal length in section 5.2
λ_m	macroscopic stretch
$\lambda_{nl} = r/\xi$	link stretch
l	internal length
μ	Lamé constant, shear modulus
M_j	stiffness moment of order j
$M(k)$	one-dimensional non-local acoustic tensor
$\boldsymbol{M}$	non-local acoustic tensor (second order)
ν	Poisson's ratio
N_j	dimension-less stiffness moment of order j
Ω	body, set of positions in reference configuration
$\partial\Omega$	boundary of a body
Ω_u	part of body on which displacements (or positions) are prescribed
$\partial\Omega_u$	boundary of Ω_u
Ω_b	part of body that is subject to external body forces (which may be zero)
$\partial\Omega_b$	boundary of Ω_b
Ω_y	deformed body; set of positions in current configuration
ω	wave frequency
Ψ	total Helmholtz free energy
$\bar{\psi}$	Helmholtz free energy density
ψ	pair-wise Helmholtz free energy
Ψ_{el}	total elastic energy

$\bar{\psi}_{el}$	elastic energy density
ψ_{el}	pair-wise elastic energy
ρ	mass per current volume
ρ_0	mass per reference volume
$\boldsymbol{r} = \boldsymbol{y}' - \boldsymbol{y}$	distance vector in current configuration
$r = \lvert\boldsymbol{r}\rvert$	2d/3d: scalar distance in current configuration (always positive)
$r = y' - y$	1d: distance with sign indicating the direction
$\boldsymbol{\sigma}$	Cauchy stress tensor
$\boldsymbol{\sigma}_0$	first Piola-Kirchhoff stress
$\boldsymbol{\sigma}_{\text{2pk}}$	second Piola-Kirchhoff stress
$\dot{\boldsymbol{s}} = \dot{s}\boldsymbol{n}$	normal velocity of a surface in the reference configuration
$\boldsymbol{u} = \boldsymbol{y} - \boldsymbol{x}$	displacement vector
$u = y - x$	displacement in 1d
$\boldsymbol{u}_*$	prescribed displacement on Ω_u
W_{diss} ($\dot{W}_{diss}$)	(rate of) dissipated energy
$\bar{w}_{diss}$ ($\dot{\bar{w}}_{diss}$)	(rate of) dissipated energy density
w_{diss} ($\dot{w}_{diss}$)	(rate of) pair-wise dissipated energy
$\dot{W}_{ext}$	rate of total external work
W_{ext}	potential of total external work
$\dot{W}_{int}$	rate of internal work
$\dot{\bar{w}}_{int}$	rate of internal work density
$\dot{w}_{int}$	rate of pair-wise internal work
$\boldsymbol{\xi} = \boldsymbol{x}' - \boldsymbol{x}$	distance vector in reference configuration
$\xi = \lvert\boldsymbol{\xi}\rvert$	scalar distance in reference configuration (always positive)
$\boldsymbol{x}$	position in reference configuration and identification label of a particle
x	position in reference configuration in 1d
$\boldsymbol{y}$	position in current configuration
y	position in current configuration in 1d
$\boldsymbol{\zeta}$	vector of generic internal variables

Notation: Constitutive functions have a hat. Integral transforms are marked with a bar.

Chapter 1

Introduction

1.1 Problem Statement

Solid bodies usually have an intractable number of degrees of freedom and only few of them are relevant for their macroscopic behavior. Classical continuum mechanics is a powerful tool, because it eliminates the detailed microstructure while keeping what is macroscopically relevant, creating mathematical models that can be treated either analytically or numerically. Material behavior is expressed by relations between stress and strain, which are the response of a representative volume element of the material to homogeneous deformation. The size of the volume element depends on the resolution of the model. It can be on the order of Ångstroms for crystal lattices, microns for metals with grains, or centimeters for heterogeneous materials like concrete.

Classical continuum models are applicable when the characteristic length of the deformation is sufficiently larger than the representative volume element of the body. If deformations localize, the continuum model begins to break down, and finally fails when deformations are non-smooth or discontinuous. The inability to describe localized deformation is reflected in the mathematical structure of continuum mechanics. Constitutive relations are formulated with deformation gradients (and their derivatives). If a deformation is non-smooth, the deformation gradient is not defined in a classical sense. This is the case for cracks where displacements are discontinuous across the crack faces or for phase boundaries where the strain field is discontinuous.

The classical remedy has been to treat regions that have an undefined deformation gradient separately. Crack lips are considered body surfaces with particular boundary conditions. Crack tips satisfy a particular energy balance that is different from the rest of the body. Phase boundaries are surfaces inside the body that satisfy particular jump conditions and kinetic relations.

This treatment relies on efficient bookkeeping of degrees of freedom. The bulk part of the body is sufficiently described by regular continuum mechanics, while the effective behavior of the defects is described by physical laws containing only the information that is relevant for the macroscopic behavior of the body. It may be difficult and costly, however, to keep track of defects. Analytical work becomes more complicated with more boundaries and irregular geometries. Numerical approximation methods must rely on expensive techniques like remeshing to make the propagation of defects possible. In addition, the physical laws governing defects may not be sufficiently characterized. This is why a theory that works *off and on defects* is useful.

The *peridynamic theory* introduced by Silling [61] is a continuum theory that does *not* require well-defined deformation gradients. Constitutive information is provided entirely on the basis of *positions* of (continuum) particles of the body. It resembles the formal structure of molecular dynamics in that it sums forces between pairs of particles. Therefore, it provides a good framework for including relevant parts of the microstructure into the constitutive description of the body. As particles interact at finite distance, the theory is *non-local* and has an internal length.

The purpose of this thesis is to explore the ability of peridynamic theory to model defects as a natural part of the body without special treatment.

1.2 Existing Approaches

Non-local Theories. Material models that are invariant with respect to rescaling of spatial variables are called *simple* by Noll [54], *strictly local* by Rogula [58] or just *local* by Kunin [48]. These materials have no internal characteristic length with reference to the underlying microstructure.

Models that are not invariant with respect to rescaling of spatial coordinates are called non-local and have an internal length. This makes them better suited for modeling phenomena at small scales. *Weakly non-local* models have constitutive relations that depend on higher order gradients. For a general treatment of gradient models see Rogula [58], for a variational formulation, see Mindlin [53]. For strain gradient plasticity see Fleck and Hutchinson [31]. In *Strictly non-local* or *integral-type non-local* models, the stress depends on the deformation of a finite environment of a continuum point. Early studies of *Non-local Elasticity* aimed at improving the agreement between continuum theories and crystal lattices (see Rogula [59]). Attention was typically focused on removing stress and strain singularities at the cores of dislocations (see Eringen [28]) or crack tips (see Eringen [29]), determining elastic energies of defects (see Gairola [35]), or accounting for boundary layers in the deformation of small bodies (see Picu [55]). Overviews of the theory can be found in Kröner [46], Rogula [59], and Kunin [48, 49]. For a recent review focused on lattice dynamics and phonon dispersion, see Chen et al. [19]. In all these cases, the non-locality of the model represents the non-local character of interatomic forces.

A different motivation for non-local models comes from statistical continuum mechanics. Here, long-range forces describe the effective behavior of heterogeneous materials. Their interaction length is associated with the statistical correlation length of heterogeneities, see for example Kröner [47] and Kunin [49]. For recent work in the context of elastic deformation of composite materials, see Drugan and Willis [24]. A mixed probabilistic-atomistic approach is presented in Banach [8].

Extensions of integral-type non-local theories to plasticity were proposed by Eringen [27] and to damage mechanics by Bažant [10]. Non-local mechanics found ample application in the modeling of the failure of brittle heterogeneous materials such as concrete. Concrete undergoes strain softening under failure, making the well-posedness of a mathematical description depend on the existence of an internal length in the model (see Bažant [11] or Jirásek [43]). The internal length was again a statistical length accounting for the heterogeneity of the material. For a recent survey of non-local integral-type theories applied to plasticity and damage of heterogeneous

materials, see Bažant and Jirásek [12].

For current work on non-linear integral-type non-local models in the context of phase transitions see Truskinovsky and Zanzotto [70] and Ren and Truskinovsky [57].

Most non-local models improve the ability to model the microstructure of a material and its defects. They share the property, however, that they (with a few exceptions) rely on spatial derivatives of the displacement fields in their constitutive description.

Handshake Methods. A different approach that models the effect of defects splits the body into different regions. Each region is simulated by a model on the appropriate scale. This is an efficient way to account for the microstructure and to save resources at the same time. Typically, a macroscopic Finite Element model is coupled with Molecular Dynamics, e.g., in the quasicontinuum method which was introduced by Tadmor et al. [66] and recently reviewed by Miller and Tadmor [52]. Sometimes, even the quantum scale is included, see Abraham et. al. [5] or Broughton and Abraham [16]. The disadvantage of handshake methods are wave reflection or unphysical "ghost forces" at the interfaces of different scales. In addition, interfaces require special attention. They need to be moved, which typically necessitates remeshing.

Macroscopic Treatment of Defects. Cohesive surface models like the one used by Camacho and Ortiz [17], can create cracks in arbitrary directions by letting Finite Elements separate. The advantage of this approach is that macroscopically relevant properties (like friction on crack faces) can be represented efficiently. However, it is necessary to follow every crack tip individually.

The Virtual Internal Bond Model proposed by Gao and Klein [36] provides a macroscopic approach derived directly from atomistic laws. A Finite Element framework represents an atomistic structure accurately for small element sizes. Again, fine spatial resolution of the numerical framework is necessary at the zones of interest. Remeshing is therefore necessary.

Work on peridynamic theory. The theory was first introduced by Silling [61] and applied to the numerical simulation of impact in [62]. Silling and Bobaru [63] developed a peridynamic constitutive model for rubber and applied it in the numerical simulation of failure in membranes and fibers. Initial analytical work on the theory was done by Silling et al. [64] and Weckner and Abeyaratne [72].

1.3 Scope

Chapter 2 provides a systematic presentation of the fundamentals of peridynamic theory. The local equation of motion postulated by Silling [61] is helpful in immediately understanding the formal similarity of the theory to atomistic systems and providing an important initial motivation for the theory. The approach adopted here is different in that it starts from global balance laws and then derives the local laws, as in classical continuum mechanics. The chapter puts special emphasis on discontinuous and non-smooth deformations. It is shown that the balance of linear and angular momentum, the balance of mechanical power and energy, and the variational formulation do not have a jump term which would require special treatment of discontinuity surfaces. A basic constitutive theory is presented for plastic materials and materials that can undergo failure. A notion of stress is introduced and motivated. The framework of linear peridynamic theory is presented and applied to wave dispersion. It is shown how a body can become unstable due to the action of long-range forces. The special equations of motion for plane and one-dimensional deformations are derived.

Chapter 3 explores how peridynamic theory relates to other models of solid bodies. In particular, it is shown how peridynamic theory can be approximated by a strain gradient theory of infinite order (if the deformation is sufficiently smooth), how local continuum theory is recovered by letting the internal length disappear, and finally, how atomistic theory is included in the peridynamic theory as a heterogenous body with its mass concentrated on discrete points. All the continuum theories are then contrasted with focus on their ability to approximate the linear elastic behavior of a discrete system. The role of the Brillouin zone is discussed.

Chapter 4 presents several force laws to either approximate atomistic dynamics or to be used on a macroscale. Of particular importance for general macroscopic bodies are force laws with resolution length. The internal length and the peridynamic continuum are interpreted.

Chapter 5 provides a brief review of analytical solution techniques. A perturbation method is introduced that captures the behavior of displacement discontinuities. The Ritz approximation method and the collocation method are presented.

Chapter 6 defines the basic concepts of brittle material failure in peridynamic theory. Crack propagation in a strip is simulated to verify the ability of peridynamic theory to predict the onset of failure. Finally, autonomous crack growth in an asymmetrically pre-cracked body is simulated.

For clarity, most derivations of fundamental relations were moved to the appendix. The reader is encouraged to refer to them as necessary.

Chapter 2

Fundamentals

2.1 Mass and Motion

A body is modeled in peridynamic theory as a continuum. It consists of a continuous set of material points or particles and is denoted by Ω. Particles are identified by their position $\boldsymbol{x}$ in the reference configuration. They are particles in the continuum sense (see Truesdell and Noll [69]) and are assigned a mass density, rather than a mass. The mass density at $\boldsymbol{x}$ represents mass per reference volume. It does not depend on time and is denoted by the bounded and piece-wise continuous function $\rho_0 = \rho_0(\boldsymbol{x})$.

The position $\boldsymbol{y}$ of a particle $\boldsymbol{x}$ at time t is given by the *motion* $\boldsymbol{y} = \boldsymbol{y}(\boldsymbol{x}, t)$. Displacements from the reference configuration into the current configuration are denoted by $\boldsymbol{u} = \boldsymbol{y} - \boldsymbol{x}$. A continuum particle has only three translational degrees of freedom and is therefore a *medium of simple structure* in the sense of Kunin [48]. The material time derivatives of $\boldsymbol{y}$ are the velocity $\dot{\boldsymbol{y}} = \dot{\boldsymbol{y}}(\boldsymbol{x}, t)$ and the acceleration $\ddot{\boldsymbol{y}} = \ddot{\boldsymbol{y}}(\boldsymbol{x}, t)$.

If a particle is separated from the neighborhood it had in the reference configuration, the fields of displacements and positions are discontinuous. It is assumed that $\boldsymbol{y}$ is bounded and at least piece-wise continuous, meaning that at least some parts of the body will stick together rather than losing connection entirely. The magnitude of

a discontinuity is quantified by the *jump operator*

$$[[\varphi]] = [[\varphi]](\boldsymbol{x}, \boldsymbol{n}, t) = \lim_{\varepsilon \to 0} \left[\varphi(\boldsymbol{x} + \varepsilon \boldsymbol{n}, t) - \varphi(\boldsymbol{x} - \varepsilon \boldsymbol{n}, t)\right]. \tag{2.1}$$

A *discontinuity surface* $S = S_\varphi(t)$ in the body Ω is defined as the set of points $\boldsymbol{x}$ on which the jump operator applied to the quantity of interest, here φ, gives a non-zero value. Note that this surface lies in the reference configuration. Assume that all surfaces are piece-wise smooth, but not necessarily connected. The vector $\boldsymbol{n}$ will from now on be used in this context as normal vector of the surface S_φ at $\boldsymbol{x}$. On smooth parts of the surface, the normal surface velocity reads $\dot{\boldsymbol{s}} = \dot{s}\boldsymbol{n}$, with $\dot{s}$ being the propagation speed. On the boundaries of smooth parts, like kinks or lines where the surface ends, the surface may propagate into the non-normal direction.

A *crack in the classical sense*[1] is represented by a discontinuity surface $S_{\boldsymbol{y}}$ associated with the field of positions where

$$[[\boldsymbol{y}]] \cdot \boldsymbol{n} > \boldsymbol{0}. \tag{2.2}$$

The boundary line of this surface inside the body Ω represents a crack front.

A *phase boundary in the classical sense* is represented by a surface $S_{\boldsymbol{F}}$, associated with a discontinuous field of deformation gradients. Following Abeyaratne and Knowles [3, page 348], the continuity of $\boldsymbol{y}$ at all times implies that at each instant of time $\frac{d}{dt}[[\boldsymbol{y}]]_{\boldsymbol{x} \in S_{\boldsymbol{F}}} = \boldsymbol{0}$ and therefore

$$[[\dot{\boldsymbol{y}}]] = -[[\boldsymbol{F}]]\dot{s}\boldsymbol{n}. \tag{2.3}$$

[1] a definition of a crack in a non-classical sense that is more meaningful in the context of this theory is given in chapter 6

2.2 Forces

2.2.1 Balance Laws

The sum of all forces acting on a continuum particle of the body is represented by the density field $\boldsymbol{b}_{tot}$ with the dimension of force per reference volume. *Surface tractions are excluded from the model.* Sometimes $\boldsymbol{b}_{tot}$ is also referred to as "force", in particular when the theory is compared to atomistic theories. A force is then to be understood in a generalized sense, including classical forces and force densities.

$\boldsymbol{b}_{tot}$ is assumed to be bounded: singular or point forces are excluded, unless otherwise stated. The effects of concentrating forces in a limit process are discussed in section 2.5.3. Forces can be due to the deformation of the body or external sources, e.g., gravity. A body Ω has to satisfy the global balance of linear momentum

$$\frac{d}{dt}\int_{\Omega} \rho_0 \dot{\boldsymbol{y}}\, dV = \int_{\Omega} \boldsymbol{b}_{tot}\, dV \tag{2.4}$$

and the global balance of angular momentum

$$\frac{d}{dt}\int_{\Omega} \boldsymbol{y} \times \rho_0 \dot{\boldsymbol{y}}\, dV = \int_{\Omega} \boldsymbol{y} \times \boldsymbol{b}_{tot}\, dV. \tag{2.5}$$

Any part of a body Ω is a also a body, which by itself has to satisfy both global balance laws. A consequence of this is that (2.4) and (2.5) are *equivalent* to two local balance laws, the local balance of linear momentum

$$\rho_0 \ddot{\boldsymbol{y}} = \boldsymbol{b}_{tot}, \tag{2.6}$$

and the local balance of angular momentum

$$\boldsymbol{y} \times (\rho_0 \ddot{\boldsymbol{y}} - \boldsymbol{b}_{tot}) = \boldsymbol{0}, \tag{2.7}$$

respectively. The equivalence is shown in the appendix A.1. Both local balance laws (2.6) and (2.7) have to be satisfied almost everywhere on Ω.

The equivalence of global and local balance laws holds *without extra jump conditions* on discontinuity surfaces. There are conditions on certain discontinuity surfaces – but they are implied by both, the local *and* the global balance of linear momentum.

An important example is the condition on the discontinuity surface $S_{\rho_0 \dot{\boldsymbol{y}}}$ associated with the specific linear momentum $\rho_0 \dot{\boldsymbol{y}}$. Such surfaces occur when a discontinuity in the field of positions (like a crack in the classical sense) opens up or when a discontinuity in the field of deformation gradients moves (like a shock or a classical phase boundary). In these cases, $[[\dot{\boldsymbol{y}}]] \neq \mathbf{0}$. A consequence of the conservation of linear momentum is that the normal speed of $S_{\rho_0 \dot{\boldsymbol{y}}}$ has to be zero, as shown in the appendix A.1. This implies that, first, a discontinuity in the field of positions, e.g., a crack in the classical sense, can only extend through its crack front but cannot propagate in its normal direction. Second, shock waves in the classical sense do not exist. A phase boundary in the classical sense *cannot move* in its normal direction.

The local balance of linear momentum (2.6) implies the local balance of angular momentum (2.7). Due to the equivalence to their global forms, it can be stated in more general terms that conservation of linear momentum implies the conservation of angular momentum.

In summary, removing surface tractions from the continuum model has the following consequences:

1. Stress tensors do not naturally appear as a field quantity.

2. Jump conditions are not complementary to local balance laws, but rather a *consequence* of them.

3. Surfaces of discontinuous deformation gradients $S_{\boldsymbol{F}}$, like shock waves or phase boundaries, cannot propagate in their normal direction.

4. The balance of angular momentum is a consequence of the balance of linear momentum.

2.2.2 Interaction Forces and Links

Two kinds of forces act on a continuum particle: interaction forces $\boldsymbol{b}_{int}$ that the body exerts on itself, and external forces $\boldsymbol{b}$, the source of which lies outside the body. They sum up to

$$\boldsymbol{b}_{tot} = \boldsymbol{b}_{int} + \boldsymbol{b}. \tag{2.8}$$

The interaction forces are required to be such that in the absence of external forces the body does not change its linear or angular momentum. Thus, from (2.4) and (2.5) follows that

$$\int_{\Omega} \boldsymbol{b}_{int}\, dV = \boldsymbol{0} \tag{2.9}$$

and

$$\int_{\Omega} \boldsymbol{y} \times \boldsymbol{b}_{int}\, dV = \boldsymbol{0}, \tag{2.10}$$

respectively. An arbitrary subsection of the body $\Omega_{sub} \subset \Omega$ also constitutes a body, and (2.9) and (2.10) have to be satisfied for Ω_{sub} as well.

A two-body type interaction is assumed[2]. One restriction of this assumption is that Poisson's ratio has to be $\nu = 1/4$, as shown in section 2.7.4. Ways to remove this restriction involve multi-particle interaction. More complicated interaction forces are not considered here to keep the formal structure of the theory simple.

A *link* of two continuum particles is defined as their ability to exert forces on each other. Alternatively, a link may be called *bond*. It should then be carefully distinguished from atomistic or chemical bonds.

The interaction force acting on $\boldsymbol{x}$ is the sum of all *pair-wise forces* $\boldsymbol{f} = \boldsymbol{f}(\boldsymbol{x}', \boldsymbol{x}, t)$ exerted by particles $\boldsymbol{x}'$:

$$\boldsymbol{b}_{int}(\boldsymbol{x}) = \int_{\Omega} dV'\, \boldsymbol{f}(\boldsymbol{x}', \boldsymbol{x}, t). \tag{2.11}$$

Combining (2.11) with (2.9) and (2.10) yields, first, the microscopic version of *actio*

[2]Two-body potentials are used in atomistic simulations to understand the qualitative behavior of bodies. A typical example is the Lennard-Jones 12-6 potential, see Allen and Tildesley [6, chap. 1.3]. For better agreements with real systems, multi-body potentials are preferred, e.g., the embedded atom potential for the simulation of metals, see Daw et al. [23].

= *reactio* (see derivation in the appendix A.2),

$$\boldsymbol{f}(\boldsymbol{x}', \boldsymbol{x}, t) = -\boldsymbol{f}(\boldsymbol{x}, \boldsymbol{x}', t), \tag{2.12}$$

and, second, the requirement that $\boldsymbol{f}$ be a central force (see A.3),

$$\boldsymbol{f} \parallel \boldsymbol{e}_r \quad \Rightarrow \quad \boldsymbol{f} = f\boldsymbol{e}_r, \tag{2.13}$$

where $f = f(\boldsymbol{x}', \boldsymbol{x}, t)$.

2.2.3 Equation of Motion

The equation of motion is the local balance of linear momentum (2.6) combined with the assumption that external and interaction forces act on a continuum particle, and that interaction forces are pair-wise central forces:

$$\rho_0(\boldsymbol{x})\ddot{\boldsymbol{y}}(\boldsymbol{x}, t) = \int_\Omega dV'\, f(\boldsymbol{x}', \boldsymbol{x}, t)\boldsymbol{e}_r + \boldsymbol{b}(\boldsymbol{x}, t). \tag{2.14}$$

This is an integro-differential equation reminiscent of the equation of motion in molecular dynamics.

2.3 Balance of Mechanical Power and Energy

General Balance of Power and Definitions. The balance of energy can be derived from the local balance of momentum. Unlike in classical theories, no jump terms emerge on discontinuities of the displacement or the strain field. For the derivation, see appendix A.4. The general global power balance reads

$$\frac{d}{dt}E + \dot{W}_{int} = \dot{W}_{ext}, \tag{2.15}$$

where E is the *kinetic energy*

$$E = \int_\Omega \frac{1}{2}\rho_0 \dot{\boldsymbol{y}} \cdot \dot{\boldsymbol{y}}\, dV, \tag{2.16}$$

and $\dot{W}_{int}$ is the *rate of internal work*

$$\dot{W}_{int} = -\int_\Omega \boldsymbol{b}_{int} \cdot \dot{\boldsymbol{y}}\, dV, \tag{2.17}$$

and $\dot{W}_{ext}$ is the *rate of external work*

$$\dot{W}_{ext} = \int_\Omega \boldsymbol{b} \cdot \dot{\boldsymbol{y}}\, dV. \tag{2.18}$$

The *potential of external work* is defined as

$$W_{ext} = \int_\Omega \boldsymbol{b} \cdot \boldsymbol{u}\, dV. \tag{2.19}$$

If the external force field does not change with time, then $\dot{W}_{ext} = \frac{d}{dt} W_{ext}$.

A useful and intuitive expression for the rate of internal work is derived (in the appendix A.5) from (2.11), (2.12) and (2.13) and the definition $\boldsymbol{r} = \boldsymbol{y}' - \boldsymbol{y}$:

$$\dot{W}_{int} = \int_\Omega dV \left[\frac{1}{2} \int_\Omega dV'\, f\dot{r} \right]. \tag{2.20}$$

The *rate of pair-wise internal work* can then be identified as

$$\dot{w}_{int} = \dot{w}_{int}(\boldsymbol{x}', \boldsymbol{x}, t) = f\dot{r}.$$

The *rate of internal work density* reads

$$\dot{\bar{w}}_{int} = \dot{\bar{w}}_{int}(\boldsymbol{x}, t) = \frac{1}{2} \int_\Omega dV'\, \dot{w}_{int}, \tag{2.21}$$

where the integral adds the work done on a particular link to the work density at both points $\boldsymbol{x}'$ and $\boldsymbol{x}$ at equal share (therefore the factor of $\frac{1}{2}$).

Helmholtz Free Energy. To keep the similarity to the formal structure of classical continuum mechanics, constitutive information is contained in a potential that resembles the Helmholtz free energy when the temperature is fixed. The energy that is associated with the deformation of a pair of particles is called *pair-wise Helmholtz free energy* $\psi = \psi(\boldsymbol{x}', \boldsymbol{x}, t)$. The Helmholtz-free energy is a general concept that can be used for dissipative and non-dissipative processes, with or without internal variables (see section 2.4), or an explicit temperature field.

Similarly to (2.21), the *Helmholtz free energy density* is defined as

$$\bar{\psi} = \bar{\psi}(\boldsymbol{x}, t) = \frac{1}{2} \int_{\Omega} dV' \; \psi(\boldsymbol{x}', \boldsymbol{x}, t). \tag{2.22}$$

and the *total Helmholtz free energy* reads

$$\Psi = \Psi(t) = \int_{\Omega} dV \; \bar{\psi}(\boldsymbol{x}, t). \tag{2.23}$$

Dissipation. In a purely mechanical setting, dissipated energy is defined as the part of internal work that is not stored as Helmholtz free energy, and, thus, not available to do mechanical work anymore. Dissipation is the rate of dissipated energy and is required to be zero or positive for each link. For the *pair-wise dissipation* the Clausius-Duhem-type inequality

$$\dot{w}_{diss} = \dot{w}_{diss}(\boldsymbol{x}', \boldsymbol{x}, t) = \dot{w}_{int} - \frac{d}{dt}\psi \geq 0 \tag{2.24}$$

has to be satisfied. The *total dissipation*, which is also required to be zero or positive, is defined as

$$\dot{W}_{diss} = \dot{W}_{diss}(t) = \dot{W}_{int} - \frac{d}{dt}\Psi \geq 0. \tag{2.25}$$

For general dissipative processes, the pair-wise Helmholtz free energy depends on internal variables, see section 2.4,

$$\psi = \psi(\boldsymbol{x}', \boldsymbol{x}, t) = \hat{\psi}(r, \boldsymbol{\zeta}, \boldsymbol{x}', \boldsymbol{x}),$$

where $\boldsymbol{\zeta}$ denotes a set of generic internal variables. The *non-equilibrium force* is defined by

$$f_{\text{neq}} = f - \frac{\partial \hat{\psi}}{\partial r}. \tag{2.26}$$

Non-equilibrium forces may be viscous forces, for example. From (2.24) follows that

$$\dot{w}_{diss} = f_{\text{neq}}\, \dot{r} + \frac{\partial \hat{\psi}}{\partial \boldsymbol{\zeta}} \cdot \dot{\boldsymbol{\zeta}} \geq 0 \qquad \forall \dot{r}, \dot{\boldsymbol{\zeta}},$$

implying the restrictions on f_{neq}

$$f_{\text{neq}} \dot{r} \geq 0,$$

and on $\hat{\psi}$

$$\frac{\partial \hat{\psi}}{\partial \boldsymbol{\zeta}} \cdot \dot{\boldsymbol{\zeta}} \geq 0.$$

Non-dissipative Processes and Conservation of Energy. If the pair-wise Helmholtz free energy depends only on the current state of deformation, then it is called *pair-wise elastic energy* $\hat{\psi}_{el}(r, \boldsymbol{x}', \boldsymbol{x})$. The *elastic energy density* is defined as

$$\bar{\psi}_{el}(\boldsymbol{x}, t) = \frac{1}{2} \int_{\Omega} dV'\, \hat{\psi}_{el}(r, \boldsymbol{x}', \boldsymbol{x})$$

and the *total elastic energy* as

$$\Psi_{el}(t) = \int_{\Omega} dV\, \bar{\psi}_{el}(\boldsymbol{x}, t).$$

It is shown in the appendix A.6 that the time derivative of Ψ_{el} does not include jump terms in the presence of discontinuities, provided that motions satisfy the balance of linear momentum. Therefore,

$$\frac{d}{dt}\Psi_{el} = \int_{\Omega} dV \left[\frac{1}{2} \int_{\Omega} dV'\, \frac{\partial \hat{\psi}_{el}}{\partial r} \dot{r} \right], \tag{2.27}$$

If a body has only elastic energy and the non-equilibrium forces are zero, pairs do not dissipate energy because of (2.24). Then, by (2.20) and (2.27),

$$\dot{W}_{int} = \frac{d}{dt}\Psi_{el}$$

and finally with (2.25)

$$\dot{W}_{diss} = 0,$$

without jump terms. By contrast, bodies in local theories may dissipate energy at moving strain discontinuities, see, e.g., Abeyaratne et al. [1]. In peridynamic theory however, the dissipation is zero if the force law is elastic.

If the external force field does not change with time, i.e., $\boldsymbol{b} = \boldsymbol{b}(\boldsymbol{x})$, the integral of the power balance (2.15) is the *energy conservation law* for non-dissipative processes,

$$E + \Psi_{el} = W_{ext}. \tag{2.28}$$

2.4 Constitutive Theory

2.4.1 Objective Constitutive Relations

The magnitude of the pair-wise interaction force is determined by the *deformation history* of the particles $\boldsymbol{x}'$ and $\boldsymbol{x}$, formally expressed by a constitutive relation

$$f = f(\boldsymbol{x}', \boldsymbol{x}, t) = \hat{f}[\boldsymbol{y}(\boldsymbol{x}', t), \boldsymbol{y}(\boldsymbol{x}, t), \boldsymbol{x}', \boldsymbol{x}]_t \tag{2.29}$$

where $\hat{f}[\boldsymbol{y}', \boldsymbol{y}, \boldsymbol{x}', \boldsymbol{x}]_t$ is a functional that requires two time-dependent motions as arguments.

Constitutive relations are required to obey the rules of *material objectivity*. Let there be a motion of a material point that is seen by one observer as $\boldsymbol{y} = \boldsymbol{y}(t)$, while a different observer sees $\boldsymbol{y}^* = \boldsymbol{y}^*(t)$. Both observers have the same time. The frames of the two observers rotate by $\boldsymbol{Q} = \boldsymbol{Q}(t)$ and translate by $\boldsymbol{d} = \boldsymbol{d}(t)$ relatively to each

other. Then $\boldsymbol{y}$ and $\boldsymbol{y}^*$ are related by

$$\boldsymbol{y}^* = \boldsymbol{Q}\boldsymbol{y} + \boldsymbol{d}. \tag{2.30}$$

If the two observers measure magnitude and orientation of the same force from their individual perspective, they may obtain different values. The first requirement of material objectivity is that the measurements differ by the rotation of their reference frames $\boldsymbol{Q}$, i.e., $\boldsymbol{f}^* = \boldsymbol{Q}\boldsymbol{f}$; from (2.13) follows that $f^* = f$. As a second requirement, both forces have to be given by the same constitutive relation. Thus, $\hat{f}$ has to satisfy $\hat{f}[\boldsymbol{y}^{*\prime}, \boldsymbol{y}^*, \boldsymbol{x}', \boldsymbol{x}]_t = \hat{f}[\boldsymbol{y}', \boldsymbol{y}, \boldsymbol{x}', \boldsymbol{x}]_t$, or with (2.30)

$$\hat{f}[\boldsymbol{Q}\boldsymbol{y}' + \boldsymbol{d}, \boldsymbol{Q}\boldsymbol{y} + \boldsymbol{d}, \boldsymbol{x}', \boldsymbol{x}]_t = \hat{f}[\boldsymbol{y}', \boldsymbol{y}, \boldsymbol{x}', \boldsymbol{x}]_t$$

for arbitrary $\boldsymbol{Q}$ and $\boldsymbol{d}$, i.e., for arbitrary changes of reference frames. Due to this arbitrariness, the pair-wise force can only depend on the scalar distance (history) $r = |\boldsymbol{y}' - \boldsymbol{y}|$ of the two particles, i.e.,

$$f = \hat{f}[r, \boldsymbol{x}', \boldsymbol{x}]_t. \tag{2.31}$$

Any constitutive function derived from the relation (2.31) keeps this structure.

2.4.2 Homogeneity and Isotropy

A constitutive relation is *homogeneous* if it is invariant under a translation $\boldsymbol{d}$ of the reference configuration to any other point pertaining to the same homogeneous part. In other words

$$\hat{f}[r, \boldsymbol{x}', \boldsymbol{x}]_t = \hat{f}[r, \boldsymbol{x}' + \boldsymbol{d}, \boldsymbol{x} + \boldsymbol{d}]_t. \tag{2.32}$$

for all admissible $\boldsymbol{d}$. Then, on this homogeneous region

$$f = \hat{f}[r, \boldsymbol{\xi}]_t \tag{2.33}$$

holds with $\boldsymbol{\xi} = \boldsymbol{x}' - \boldsymbol{x}$.

A constitutive relation is *isotropic* at $\boldsymbol{x}$, if the interaction forces between $\boldsymbol{x}$ and particles from its environment $\boldsymbol{x}'$ do not depend on their spatial orientation in the reference configuration. The orientation of two particles is contained in the distance vector $\boldsymbol{\xi} = \boldsymbol{x}' - \boldsymbol{x}$, with which the constitutive relation (2.31) can be equivalently rewritten as

$$f = \hat{f}[r, \boldsymbol{\xi}, \boldsymbol{x}]_t. \tag{2.34}$$

Isotropy for $\boldsymbol{x}$ implies that

$$\hat{f}[r, \boldsymbol{\xi}, \boldsymbol{x}]_t = \hat{f}[r, \boldsymbol{Q}\boldsymbol{\xi}, \boldsymbol{x}]_t \tag{2.35}$$

for arbitrary rotations $\boldsymbol{Q}$. Consequently, the most general isotropic constitutive relation at $\boldsymbol{x}$ is

$$f = \hat{f}[r, \xi, \boldsymbol{x}]_t. \tag{2.36}$$

In many practical problems, the body of interest has a constitutive relation that is homogeneous and isotropic, i.e.,

$$f = \hat{f}[r, \xi]_t. \tag{2.37}$$

Undergoing a permanent deformation with failure or deforming plastically may change the material behavior of a body, and thus its homogeneity or material symmetry. Close to a crack lip, e.g., the interaction with the part of the body beyond the crack was eliminated by the propagating crack. In the sense of the definitions above, this part may have homogeneous or isotropic constitutive relations, and still behave non-homogeneously or anisotropically. Due to the non-local character of the theory, isotropy and homogeneity at a point $\boldsymbol{x}$ may be affected by a deformation process beyond its immediate neighborhood.

2.4.3 Elasticity

General Elastic Force Function

If the pair-wise interaction force f depends only on the current deformation of a pair of particles rather than on its deformation history, the constitutive relation is called *elastic*. For a pair of particles $\boldsymbol{x}'$ and $\boldsymbol{x}$ the force is given by

$$f = \hat{f}(r, \boldsymbol{x}', \boldsymbol{x}), \tag{2.38}$$

or by the potential $\hat{\psi}_{el}$ with

$$f = \frac{\partial \hat{\psi}_{el}}{\partial r}(r, \boldsymbol{x}', \boldsymbol{x}). \tag{2.39}$$

The potential $\hat{\psi}_{el}$ is the pair-wise elastic energy, as defined in section 2.3. It is of the type of a Helmholtz free energy and is used under the assumption that, first, the temperature is constant and, second, $\hat{\psi}_{el}$ depends only on the current deformation. For different forms of the Helmholtz free energy that do not only depend on the current state of deformation, see section 2.4.4.

Separable Force Functions

A special intuitive simplification of the force function is obtained by assuming that the interaction force is the product of a modulus $E(\boldsymbol{x}', \boldsymbol{x})$ and a possibly non-linear constitutive function $\hat{s}$ depending on the strain of a link $\varepsilon_{nl} = r/\xi - 1$

$$\hat{f}(r, \boldsymbol{x}', \boldsymbol{x}) = E(\boldsymbol{x}', \boldsymbol{x})\ \hat{s}(\varepsilon_{nl}). \tag{2.40}$$

In the isotropic case, when $\hat{f}(r, \xi) = E(\xi)\hat{s}(\varepsilon_{nl})$, $\hat{s}$ can be measured in an experiment: Let $\boldsymbol{F} = (\varepsilon_{nl} + 1)\mathbf{1}$, then $\boldsymbol{\sigma}_0 = 5\lambda\hat{s}(\varepsilon_{nl})\mathbf{1}$, where λ is Lame's constant, see section 2.7.

At a displacement discontinuity, the strain of a link is unbounded for $\xi \to 0$. Therefore, the functions E and $\hat{s}$ have to be chosen appropriately in order to ensure regular behavior.

Linear-Elastic Force Functions

Key ingredient of an elastic force function that is linear in the deformation is the *stiffness distribution* $C(\boldsymbol{x}', \boldsymbol{x})$ and the *reference force* $\hat{f}_0(\boldsymbol{x}', \boldsymbol{x})$, representing the force exerted by particle $\boldsymbol{x}'$ on $\boldsymbol{x}$ in the undeformed reference configuration:

$$\hat{f}(r, \boldsymbol{x}', \boldsymbol{x}) = C(\boldsymbol{x}', \boldsymbol{x})(r - \xi) + \hat{f}_0(\boldsymbol{x}', \boldsymbol{x}). \tag{2.41}$$

More specifically, the force function for an isotropic and homogeneous material with zero-valued reference force reads

$$\hat{f}(r, \xi) = C(\xi)(r - \xi). \tag{2.42}$$

All constitutive information is now contained in the stiffness distribution C. (2.42) is also a separable force function with $C(\xi)\xi = E(\boldsymbol{x}, \boldsymbol{x}')$ and $\hat{s}(\alpha) = \alpha - 1$.

Non-linear force functions $\hat{f}$ can be approximated by (2.41) or (2.42) by setting $C(\boldsymbol{x}', \boldsymbol{x}) = \frac{\partial \hat{f}}{\partial r}(\xi, \boldsymbol{x}', \boldsymbol{x})$, $\hat{f}_0(\boldsymbol{x}', \boldsymbol{x}) = \hat{f}(\xi, \boldsymbol{x}', \boldsymbol{x})$ or $C(\xi) = \frac{\partial \hat{f}}{\partial r}(\xi, \xi)$, respectively.

The general vectorial force between particles $\boldsymbol{f} = \hat{f}\boldsymbol{e}_r$ *cannot be linear* in $\boldsymbol{r}$ due to the kinematic non-linearity in $\boldsymbol{e}_r = \boldsymbol{r}/r$. Linearity of the scalar force function $\hat{f}$ is therefore insufficient to create a linear system. Linear systems may be obtained only by linearizing, as shown in section 2.8.

Structure-less Force Functions

Forces in atomistic systems depend formally only on the current positions of interacting particles. This concept motivates in the peridynamic framework the definition of *structure-less* force functions, as first introduced by Silling [61]. The general elastic force function (2.38) without connection to the reference state reads

$$f = \hat{f}(r). \tag{2.43}$$

It turns out that the concept of structure-less force functions is not useful within the context of the peridynamic framework, as will be explained in section 3.2.5.

2.4.4 Inelasticity

Internal Variables

The general functional dependence of the pair-wise force function (2.31) on the entire deformation history can be specialized to a more convenient mathematical description: the pair-wise force depends for each pair on the state of deformation at the current time and on *internal variables* in order to account for inelastic or irreversible deformation. For a general description in the context of classical continuum mechanics, see Coleman and Gurtin [21] or Holzapfel [41, page 278].

The *pair-wise Helmholtz free energy* with internal variables reads

$$\psi = \hat{\psi}(r, \boldsymbol{\zeta}, \boldsymbol{x}', \boldsymbol{x}), \tag{2.44}$$

with $\boldsymbol{\zeta}$ being a set of generic internal variables. The pair-wise force is the derivative with respect to the deformation r,

$$f = \frac{\partial \hat{\psi}}{\partial r}.$$

The internal variables must be equipped with evolution laws like

$$\frac{d}{dt}\boldsymbol{\zeta} = \boldsymbol{A}(r, \boldsymbol{\zeta}, \boldsymbol{x}', \boldsymbol{x}). \tag{2.45}$$

The choice of internal variables and their evolution laws depend on the inelastic mechanism; considered here are plastic deformation and failure in the sense of damage.

As constitutive relations in peridynamic theory are only required for pairs, one can conveniently apply one-dimensional models of classical continuum theory, and, thus, import the essential underlying deformation characteristics. For one-dimensional models of plasticity and visco-elasticity see Simo and Hughes [65]; for damage, see

Gurtin and Francis [39], and Krajcinovic and Lemaitre [45].

Rate-Independent Perfectly-Plastic Force Law

From the model in Simo and Hughes [65, page 13], a peridynamic constitutive relation describing rate-independent perfectly-plastic and linear elastic behavior is derived. The pair-wise Helmholtz free energy ψ reads

$$\psi = \hat{\psi}(r, r_p, \boldsymbol{x}', \boldsymbol{x}) = \frac{1}{2} C(\boldsymbol{x}', \boldsymbol{x})(r - \xi - r_p)^2$$

with r_p being the measure of plastic deformation. The evolution of r_p depends on the *yield strength* $f_Y = f_Y(\boldsymbol{x}', \boldsymbol{x})$ and the *yield condition*

$$\mathcal{F}(f, \boldsymbol{x}', \boldsymbol{x}) = |f| - f_Y(\boldsymbol{x}', \boldsymbol{x}) \leq 0.$$

The complete evolution law reads

$$\dot{r}_p = \gamma \, \mathrm{sign} f,$$

where γ is the *slip rate* for which

$$\begin{aligned} &\gamma = \dot{r} \, \mathrm{sign} f && \text{if} \qquad \mathcal{F} = \dot{\mathcal{F}} = 0 \\ &\gamma = 0 && \text{otherwise} \end{aligned} \tag{2.46}$$

holds. The effective force law reads in incremental form:

$$\dot{f} = \begin{cases} C(\boldsymbol{x}', \boldsymbol{x}) \, \dot{r} & \gamma = 0 \\ 0 & \gamma > 0 \end{cases} \tag{2.47}$$

Extensions to viscoplasticity or plasticity with hardening can also be found in Simo and Hughes [65].

Elastic Force Law with Brittle Failure

To model the failure of a link that connects a pair, the simple model of homogeneous damage evolution in a one-dimensional bar, as described in Gurtin and Francis [39], is adopted and further simplified. The key idea is that a link ceases to interact at a critical deformation and cannot recover connectivity thereafter. Failure is assumed to occur under tension.

The critical deformation is reached, when the *link failure criterion* is satisfied, i.e.,

$$\kappa = \kappa(r_{\max}, \boldsymbol{x}', \boldsymbol{x}) \geq 0. \tag{2.48}$$

The value of κ depends on the internal variable $r_{\max}$ that measures the maximum tensile deformation of a link. $r_{\max}$ can only grow and has the evolution law

$$r_{\max}(t) = \max_{\tau \leq t} \; r(\tau). \tag{2.49}$$

The pair-wise Helmholtz free energy reads

$$\psi = \hat{\psi}(r, r_{\max}, \boldsymbol{x}', \boldsymbol{x}) = \begin{cases} \hat{\psi}_{el}(r, \boldsymbol{x}', \boldsymbol{x}) & \kappa(r_{\max}, \boldsymbol{x}', \boldsymbol{x}) \leq 0 \\ 0 & \kappa(r_{\max}, \boldsymbol{x}', \boldsymbol{x}) > 0 \end{cases} \tag{2.50}$$

Note that $\hat{\psi}$ is in general discontinuous in $r_{\max}$. The associated force law reads

$$f = \begin{cases} \frac{\partial \hat{\psi}_{el}}{\partial r}(r, \boldsymbol{x}', \boldsymbol{x}) & \kappa(r_{\max}, \boldsymbol{x}', \boldsymbol{x}) \leq 0 \\ 0 & \kappa(r_{\max}, \boldsymbol{x}', \boldsymbol{x}) > 0 \end{cases} \tag{2.51}$$

It is possible to include more complicated damage mechanisms, e.g. to model fatigue. An overview over these mechanisms in the context of classical continuum damage mechanisms is given in Krajcinovic and Lemaitre [45].

2.5 Initial Boundary Value Problems

2.5.1 Local Formulation with Equation of Motion

A peridynamic problem statement is called *initial boundary value problem*. It resembles initial boundary value problems of classical continuum theories in that it includes the local equation of motion[3], constitutive relations, information about the geometry of the body Ω, and boundary conditions. Unlike in classical theories, however, boundary displacements and forces are prescribed on a boundary *region* with non-zero volumetric measure, as opposed to a geometric boundary in the strict mathematical sense. The reason for this is given in section 2.5.3. A complete initial boundary value problem in local form reads in peridynamic theory:

Let there be a body $\Omega = \Omega_u \cup \Omega_b$ and the given fields of initial displacements $\boldsymbol{u}_0(\boldsymbol{x})$ on Ω_b, initial velocities $\dot{\boldsymbol{u}}_0(\boldsymbol{x})$ on Ω_b, external forces $\boldsymbol{b}_*(\boldsymbol{x}, t)$ on Ω_b and boundary displacements $\boldsymbol{u}_*(\boldsymbol{x}, t)$ on Ω_u. Then, the displacement field $\boldsymbol{u}(\boldsymbol{x}, t)$ has to satisfy:

$$\left.\begin{aligned}
&\boldsymbol{x} \in \Omega_b : && \rho_0(\boldsymbol{x})\ddot{\boldsymbol{u}}(\boldsymbol{x}, t) = \textstyle\int_\Omega dV' \, \boldsymbol{f}(\boldsymbol{x}', \boldsymbol{x}, t) + \boldsymbol{b}_*(\boldsymbol{x}, t) \\
&\boldsymbol{x}, \boldsymbol{x}' \in \Omega : && \boldsymbol{f}(\boldsymbol{x}', \boldsymbol{x}, t) = \hat{f}[r, \boldsymbol{x}', \boldsymbol{x}]_t \boldsymbol{e}_r \\
&\boldsymbol{x} \in \Omega_b : && \boldsymbol{u}(\boldsymbol{x}, 0) = \boldsymbol{u}_0(\boldsymbol{x}), \quad \dot{\boldsymbol{u}}(\boldsymbol{x}, 0) = \dot{\boldsymbol{u}}_0(\boldsymbol{x}) \\
&\boldsymbol{x} \in \Omega_u : && \boldsymbol{u}(\boldsymbol{x}, t) = \boldsymbol{u}_*(\boldsymbol{x}, t)
\end{aligned}\right\} \tag{2.52}$$

In classical continuum mechanics, an (initial) boundary value problem that is stated in a local form like (2.52) contains typically a (partial) differential equation and admits only smooth solutions. It is called the *strong form*, and its solutions are *strong solutions*. By contrast, the peridynamic local formulation of a boundary value problem by (2.52) admits smooth, non-smooth and discontinuous solutions.

2.5.2 Variational Formulation

The variational formulation is derived by multiplying the local equation of motion (2.14) by an arbitrary *test function* $\boldsymbol{v} = \boldsymbol{v}(\boldsymbol{x})$ and integrating over the entire body.

[3] Equation (2.14) in the peridynamic framework.

Rather than applying Gauss' theorem, as in classical continuum mechanics, the term with interaction forces is rearranged, yielding a difference expression (the derivation is similar to the one in the appendix A.5). The variational problem statement is *equivalent* to local formulation *without jump terms*. The complete variational problem reads:

Let there be a body $\Omega = \Omega_u \cup \Omega_b$ and the given fields of initial displacements $\boldsymbol{u}_0(\boldsymbol{x})$ on Ω_b, initial velocities $\dot{\boldsymbol{u}}_0(\boldsymbol{x})$ on Ω_b, external forces $\boldsymbol{b}_*(\boldsymbol{x},t)$ on Ω_b and boundary displacements $\boldsymbol{u}_*(\boldsymbol{x},t)$ on Ω_u. Then, the displacement field $\boldsymbol{u}(\boldsymbol{x},t)$ has to satisfy:

$$\left.\begin{aligned} \textstyle\int_\Omega dV\,[\rho_0(\boldsymbol{x})\ddot{\boldsymbol{y}}(\boldsymbol{x},t) - \boldsymbol{b}_*(\boldsymbol{x},t)]\cdot\boldsymbol{v}(\boldsymbol{x}) & \\ = -\tfrac{1}{2}\textstyle\int_\Omega dV \int_\Omega dV'\,\boldsymbol{f}(\boldsymbol{x}',\boldsymbol{x},t)\cdot[\boldsymbol{v}(\boldsymbol{x}') - \boldsymbol{v}(\boldsymbol{x})] & \\ \boldsymbol{f}(\boldsymbol{x}',\boldsymbol{x},t) = \hat{f}[r,\boldsymbol{x}',\boldsymbol{x}]_t\boldsymbol{e}_r & \\ \textstyle\int_{\Omega_b} dV\ \boldsymbol{u}(\boldsymbol{x},0)\cdot\boldsymbol{v}(\boldsymbol{x}) = \int_{\Omega_b} dV\ \boldsymbol{u}_0(\boldsymbol{x})\cdot\boldsymbol{v}(\boldsymbol{x}) & \\ \textstyle\int_{\Omega_b} dV\ \dot{\boldsymbol{u}}(\boldsymbol{x},0)\cdot\boldsymbol{v}(\boldsymbol{x}) = \int_{\Omega_b} dV\ \dot{\boldsymbol{u}}_0(\boldsymbol{x})\cdot\boldsymbol{v}(\boldsymbol{x}) & \\ \boldsymbol{u}(\boldsymbol{x},t) = \boldsymbol{u}_*(\boldsymbol{x},t) \quad \boldsymbol{x}\in\Omega_u & \end{aligned}\right\} \tag{2.53}$$

for all $\boldsymbol{v}$ at all times t with $\boldsymbol{v}(\boldsymbol{x}) = \boldsymbol{0}$ for $\boldsymbol{x}\in\Omega_u$.

In equilibrium, the solution to the variational problem (2.53) is a stationary point of the potential energy, if certain conditions are satisfied, see section 2.6.3.

In peridynamic theory, the local formulation with the equation of motion (2.52) and the variational formulation (2.53) are equivalent and allow both for non-smooth and even discontinuous solutions. By contrast, in classical continuum mechanics, the class of admissible solutions to the variational formulation (also called the weak form) is still restricted to continuous functions (extensions to discontinuous solutions are made by introducing boundaries inside the body).

In local classical continuum theory, jump terms in the variational form indicate the necessity of additional constitutive relations on the discontinuity surface, e.g. the relation between cohesive forces and the crack opening in the cohesive surface model as explained by Ruiz and Ortiz [60]. As no jump terms appear in the variational formulation in the peridynamic theory, there is no necessity for extra constitutive relations.

2.5.3 Reaction to Surface Displacements and Tractions

Prescribed *finite displacements on a region of zero volumetric* measure[4] do not affect the deformation of the rest of the body. The pair-wise Helmholtz free energy of a material is bounded if the displacements are bounded. Therefore, displacements on a region of zero volumetric measure do not change the value of the Helmholtz free energy density. Displacement fields that are equal almost everywhere pertain to the same equivalence class of deformations, even if they differ on their boundary.

The response to *singular forces* (i.e., of the type of a Dirac delta function distribution) was analyzed by Silling et al. [64] in the context of linear equilibrium problems for long bodies. It was found that a singular force on a peridynamic continuum causes singular displacements. This result can be generalized for non-linear bodies: assume singular forces do not cause singular displacements on a region with measure zero. Then, the finite deformation of this particular region does not affect the deformation of the rest of the body. This, however, is impossible, as, by the balance of linear momentum, the volumetric measure of the force which is not zero has to be balanced by the body. This contradiction explains why singular forces lead to singular displacements.

The inability to resist the displacement of one single point is identical with the inability to withstand concentrated forces without forming a displacement discontinuity. This is caused by missing *local stiffness*, as is explained in section 3.3.7. Unlike local materials, peridynamic materials cannot have local stiffness. Therefore, it is necessary to formulate initial-boundary value problems such that boundary displacements or forces are prescribed on regions with non-zero volumetric measure. The distinction between boundary forces and body forces is obsolete. Small regions of prescribed displacements Ω_u have less influence than large regions. In general, a displacement discontinuity forms at the interface between Ω_b and Ω_u that increases upon decreasing Ω_u in size. For examples, see section 5.2.

[4] A region of zero volumetric measure is a point in a one-dimensional body, a point or a line in a two dimensional body, or a point, a line or a surface in a three dimensional body Ω.

2.6 Equilibria

2.6.1 Equilibrium Problem and Equilibrium Condition

The equilibrium problem derived from (2.52) reads: For a body $\Omega = \Omega_u \cup \Omega_b$ and the given fields of external forces $\boldsymbol{b}_*(\boldsymbol{x})$ on Ω_b (dead load) and boundary displacements $\boldsymbol{u}_*(\boldsymbol{x})$ on Ω_u, the displacement field $\boldsymbol{u}(\boldsymbol{x})$ has to satisfy

$$\left.\begin{array}{ll} \boldsymbol{x} \in \Omega_b : & \int_\Omega dV' \, \boldsymbol{f}(\boldsymbol{x}', \boldsymbol{x}) + \boldsymbol{b}_*(\boldsymbol{x}) = \boldsymbol{0} \\ \boldsymbol{x}, \boldsymbol{x}' \in \Omega : & \boldsymbol{f}(\boldsymbol{x}', \boldsymbol{x}) = \hat{f}[r, \boldsymbol{x}', \boldsymbol{x}]_t \boldsymbol{e}_r \\ \boldsymbol{x} \in \Omega_u : & \boldsymbol{u}(\boldsymbol{x}) = \boldsymbol{u}_*(\boldsymbol{x}) \end{array}\right\} \tag{2.54}$$

The integral equation in (2.54) is called *equilibrium condition*.

2.6.2 Variational Equilibrium Problem

The variational equilibrium problem derived from (2.53) reads: For a body $\Omega = \Omega_u \cup \Omega_b$ and the given fields of external forces $\boldsymbol{b}_*(\boldsymbol{x})$ on Ω_b (dead load) and boundary displacements $\boldsymbol{u}_*(\boldsymbol{x})$ on Ω_u, the displacement field $\boldsymbol{u}(\boldsymbol{x})$ has to satisfy

$$\left.\begin{array}{c} \frac{1}{2} \int_\Omega dV \int_\Omega dV' \, \boldsymbol{f}(\boldsymbol{x}', \boldsymbol{x}) \cdot [\boldsymbol{v}(\boldsymbol{x}') - \boldsymbol{v}(\boldsymbol{x})] + \int_\Omega dV \; \boldsymbol{b}_*(\boldsymbol{x}) \cdot \boldsymbol{v}(\boldsymbol{x}) = \boldsymbol{0} \\ \boldsymbol{f}(\boldsymbol{x}', \boldsymbol{x}) = \hat{f}[r, \boldsymbol{x}', \boldsymbol{x}]_t \boldsymbol{e}_r \\ \boldsymbol{u}(\boldsymbol{x}) = \boldsymbol{u}_*(\boldsymbol{x}) \quad \boldsymbol{x} \in \Omega_u \end{array}\right\} \tag{2.55}$$

for all $\boldsymbol{v}$ with $\boldsymbol{v}(\boldsymbol{x}) = \boldsymbol{0}$ for $\boldsymbol{x} \in \Omega_u$.

2.6.3 Stationary and Minimum Potential Energy

Solutions to the equilibrium problems (2.54) and (2.55) are stationary points of the total potential energy

$$\Pi[\boldsymbol{u}] = \Psi[\boldsymbol{u}] - \int_{\Omega_b} dV \; \boldsymbol{b}_*(\boldsymbol{x}) \cdot \boldsymbol{u}(\boldsymbol{x}), \tag{2.56}$$

where $\boldsymbol{u}$ is of the class of possibly discontinuous functions with $\boldsymbol{u}(\boldsymbol{x}) = \boldsymbol{u}_*(\boldsymbol{x})$ for $\boldsymbol{x} \in \Omega_u$, under the following conditions (for derivation see appendix A.7):

1. The material is elastic, i.e., the pair-wise Helmholtz free energy is the pair-wise elastic energy.

2. Stationarity is measured with respect to incremental and possibly discontinuous deformations including the formation and the extension of a (reversible) crack, and the formation and motion of phase boundaries (in the classical sense)[5]. According to Gelfand and Fomin [37, page 13], the equilibrium condition in (2.54) is therefore a necessary criterion for a *strong extremum*.

If variations with non-smooth increments are considered in classical theory (like the propagation of phase boundaries in the classical sense), extra conditions on the surface of non-smoothness have to be satisfied in order to ensure that the equilibrium is at a stationary point: the so-called *Weierstrass-Erdmann corner conditions* guarantee that the energy of the system does not increase or decrease at first order with the change of the location of a kink. For the general mathematical description see Gelfand and Fomin [37, page 63]; for the application to phase boundaries, see Abeyaratne et al. [1, sec. 4]. In peridynamic theory, satisfying the equilibrium condition is *sufficient* to be at a stationary point of potential energy.

An equilibrium at a deformed state is *(infinitesimally) stable* if the deformation is a (relative) minimum of the potential energy. Conditions for infinitesimal stability of an elastic material in equilibrium are considered in section 2.8.4.

2.7 Stress

2.7.1 Non-local Stress

The notion of stress is not conceptually necessary in peridynamic theory. However it is useful, as one can use it to, first, compare force-like boundary conditions in

[5]The actual motion of phase boundaries in the classical sense is not possible by the conservation of linear momentum, see section 2.2.1. Therefore, the statement here concerns only the energy landscape of deformations.

non-local theory to traction boundary conditions in classical theory and, second, to formulate stress-strain relations. If the stress-strain relation is known, constitutive models can be calibrated; e.g., by choosing $\hat{f}$ such that stiffness moduli correspond to measured material values.

In classical continuum mechanics, stress is a set of traction values, each of which represents the force that one part of a body exerts on another part, see e.g. Truesdell [68]. The existence of tractions is assumed from the beginning; the idea of equivalently replacing the influence of one part of a body onto another by traction values on an arbitrarily oriented cutting plane leads to the notion of a stress tensor. Thus, the concepts of tractions and stress are complementary.

Physically, a traction can be thought of as the sum of (possibly) many microscopic interaction forces between elementary particles like atoms. Tractions do not contain information about the origin of atomistic forces. Instead, tractions act directly on surfaces like cutting planes (with zero volumetric measure). Tractions and stresses are modeling concepts containing macroscopically relevant information drawn from microscopic details.

The standard formulation of peridynamic theory does not postulate tractions in the sense of classical continuum mechanics; therefore, stress is not a natural component. There are two ways to introduce *non-local stress*: first, an energetic approach that makes use of the fact that in classical continuum mechanics, stress is energy-conjugate to strain, and, second, the dynamic approach that defines stress as sum of particle forces, as presented by Born [15]. Both methods lead to the same result under homogeneous deformation and are presented in the subsequent sections.

The stress definitions presented here differ for general deformations from the one used by Silling [61]; however, they are equal under homogeneous deformations.

2.7.2 Stress as Energy-Conjugate Quantity

For homogeneous deformations with deformation gradient $\boldsymbol{F}$, non-local stress is defined as the energy conjugate quantity to the deformation gradient. In this sense the definition corresponds to the stress of classical continuum mechanics.

Consider a sufficiently large body such that Ω can be approximated by $\mathbb{R}^3$. Assume the body is isotropic and homogeneous with the pair-wise Helmholtz free energy $\hat{\psi}(r, \xi)$ at a certain fixed state of internal variables, and interaction force

$$\boldsymbol{f} = \frac{\partial \hat{\psi}(r, \xi)}{\partial \boldsymbol{r}} = \hat{f}(r, \xi)\, \boldsymbol{e}_r. \tag{2.57}$$

Let this body be subject to the homogeneous deformation

$$\boldsymbol{y} = \boldsymbol{F}\boldsymbol{x} \quad \Rightarrow \quad \boldsymbol{r} = \boldsymbol{F}\boldsymbol{\xi}. \tag{2.58}$$

The Helmholtz free energy density can now be written as a function of the deformation gradient

$$\bar{\psi}(\boldsymbol{F}) = \frac{1}{2} \int_{\mathbb{R}^3} dV_\xi\ \hat{\psi}(|\boldsymbol{F}\boldsymbol{\xi}|, |\boldsymbol{\xi}|). \tag{2.59}$$

If the pair-wise force function goes to zero sufficiently fast for large ξ, the value of the integral (2.59) is the same for a finite body, provided it is evaluated sufficiently far away from the boundary.

In classical continuum mechanics, the first Piola-Kirchhoff stress $\boldsymbol{\sigma}_0$ is given by

$$\boldsymbol{\sigma}_0 = \frac{d\bar{\psi}}{d\boldsymbol{F}}. \tag{2.60}$$

Combining (2.60) and (2.59) yields for the non-local continuum in the special case of a homogeneous deformation the stress-strain relation

$$\hat{\boldsymbol{\sigma}}_0(\boldsymbol{F}) = \frac{1}{2} \int_{\mathbb{R}^3} dV_\xi\ \hat{f}(|\boldsymbol{F}\boldsymbol{\xi}|, |\boldsymbol{\xi}|)\ \boldsymbol{e}_r \otimes \boldsymbol{\xi}. \tag{2.61}$$

Additionally, (2.61) motivates a definition of non-local stress as a pure field function for the body Ω that is independent of material properties:

$$\boldsymbol{\sigma}_0(\boldsymbol{x}, t) = \frac{1}{2} \int_{\Omega} dV'\ \boldsymbol{f}(\boldsymbol{x}', \boldsymbol{x}, t) \otimes (\boldsymbol{x}' - \boldsymbol{x}). \tag{2.62}$$

This expression includes positions in the reference configuration accounting for the

fact that the first Piola-Kirchhoff stress is a measure related to the reference geometry. A stress measure in the current configuration uses a pair-wise force that is measured with respect to the current volume:

$$\boldsymbol{f}_y = \boldsymbol{f}/J^2 \qquad \boldsymbol{f}_y = \boldsymbol{f}_y(\boldsymbol{y}', \boldsymbol{y}, t) \qquad J = \det \boldsymbol{F}. \tag{2.63}$$

Cauchy stress and the first Piola-Kirchhoff stress are related by $\boldsymbol{\sigma} = J\boldsymbol{\sigma}_0\boldsymbol{F}^T$, thus,

$$\boldsymbol{\sigma}(\boldsymbol{y}, t) = \frac{1}{2}\int_{\Omega_y} dV_y' \; \boldsymbol{f}_y(\boldsymbol{y}', \boldsymbol{y}, t) \otimes (\boldsymbol{y}' - \boldsymbol{y}) \tag{2.64}$$

with Ω_y being the current volume of the body. The corresponding stress-strain relation for the the second Piola-Kirchhoff stress reads

$$\hat{\boldsymbol{\sigma}}_{2\mathrm{pk}}(\boldsymbol{C}) = \frac{1}{2}\int_{\mathbb{R}^3} dV_\xi \; \frac{\hat{f}(\sqrt{\boldsymbol{\xi}\cdot\boldsymbol{C}\boldsymbol{\xi}}, \xi)}{\sqrt{\boldsymbol{\xi}\cdot\boldsymbol{C}\boldsymbol{\xi}}} \boldsymbol{\xi} \otimes \boldsymbol{\xi}, \tag{2.65}$$

where $\boldsymbol{C} = \boldsymbol{F}^T\boldsymbol{F}$ is the right Cauchy-Green tensor. Finally, the material-independent definition reads

$$\boldsymbol{\sigma}_{2\mathrm{pk}}(\boldsymbol{x}, t) = \frac{1}{2}\int_{\Omega} dV' \; \boldsymbol{F}^{-1}\boldsymbol{f}(\boldsymbol{x}', \boldsymbol{x}, t) \otimes (\boldsymbol{x}' - \boldsymbol{x}). \tag{2.66}$$

2.7.3 Cauchy's Dynamic Notion of Stress

In this section, the Cauchy stress tensor is constructed following Born [15] and then shown to be equal to (2.64). The Cauchy stress tensor in a crystal lattice is the quantity that maps normal vectors onto traction values that are the sum of forces per unit area between pairs of atoms. Considered are only those pairs of atoms which are connected by a line going through a finite surface area where the state of stress is to be determined. If $\boldsymbol{f}_\Phi$ denotes the interaction force between two discrete particles,

the definition of the Cauchy stress $\boldsymbol{\sigma}$ reads:

$$\boldsymbol{t}(\boldsymbol{n}) = \boldsymbol{\sigma}\boldsymbol{n} \qquad \boldsymbol{t} = \frac{1}{A}\sum_{(i,j)} \boldsymbol{f}_\Phi(\boldsymbol{y}_i, \boldsymbol{y}_j) \tag{2.67}$$

$$(i,j) = \left\{ i,j \in \mathbb{N} \mid \exists s \in \mathbb{R},\ \boldsymbol{y}_i + s(\boldsymbol{y}_j - \boldsymbol{y}_i) \in A \right\} \tag{2.68}$$

The surface A is to be chosen such that it is (a) small enough that, in some sense, it can be associated with one point and (b) big enough that the stress field is sufficiently smooth and the following assumption can be made: the number of pairs of atoms with relative position $\boldsymbol{r}_{ij} = \boldsymbol{y}_j - \boldsymbol{y}_i$ contained in the sum in (2.67) is given by $\boldsymbol{r}_{ij} \cdot \boldsymbol{n}\, A/V_c$ where V_c denotes the volume of a unit cell or the volume occupied by one atom in a homogeneous deformation. Then, the sum over indices i, j can be replaced by a sum over relative distance vectors with $\boldsymbol{r}_{ij} \cdot \boldsymbol{n} \geq 0$,

$$\boldsymbol{t} = \left[\frac{1}{V_c} \sum_{\boldsymbol{r}_{ij} | \, \boldsymbol{r}_{ij} \cdot \boldsymbol{n} \geq 0} \boldsymbol{f}_\Phi(\boldsymbol{y}_j, \boldsymbol{y}_i) \otimes \boldsymbol{r}_{ij} \right] \boldsymbol{n}.$$

Making use of $\boldsymbol{f}_y(\boldsymbol{y}_j, \boldsymbol{y}_i) = -\boldsymbol{f}_y(\boldsymbol{y}_i, \boldsymbol{y}_j)$ yields

$$\boldsymbol{t} = \left[\frac{1}{2V_c} \sum_{\boldsymbol{r}_{ij}} \boldsymbol{f}_\Phi(\boldsymbol{y}_j, \boldsymbol{y}_i) \otimes \boldsymbol{r}_{ij} \right] \boldsymbol{n}.$$

with the sum being extended over all possible $\boldsymbol{r}_{ij}$. The interaction force for discrete particles can be expressed in terms of a force density in the peridynamic sense with dimensions force/length[6],

$$\boldsymbol{f}_\Phi = V_c V_c \boldsymbol{f}_y.$$

Finally, in the continuum limit when $V_c \to 0$, the Cauchy stress (2.64) can be identified:

$$\boldsymbol{t} = \left[\frac{1}{2} \sum_{\boldsymbol{r}_{ij}} V_c\ \boldsymbol{f}_y(\boldsymbol{y}_j, \boldsymbol{y}_i) \otimes \boldsymbol{r}_{ij} \right] \boldsymbol{n} \to \left[\frac{1}{2} \int_{\Omega_y} dV_y\ \boldsymbol{f}_y(\boldsymbol{y}', \boldsymbol{y}) \otimes (\boldsymbol{y}' - \boldsymbol{y}) \right] \boldsymbol{n} = \boldsymbol{\sigma}\boldsymbol{n}.$$

2.7.4 Non-local Stiffness

One purpose of the stress strain relations (2.61) and (2.65) is to calibrate the constitutive function $\hat{f}$. For many materials, however, rather than the complete stress strain response, only stiffness values are known (and relevant). In this section, stiffness values are extracted from the non-local stress-strain relations, using the definition of the fourth-order stiffness tensor $\boldsymbol{\mathcal{C}}$,

$$\boldsymbol{\mathcal{C}} = \frac{d\hat{\boldsymbol{\sigma}}_{\text{2pk}}}{d\boldsymbol{E}},$$

where $\boldsymbol{E} = \frac{1}{2}(\boldsymbol{C} - \mathbf{1})$ is the Lagrangian strain. From (2.65) follows the stiffness tensor at deformed states

$$\boldsymbol{\mathcal{C}}(\boldsymbol{C}) = \frac{1}{2}\int_{\mathbb{R}^3} dV_\xi \, \frac{1}{r}\frac{\partial}{\partial r}\frac{\hat{f}(r,\xi)}{r}\boldsymbol{\xi}\otimes\boldsymbol{\xi}\otimes\boldsymbol{\xi}\otimes\boldsymbol{\xi} \qquad r = \sqrt{\boldsymbol{\xi}\cdot\boldsymbol{C}\boldsymbol{\xi}}$$

or the stiffness tensor at the undeformed state $\boldsymbol{C} = \mathbf{1}$, assuming that $\hat{f}(\xi,\xi) = 0$, i.e., there is no force between pairs in the reference configuration:

$$\boldsymbol{\mathcal{C}} = \boldsymbol{\mathcal{C}}(\mathbf{1}) = \frac{1}{2}\int_{\mathbb{R}^3} dV_\xi \;\; \xi^2 C(\xi)\, \boldsymbol{e}_\xi\otimes\boldsymbol{e}_\xi\otimes\boldsymbol{e}_\xi\otimes\boldsymbol{e}_\xi \qquad \boldsymbol{e}_\xi = \boldsymbol{\xi}/\xi. \tag{2.69}$$

$C(\xi) = \frac{\partial \hat{f}}{\partial r}(\xi,\xi)$ is the pair-wise stiffness distribution. For two- and three-dimensional bodies, the expression (2.69) can be further simplified to

$$\boldsymbol{\mathcal{C}} = \lambda\, \mathbf{1}\otimes\mathbf{1} + 2\mu\, \boldsymbol{I}_{\text{sym}} \qquad (\boldsymbol{I}_{\text{sym}})_{ijkl} = \frac{1}{2}(\delta_{ik}\delta_{jl} + \delta_{il}\delta_{jk}),$$

where $\boldsymbol{I}_{\text{sym}}$ is a fourth-order tensor that maps a tensor onto its symmetric part.

For three-dimensional bodies, λ and μ are Lame's constants, now given in terms of the stiffness distribution $C(\xi)$ as

$$\lambda = \mu = \frac{2\pi}{15}\int_0^\infty d\xi \; \xi^4 C(\xi). \tag{2.70}$$

The associated Poisson's ratio and Young's Modulus read

$$\nu = 1/4, \qquad E = \frac{\pi}{3}\int_0^\infty d\xi\ \xi^4 C(\xi). \tag{2.71}$$

In two dimensions, λ and μ are Lame's constants, if the system represents a three-dimensional body under plane-strain conditions (see section 2.8.6). Then

$$\lambda = \mu = \frac{\pi}{8}\int_0^\infty d\xi\ \xi^3 C(\xi). \tag{2.72}$$

For one-dimensional bodies, (2.69) simplifies to

$$\mathcal{C} = \int_0^\infty d\xi\ \xi^2 C(\xi), \tag{2.73}$$

where $\mathcal{C}$ is a general stiffness constant. For a bar that can deform freely in y- and z-direction, $\mathcal{C} = E$. For other examples, see section 2.8.7.

2.8 Linear Theory

2.8.1 Linearization

Linearization is an approximation technique that is useful for the analysis of neighborhoods of known states of deformation. This includes:

- Stability analyses in order to find out if an equilibrium state has a neighborhood that is energetically more or less favorable than the equilibrium state itself.
- Acoustic analyses or the analysis of small amplitude waves.
- Equilibrium analysis or the analysis of small static displacements under given loads.

The linear theory is developed for a body consisting of a general material that may be rate dependent. The pair-wise force can be approximated by the sum of, first, the

force associated with the current state of deformation $\boldsymbol{r}_0 = \boldsymbol{y}_0' - \boldsymbol{y}_0$ (possibly, but not necessarily the reference configuration)

$$\hat{\boldsymbol{f}}_0 = \hat{f}_0(\boldsymbol{r}_0, \boldsymbol{x}', \boldsymbol{x})\boldsymbol{e}_{r_0} = \hat{f}(r = |\boldsymbol{r}_0|, \dot{r} = 0, \boldsymbol{x}', \boldsymbol{x})\boldsymbol{e}_{r_0} \tag{2.74}$$

and, second, a force increment that is linear in the deformation increment $d\boldsymbol{r} = \boldsymbol{r} - \boldsymbol{r}_0$ and linear in the velocity $\dot{\boldsymbol{r}}$

$$d\boldsymbol{f} = d\left(\hat{f}(r, \dot{r}, \boldsymbol{x}', \boldsymbol{x})\boldsymbol{e}_r\right) = \boldsymbol{C}d\boldsymbol{r} + \boldsymbol{D}d\dot{\boldsymbol{r}}.$$

$\boldsymbol{C}$ is the *tangential stiffness tensor* of second order with

$$\boldsymbol{C} = \left[\frac{\partial \hat{f}}{\partial r}\,\boldsymbol{e}_r \otimes \boldsymbol{e}_r + \frac{\hat{f}}{r}(\boldsymbol{1} - \boldsymbol{e}_r \otimes \boldsymbol{e}_r)\right]_{\boldsymbol{r}=\boldsymbol{r}_0,\,\dot{\boldsymbol{r}}=\boldsymbol{0}} \tag{2.75}$$

and $\boldsymbol{D}$ is the *tangential viscosity tensor* of second order with

$$\boldsymbol{D} = \left[\frac{\partial \hat{f}}{\partial \dot{r}}\,\boldsymbol{e}_r \otimes \boldsymbol{e}_r\right]_{\boldsymbol{r}=\boldsymbol{r}_0,\,\dot{\boldsymbol{r}}=\boldsymbol{0}}.$$

Both, $\boldsymbol{C}$ and $\boldsymbol{D}$ are symmetric tensors. The linear approximation of the force function reads

$$\hat{\boldsymbol{f}}_{\text{lin}}(\boldsymbol{r}, \dot{\boldsymbol{r}}, \boldsymbol{x}', \boldsymbol{x}) = \hat{\boldsymbol{f}}_0 + \boldsymbol{C}(\boldsymbol{r} - \boldsymbol{r}_0) + \boldsymbol{D}\dot{\boldsymbol{r}}. \tag{2.76}$$

In an equilibrium state, there is no acceleration due to material interaction and, thus, there is no (internal) net force acting on any particle. The forces $\hat{\boldsymbol{f}}_0$ balance each other, i.e.,

$$\int_\Omega dV'\ \hat{\boldsymbol{f}}_0 = \boldsymbol{0}.$$

Note that non-zero reference forces $\hat{f}_0$ do have an effect nevertheless: they enter the stiffness tensor $\boldsymbol{C}$ in (2.75).

Finally, with the incremental small deformation $\boldsymbol{u}$ being measured from an equilibrium state, the linearized equation of motion reads

$$\begin{aligned} \rho_0(\boldsymbol{x})\ddot{\boldsymbol{u}}(\boldsymbol{x},t) &= \int_\Omega dV'\, \boldsymbol{C}\,[\boldsymbol{u}(\boldsymbol{x}',t)-\boldsymbol{u}(\boldsymbol{x},t)] \\ &+ \int_\Omega dV'\, \boldsymbol{D}\,[\dot{\boldsymbol{u}}(\boldsymbol{x}',t)-\dot{\boldsymbol{u}}(\boldsymbol{x},t)] + \boldsymbol{b}(\boldsymbol{x},t). \end{aligned} \tag{2.77}$$

The choice of the word "linearized" over "linear" emphasizes that there is no linear constitutive relation that leads to (2.77) without making an approximation by linearizing. This is also reflected by the fact that, as in classical theory of elasticity, a linearized constitutive relation $\boldsymbol{f} = \hat{\boldsymbol{f}}_{\text{lin}}$ is not objective.

If the incremental deformation is measured from the reference configuration, i.e., $\boldsymbol{r}_0 = \boldsymbol{\xi}$, then $\hat{\boldsymbol{f}}_0$ reads

$$\hat{\boldsymbol{f}}_0 = \hat{f}_0(\boldsymbol{x}',\boldsymbol{x})\boldsymbol{e}_\xi = \hat{f}(r=\xi,\dot{r}=0,\boldsymbol{x}',\boldsymbol{x})\boldsymbol{e}_\xi.$$

and

$$\boldsymbol{C} = C\,\boldsymbol{e}_\xi\otimes\boldsymbol{e}_\xi + \frac{\hat{f}_0}{\xi}(\mathbf{1}-\boldsymbol{e}_\xi\otimes\boldsymbol{e}_\xi); \qquad C = C(\boldsymbol{x}',\boldsymbol{x}) = \frac{\partial\hat{f}}{\partial r}(\xi,0,\boldsymbol{x}',\boldsymbol{x}) \tag{2.78}$$

and

$$\boldsymbol{D} = D\,\boldsymbol{e}_\xi\otimes\boldsymbol{e}_\xi; \qquad D = D(\boldsymbol{x}',\boldsymbol{x}) = \frac{\partial\hat{f}}{\partial\dot{r}}(\xi,0,\boldsymbol{x}',\boldsymbol{x}).$$

C and D are called *stiffness distribution* and *viscosity distribution*, respectively. From (2.12) follow the symmetry properties of the stiffness distribution,

$$C(\boldsymbol{x}',\boldsymbol{x}) = C(\boldsymbol{x},\boldsymbol{x}'),$$

and of the viscosity distribution,

$$D(\boldsymbol{x}',\boldsymbol{x}) = D(\boldsymbol{x},\boldsymbol{x}').$$

A special equation of motion that will often be used is derived from an elastic-inviscid constitutive relation (2.38) that is in addition homogeneous and isotropic, and has a zero reference force:

$$\begin{aligned} \rho_0(\boldsymbol{x})\ddot{\boldsymbol{u}}(\boldsymbol{x},t) &= \int_\Omega dV'\, \boldsymbol{C}\,[\boldsymbol{u}(\boldsymbol{x}',t)-\boldsymbol{u}(\boldsymbol{x},t)] + \boldsymbol{b}(\boldsymbol{x},t) \\ \boldsymbol{C} &= C(\xi)\boldsymbol{e}_\xi \otimes \boldsymbol{e}_\xi. \end{aligned} \tag{2.79}$$

This is a linear integro-differential equation where the stiffness tensor $\boldsymbol{C}$ is a symmetric *kernel*. The linearized equilibrium condition derived from (2.79),

$$\int_\Omega dV'\, \boldsymbol{C}\,[\boldsymbol{u}(\boldsymbol{x}')-\boldsymbol{u}(\boldsymbol{x})] + \boldsymbol{b}(\boldsymbol{x}) = \boldsymbol{0}, \tag{2.80}$$

is a *Fredholm equation of second kind*. For the general theory of integral equations and Fredholm equations, see Tricomi [67].

2.8.2 Dispersion Relation

Non-local particle interaction causes wave dispersion. Consider a wave $\boldsymbol{u}(\boldsymbol{x},t) = \bar{\boldsymbol{u}}(\boldsymbol{k})\exp(\omega t - i\boldsymbol{k}\cdot\boldsymbol{x})$ in a linear elastic-inviscid, isotropic, homogeneous medium, possibly at a deformed state. Let the body be large and the region of interest sufficiently far away from boundaries such that boundary effects are negligible. In this case, the body Ω can be approximated by an infinite medium $\mathbb{R}^3$. The wave has to satisfy (2.79), which leads to the *dispersion relation* in an infinite medium

$$(\boldsymbol{M}(\boldsymbol{k}) - \rho\omega^2\boldsymbol{1})\,\bar{\boldsymbol{u}}(\boldsymbol{k}) = \boldsymbol{0} \tag{2.81}$$

relating the wave frequency ω to the wave vector $\boldsymbol{k}$. $\boldsymbol{M}$ is the generalized or *non-local acoustic tensor* defined as

$$\boldsymbol{M}(\boldsymbol{k}) = \int_{\mathbb{R}^3} dV_\xi\,(1-\cos\boldsymbol{k}\cdot\boldsymbol{\xi})\,\boldsymbol{C}. \tag{2.82}$$

Note that the acoustic tensor depends on the current state of deformation $\boldsymbol{r}_0$. As $\boldsymbol{C}$ is bounded, $\boldsymbol{M}$ is finite in the limit (see Kunin [48, page 50]), when $k \to \infty$,

$$\boldsymbol{M}_\infty = \int_{\mathbb{R}^3} dV_\xi \, \boldsymbol{C}. \tag{2.83}$$

Multiplying (2.83) from both sides by a unit vector $\bar{\boldsymbol{u}}$ and making use of (2.81), shows that

$$\rho\omega_\infty^2 = \bar{\boldsymbol{u}} \cdot \boldsymbol{M}_\infty \bar{\boldsymbol{u}}. \tag{2.84}$$

Therefore, ω_∞ is finite, and ω_∞ is the same for different wave modes, if $\boldsymbol{M}$ is isotropic.

2.8.3 Waves at the Undeformed State

Consider a large body in its reference configuration with a zero reference force $\hat{\boldsymbol{f}}_0$. Far away from boundaries, the acoustic tensor reads

$$\boldsymbol{M}(\boldsymbol{k}) = \int_{\mathbb{R}^3} dV_\xi \, (1 - \cos \boldsymbol{k} \cdot \boldsymbol{\xi}) \, C(\xi) \, \boldsymbol{e}_\xi \otimes \boldsymbol{e}_\xi. \tag{2.85}$$

The dispersion relation (2.81) admits two kinds of waves (as shown in the appendix A.8):

1. Longitudinal or P-waves with $\bar{\boldsymbol{u}} \parallel \boldsymbol{k}$ and dispersion relation

$$\rho\omega_P^2(k) = \int_{\mathbb{R}^3} dV_\xi \, (1 - \cos[k\xi \, \boldsymbol{e}_\xi \cdot \boldsymbol{e}_1]) \, C(\xi) \, (\boldsymbol{e}_\xi \cdot \boldsymbol{e}_1)^2. \tag{2.86}$$

2. Shear or S-waves with $\bar{\boldsymbol{u}} \cdot \boldsymbol{k} = 0$ and dispersion relation

$$\rho\omega_S^2(k) = \int_{\mathbb{R}^3} dV_\xi \, (1 - \cos[k\xi \, \boldsymbol{e}_\xi \cdot \boldsymbol{e}_1]) \, C(\xi) \, (\boldsymbol{e}_\xi \cdot \boldsymbol{e}_2)^2. \tag{2.87}$$

The phase speeds $c_{ph} = \omega/k$ for $k = 0$ read in three and two dimensions

$$\rho c_{ph;P}^2(0) = 3\rho c_{ph;S}^2(0) = 3\lambda, \tag{2.88}$$

and in one dimension

$$\rho c_{ph}^2(0) = \mathcal{C}. \tag{2.89}$$

The stiffness constants λ and $\mathcal{C}$ are defined in (2.70), (2.72) and (2.73), respectively.

2.8.4 Infinitesimal and Small Scale Stability

An equilibrium at a deformed state is *infinitesimally stable* if the deformation is a relative minimum of the potential energy, defined in (2.56). For an elastic material with $\psi = \hat{\psi}(r, \boldsymbol{x}', \boldsymbol{x})$, this is the case when all eigenvalues β of the eigenvalue problem

$$\left.\begin{aligned} \int_\Omega dV'\, \boldsymbol{C}[\boldsymbol{v}(\boldsymbol{x}') - \boldsymbol{v}(\boldsymbol{x})] + \beta \boldsymbol{v}(\boldsymbol{x}) = \boldsymbol{0} \qquad & \boldsymbol{x} \in \Omega_b \\ \boldsymbol{v}(\boldsymbol{x}) = \boldsymbol{0} \qquad & \boldsymbol{x} \in \Omega_u \end{aligned}\right\} \tag{2.90}$$

are positive (for derivation see appendix A.9).

Small scale stability describes the reaction to perturbations with a wave length that is small compared to the body size and small compared to a characteristic length over which the deformation varies significantly. It is here only applied to regions that are sufficiently far from the boundary. The idea of small scale stability stands in contrast to overall structural stability describing the reaction to macroscopic perturbations such as beam buckling.

Based on these assumptions, the large body approximation $\Omega = \mathbb{R}^3$ for a homogeneous deformation $\boldsymbol{r} = \boldsymbol{F}\boldsymbol{\xi}$ is applied. Taking the Fourier Transform, the stability criterion (2.90) simplifies to the eigenvalue problem

$$[\boldsymbol{M}(\boldsymbol{k}) - \beta \boldsymbol{1}]\, \bar{\boldsymbol{v}}(\boldsymbol{k}) = \boldsymbol{0},$$

with $\boldsymbol{M}$ being the acoustic tensor defined in (2.82). Stability properties are all contained in the acoustic tensor, as it represents mode-specific resistance against incremental deformation. If $\boldsymbol{M}$ has zero-valued or negative eigenvalues, there is no (or negative) resistance against the deformation expressed by the eigenvector that is associated with β. The equilibrium is not small scale stable (i.e., either neutrally stable

or unstable). If all eigenvalues are positive, the system is small scale stable. Looking at the structure of $\boldsymbol{M}$ that follows from (2.82),

$$\boldsymbol{M}(\boldsymbol{k}) = \int_{\mathbb{R}^3} dV_\xi \, (1 - \cos \boldsymbol{k} \cdot \boldsymbol{\xi}) \, \left[\frac{\partial \hat{f}}{\partial r} \, \boldsymbol{e}_r \otimes \boldsymbol{e}_r + \frac{\hat{f}}{r} (\mathbf{1} - \boldsymbol{e}_r \otimes \boldsymbol{e}_r) \right], \tag{2.91}$$

reveals insight into mechanisms that cause the loss of stability (see appendix A.10 for derivation):

1. A particular pair is represented by a value of $\boldsymbol{\xi}$. This pair is called stable if the the integrand of (2.91) is positive definite for the associated value of $\boldsymbol{\xi}$.

2. If all pairs are stable, small scale stability follows. For small scale instability, it is necessary but not sufficient that pairs are unstable. In other words, unstable pairs can be stabilized by other stable pairs – or stable pairs may be destabilized by the surrounding.

3. If the force acting between particles of a pair is compressive, i.e., $\hat{f} < 0$, then the pair is unstable with respect to rotation. This instability can be interpreted as micro-buckling. The effect is due to the long-range nature of forces and due to the fact that the forces act between pairs. It does not occur in classical theory where interaction forces are local.

4. If the tangential stiffness of a pair is negative, i.e., $\frac{\partial \hat{f}}{\partial r} < 0$, then the pair is unstable with respect to extension and compression.

5. If $\hat{f} > 0$ and $\frac{\partial \hat{f}}{\partial r} > 0$, then the pair is stable.

The loss of stability caused by material behavior is typically associated with a non-convex energy, see, in the context of phase transformations, Abeyaratne and Knowles [2, 4], or, in the context of localized shear deformation in a non-local softening material, Leroy and Molinari [50]. Peridynamic theory, however, predicts instability under compression even if the elastic energy $\hat{\psi}_{el}$ is convex.

2.8.5 Existence and Uniqueness of Equilibrium Solutions

A solution of an equilibrium problem (2.54) with a linearized equilibrium condition (2.80) exists if invertibility criteria for the Fredholm integral equation are satisfied. For invertibility, see Davis [22] and Hilbert [40, page 192]. For existence of energy minimizers in a non-linear setting, see Fosdick and Mason [32, 33].

The notion of uniqueness of a solution is slightly different from classical theory: in peridynamic theory, a solution is a class of functions that are the same almost everywhere. In other words, two different functions may both represent the same solution if they differ, e.g., only at one point. In this sense, solutions to a linear equilibrium problem are unique. Uniqueness is established as in classical theory: if the potential energy is convex, then there is only one point of stationary energy. This implies, with the result of section 2.6.3, that there is only one equilibrium solution. Convexity of the potential energy implies infinitesimal stability for equilibrium points.

Functions pertaining to the same solution may differ at some points because differences on a region with a volumetric measure of zero do not change the energy integral.

2.8.6 Plane Deformation

Reducing the dimensions of a problem may simplify the analysis significantly. Consider the linearized equation of motion (2.79) for an isotropic, homogeneous and elastic body with zero-valued reference force. If the extension of a body is large in one coordinate direction and changes of the displacement field in the other two directions are more significant, the approximation of *plane deformation* is used:

- The body is assumed to be infinite in the z-direction, i.e., $\Omega = \Omega_2 \times \{-\infty, \infty\}$.
- The displacement field depends only on two spatial coordinates $\hat{\boldsymbol{x}} = (x, y) \in \Omega_2$, i.e., $\boldsymbol{u} = \boldsymbol{u}(\hat{\boldsymbol{x}}, t)$.
- The external force field depends only on the same two spatial coordinates, i.e., $\boldsymbol{b} = \boldsymbol{b}(\hat{\boldsymbol{x}}, t)$.

These assumptions combined with (2.79) yield

$$\rho_0 \ddot{\boldsymbol{u}}(\hat{\boldsymbol{x}}, t) = \int_{\Omega_2} dA' \left(\int_{-\infty}^{+\infty} dz' \, \boldsymbol{C} \right) \, [\boldsymbol{u}(\hat{\boldsymbol{x}}', t) - \boldsymbol{u}(\hat{\boldsymbol{x}}, t)] + \boldsymbol{b}(\hat{\boldsymbol{x}}, t).$$

By splitting the stiffness tensor, the displacement field and the body force into a plane strain and an anti-plane shear contribution,

$$\int_{-\infty}^{+\infty} dz' \, \boldsymbol{C} = \begin{pmatrix} & \boldsymbol{C}_{ps} & & 0 \\ & & & 0 \\ 0 & 0 & & C_{as} \end{pmatrix} \qquad \boldsymbol{u} = \begin{bmatrix} \boldsymbol{u}_{ps}(\hat{\boldsymbol{x}}, t) \\ u_{as}(\hat{\boldsymbol{x}}, t) \end{bmatrix} \qquad \boldsymbol{b} = \begin{bmatrix} \boldsymbol{b}_{ps}(\hat{\boldsymbol{x}}, t) \\ b_{as}(\hat{\boldsymbol{x}}, t) \end{bmatrix}$$

the equations of motion become uncoupled and can be separately expressed for *plane strain* as two-dimensional vector equation,

$$\rho_0 \ddot{\boldsymbol{u}}_{ps}(\hat{\boldsymbol{x}}, t) = \int_{\Omega_2} dA' \; \boldsymbol{C}_{ps}[\boldsymbol{u}_{ps}(\hat{\boldsymbol{x}}', t) - \boldsymbol{u}_{ps}(\hat{\boldsymbol{x}}, t)] + \boldsymbol{u}_{ps}(\hat{\boldsymbol{x}}, t), \tag{2.92}$$

with

$$\begin{aligned} \boldsymbol{C}_{ps} &= C_{ps}(\hat{\xi}) \boldsymbol{e}_{\hat{\xi}} \otimes \boldsymbol{e}_{\hat{\xi}}, \\ C_{ps}(\hat{\xi}) &= \int_{-\infty}^{+\infty} d\zeta \, \frac{\hat{\xi}^2}{\hat{\xi}^2 + \zeta^2} \, C(\sqrt{\hat{\xi}^2 + \zeta^2}), \\ E &= \frac{5\pi}{16} \int_0^{\infty} d\xi \, \xi^3 C_{ps}(\xi), \end{aligned} \tag{2.93}$$

and for *anti-plane shear* as scalar equation,

$$\rho_0 \ddot{u}_{as}(\hat{\boldsymbol{x}}, t) = \int_{\Omega_2} dA' \; C_{as}[u_{as}(\hat{\boldsymbol{x}}', t) - u_{as}(\hat{\boldsymbol{x}}, t)] + b_{as}(\hat{\boldsymbol{x}}, t), \tag{2.94}$$

with

$$\begin{aligned} C_{as} = C_{as}(\hat{\xi}) &= \int_{-\infty}^{+\infty} d\zeta \, \frac{\zeta^2}{\hat{\xi}^2 + \zeta^2} \, C(\sqrt{\hat{\xi}^2 + \zeta^2}), \\ E &= \frac{5\pi}{4} \int_0^{\infty} d\xi \, \xi^3 C_{as}(\xi), \end{aligned} \tag{2.95}$$

and with $\hat{\boldsymbol{\xi}} = \hat{\boldsymbol{x}}' - \hat{\boldsymbol{x}} \in \Omega_2$ and $\boldsymbol{e}_{\hat{\xi}} = \hat{\boldsymbol{\xi}}/\hat{\xi}$. The expressions for Young's Modulus (2.93) and (2.95) were derived from (2.71).

The equations of motion for plane strain and anti-plane shear were derived from the linearized equation of motion in three-dimension. In some cases, this can be done similarly in a non-linear setting. In general, however, and unlike in local theories, non-linearity in the presence of non-local forces prevents the decoupling of plane strain and anti-plane shear: shearing motion in the z-direction of a material with a non-linear force-law gives rise to forces and displacements in the x-y-direction.

The stiffness distributions for plane strain C_{ps} and anti-plane shear C_{as} are here expressed in terms of an underlying three-dimensional function C; one may argue that this is a necessary restriction on any two-dimensional model. However, it might as well be appropriate to develop truly two- or one-dimensional theories that cannot be derived from three-dimensional models – as long as they reproduce the desired macroscopic properties.

2.8.7 One-dimensional Plane Deformation

The equations of motion for plane strain (2.92) and anti-plane shear (2.94) are further reduced to one-dimensional problems. Assume that the body is long in the y-direction such that $\Omega_2 = \Omega_1 \times \{-\infty, \infty\}$, and that the deformation and the external force field only depend on one spatial variable $x \in \Omega_1$.

For *one-dimensional plane strain* the equation of motion (2.92) can be uncoupled in x- and y- direction. If $\boldsymbol{u} = u(x,t)\boldsymbol{e}_1$ and $\boldsymbol{b} = b(x,t)\boldsymbol{e}_1$, then the equation of motion reads

$$\rho_0 \ddot{u}(x,t) = \int_{\Omega_1} dx' \; C_{ps;1d}\left[u(x',t) - u(x,t)\right] + b(x,t) \tag{2.96}$$

with

$$C_{ps;1d}(\xi) = \int_{-\infty}^{+\infty} d\zeta \; \frac{1}{\xi^2 + \zeta^2} \, C_{ps}(\sqrt{\xi^2 + \zeta^2}),$$

$$E = \frac{6}{5} \int_0^{\infty} d\xi \; \xi^2 C_{ps;1d}(\xi). \tag{2.97}$$

For *one-dimensional anti-plane shear*, the equation of motion (2.94) can be rewritten

as

$$\rho_0 \ddot{u}(x,t) = \int_{\Omega_1} dx' \; C_{as;1d}\left[u(x',t) - u(x,t)\right] + b(x,t), \tag{2.98}$$

with

$$C_{as;1d}(\xi) = \int_{-\infty}^{+\infty} d\zeta \; \frac{\xi^2}{\xi^2+\zeta^2} \; C_{as}(\sqrt{\xi^2+\zeta^2}),$$

$$E = \frac{2}{5} \int_0^{\infty} d\xi \; \xi^2 C_{as;1d}(\xi). \tag{2.99}$$

As mentioned in section 2.8.6, it may be justified to use stiffness distributions that are not derived from higher dimensions.

Chapter 3

Comparison of Theories

3.1 Introduction

Non-local models are equipped with one or more internal characteristic lengths. They define scales that other lengths can be measured with respect to. Often, the lengths themselves are referred to as length scales. The physical meaning of characteristic lengths is directly related to the nature of the long-range forces. If not otherwise stated, peridynamic force laws have one internal length denoted by l.

Consider an elastic force law (2.38) that is isotropic. The value of the force between two particles should depend on the current distance of particles, their distance in the reference configuration, the internal length and some stiffness constant like Young's Modulus. The dimension of the pair-wise force is $[f] = F/L^{2n+1}$, and of Young's Modulus $[E] = F/L^n$ where L and F denote the physical dimensions of length and force, and n is the number of spatial dimensions of Ω. From dimensional analysis follows therefore that

$$\hat{f} = \hat{f}(r, \xi, l, E) \quad \Rightarrow \quad \frac{\hat{f}\, l^{n+1}}{E} = \bar{f}\left(\lambda, \bar{\xi}\right) \tag{3.1}$$

with $\lambda = \lambda_{nl} = r/\xi$ being the *non-local stretch* or *bond stretch*, and $\bar{\xi} = \xi/l$.

The further particles are apart the weaker their interaction. The range of interaction is called *horizon*. In solid mechanics, it is often practical to define a horizon

h_0 in the reference configuration. Then, the deformations have to be small. For large deformations, a horizon h_y should be defined in the current configuration, like it is done in molecular dynamics. If the range of interaction is not limited, the horizon is set formally to be ∞.

3.2 Formal Agreements with Other Models

3.2.1 Non-linear Strain Gradient Models

If the deformation and the force law of a peridynamic continuum are sufficiently smooth, the interaction integral can be written as a power series with respect to the internal length l. It is shown in the appendix A.11 that any interaction term for a force law of type (3.1) reads

$$\int_\Omega dV' \, \boldsymbol{f} = \frac{1}{l}\boldsymbol{R}_{-1} + \text{Div}\, \hat{\boldsymbol{\sigma}}_0(\boldsymbol{F}) + l\, \boldsymbol{R}_1 + l^2\, \boldsymbol{R}_2 + ... \tag{3.2}$$

where $\hat{\boldsymbol{\sigma}}_0$ is a constitutive function defined by (2.61). The functions $\boldsymbol{R}_i$ are higher order terms that are independent of l. They can be derived for arbitrary order following the procedure in A.11. At a location sufficiently far from the boundary,

$$\begin{aligned} \boldsymbol{R}_{-1} &= \boldsymbol{0} \\ (\boldsymbol{R})_{1,i} &= B_{ijklmnp}(\boldsymbol{F}) F_{jkl} F_{mnp} \end{aligned}$$

where

$$F_{jkl} = \frac{\partial^2 y_j}{\partial x_k \partial x_l}$$

is a higher order gradient. The tensor $B_{ijklmnp}$ is a constitutive function that depends only on $\boldsymbol{F}$:

$$B_{ijklmnp} = \frac{E}{8} \int_{\bar{\Omega}} d\bar{V}_\xi \, \frac{\partial^2 \bar{f}_i}{\partial \lambda_j \partial \lambda_m}(\boldsymbol{F}\boldsymbol{e}_\xi, \bar{\xi}) e_k \bar{\xi}_l e_n \bar{\xi}_p.$$

In one dimension, sufficiently far from the boundary, the series reads

$$\int_\Omega dx' \; f = \frac{d}{dx}\hat{\sigma}_0(y') + lR_1 + l^2R_2 + ... \tag{3.3}$$

with

$$R_1 = B(y')\left(y''(x)\right)^2$$

and

$$B(y') = \frac{E}{8}\int_{-\infty}^{+\infty} d\bar{\xi}\; \frac{\partial^2 \bar{f}}{\partial \lambda^2}(y', \bar{\xi})\bar{\xi}^2.$$

The expressions (3.2) and (3.3) may be used to approximate solutions of non-linear peridynamic initial boundary value problems, provided that the deformation is sufficiently smooth. In this case, the corresponding equations of motion or equilibrium conditions become partial (or ordinary) differential equations. For example, an approximation of first order of the solution $\boldsymbol{y} = \boldsymbol{y}(\boldsymbol{x}, t)$, satisfies

$$\rho_0 \ddot{\boldsymbol{y}} = \text{Div}\; \hat{\boldsymbol{\sigma}}_0\left(\frac{\partial \boldsymbol{y}}{\partial \boldsymbol{x}}\right) + l\; \boldsymbol{R}_1\left(\frac{\partial \boldsymbol{y}}{\partial \boldsymbol{x}}, \frac{\partial^2 \boldsymbol{y}}{\partial \boldsymbol{x}^2}\right) + \boldsymbol{b}(\boldsymbol{x}, t). \tag{3.4}$$

For the approximation to be good, it is necessary that

$$\left\| \frac{\partial^m \boldsymbol{y}}{\partial x_j \partial x_k ... \partial x_p} \right\| \ll \frac{1}{l^{m-1}} \qquad \forall m > 1.$$

On interfaces between regions where the body can move freely and regions where displacements are prescribed, or on locations where the external body force is discontinuous, the solution to a peridynamic boundary value problem is typically discontinuous. Approximations of strain-gradient type are in this case restricted to well-behaved parts of the body. To provide boundary conditions for (3.4), extra attention has to be paid to boundaries and interfaces. This is done for the linear case in section 5.2.

3.2.2 Non-linear Classical Elasticity

In the limit of a vanishing length scale, the interaction term, that represents the sum of all forces acting on particle $\boldsymbol{x}$, becomes for smooth deformations

$$\int_{\Omega} dV' \, \boldsymbol{f} = \text{Div } \hat{\boldsymbol{\sigma}}_0(\boldsymbol{F}). \tag{3.5}$$

The limit of solutions to (2.52) for $l \to 0$ has to satisfy the following problem statement with initial displacements $\boldsymbol{u}_0(\boldsymbol{x})$, initial velocities $\boldsymbol{v}_0(\boldsymbol{x})$, boundary displacements $\boldsymbol{u}_*(\boldsymbol{x}, t)$ and external forces $\boldsymbol{b}_*(\boldsymbol{x}, t)$ (see derivation in A.12):

$$\left.\begin{aligned}
\boldsymbol{x} \in \Omega_b : \quad & \rho_0 \ddot{\boldsymbol{u}} = \text{Div } \hat{\boldsymbol{\sigma}}_0(\boldsymbol{F}) + \boldsymbol{b}_*(\boldsymbol{x}, t) \\
& \boldsymbol{u}(\boldsymbol{x}, 0) = \boldsymbol{u}_0(\boldsymbol{x}) \\
& \dot{\boldsymbol{u}}(\boldsymbol{x}, 0) = \boldsymbol{v}_0(\boldsymbol{x}) \\
\boldsymbol{x} \in \partial\Omega_u \cap \partial\Omega_b : \quad & \boldsymbol{u}(\boldsymbol{x}, t) = \boldsymbol{u}_*(\boldsymbol{x}, t) \\
\boldsymbol{x} \in \partial\Omega_b \backslash \partial\Omega_u : \quad & \hat{\boldsymbol{\sigma}}_0(\boldsymbol{F})\boldsymbol{n} = \boldsymbol{0}
\end{aligned}\right\} \tag{3.6}$$

The problems statement (3.6) is formulated for smooth deformations, while the general peridynamic problem statement (2.52) is formulated for general non-smooth solutions. When $l \to 0$, discontinuities in the solution often disappear due to the increase of local stiffness as explained in (3.3.7). Sections 5.2.3 and 5.2.4 show deformations with a discontinuity at the interface between Ω_u and Ω_b with $[[\boldsymbol{u}]] = o(l)$. One necessary criterion for the interface discontinuity to disappear is that Ω_u has a finite measure. Another necessary criterion is that the elastic energy grows unbounded if the deformation localizes.

Formally, only zero-valued traction boundary conditions of Neumann-type appear. However, concentrated body forces on the boundary may represent tractions in the limit, when a concentration parameter approaches zero.

The problem statement (3.6) may have multiple solutions, not all of which are limits of solutions to (2.52) when $l \to 0$. *A limit of solutions to* (2.52) *necessarily satisfies* (3.6) *if it is smooth.* In this sense, a local material with a constitutive relation that can be written in the form of (2.61), is approached in peridynamic theory. The

constitutive relation (2.61) has the known restrictions, in particular a Poisson's ratio of $\nu = 1/4$ for small deformations. For the class of admissible materials, however, the theory of classical elasticity is *included* in the peridynamic framework.

For one-dimensional bodies, any local material with a constitutive relation $\sigma = \hat{\sigma}_0(\lambda)$ can be approached in peridynamic theory when $l \to 0$. Let $\hat{\sigma}_*(\lambda)$ be a given arbitrary constitutive function that is independent of l, and let $\hat{f}$ assume the form

$$\hat{f}(r, \xi) = -2d'(\xi)\hat{\sigma}_*(\lambda). \tag{3.7}$$

For dimensional reasons, d must equal

$$d(\xi) = \frac{\bar{d}(\bar{\xi})}{l},$$

where $\bar{d}$ is a dimensionless function with the properties[1] $\bar{d}(\bar{\xi}) = \bar{d}(-\bar{\xi})$ and $\bar{d} \to 0$ when $\bar{\xi} \to \infty$. If in addition

$$\int_{-\infty}^{+\infty} d\bar{\xi}\ \bar{d}(\bar{\xi}) = 1,$$

then d has the properties of a function that approaches a Dirac delta function, i.e., upon decreasing l, d becomes more and more concentrated. Then the stress (2.61) reads in one dimension

$$\hat{\sigma}_0(\lambda) = \frac{1}{2}\int_{-\infty}^{+\infty} d\xi\ \hat{f}(r, \xi)\xi = \hat{\sigma}_*(\lambda)\int_{-\infty}^{+\infty} d\bar{\xi}\ [-\bar{d}'(\bar{\xi})\bar{\xi}] = \hat{\sigma}_*(\lambda) \tag{3.8}$$

and the equation of motion becomes in the limit, when $l \to 0$,

$$\rho_0\ddot{u} = \frac{\partial}{\partial x}\hat{\sigma}_*(u') + b. \tag{3.9}$$

[1]It is convenient for one-dimensional bodies to let the distance of two particles in the reference configuration assume negative values. The sign of ξ replaces the unit vector $\boldsymbol{e}_\xi$, indicating how the particles x' and x are oriented.

3.2.3 Linear Integral-type Models with Strain Field

Linear non-local integral-type models that can be found in the literature, see Edelen [25, page 79], Kröner [46, page 338], or Rogula [58, page 142], employ the standard equation of motion

$$\rho_0 \ddot{\boldsymbol{y}} = \operatorname{Div} \boldsymbol{\sigma}_0 + \boldsymbol{b} \tag{3.10}$$

with a non-local constitutive function for the stress,

$$\boldsymbol{\sigma}_0(\boldsymbol{x}) = \boldsymbol{c}_0 \, \boldsymbol{\varepsilon}(\boldsymbol{x}) + \int_\Omega dV' \, \boldsymbol{c}(\boldsymbol{x}', \boldsymbol{x}) \, \boldsymbol{\varepsilon}(\boldsymbol{x}'), \tag{3.11}$$

where $\boldsymbol{c}_0$ is a local fourth-order stiffness tensor and $\boldsymbol{c}(\boldsymbol{x}', \boldsymbol{x})$ is a fourth-order stiffness kernel accounting for non-local material interaction.

For the case of isotropic and homogeneous materials, it is shown in the appendix A.13 that this model is equivalent to a special linearized peridynamic model – in particular for discontinuous or non-smooth deformations – provided that:

- The local stiffness tensor $\boldsymbol{c}_0$ vanishes.
- The stiffness kernel is isotropic and homogeneous, such that,

$$\boldsymbol{c}(\boldsymbol{x}', \boldsymbol{x}) = \boldsymbol{c}(\xi) = \lambda(\xi) \mathbf{1} \otimes \mathbf{1} + 2\mu(\xi) \boldsymbol{I}_{\mathrm{sym}}, \tag{3.12}$$

  where $\lambda(\xi) = \mu(\xi)$ are equal spatial distributions of Lame's constants, subject to some technical restrictions (smoothness and boundedness for $0 < \xi < \infty$, $\lambda \to 0$ for $\xi \to \infty$, and derivative has to be bounded for $\xi \to 0$).

- $\boldsymbol{x}$ is sufficiently far away from the boundary.

The corresponding peridynamic stiffness tensor reads

$$\boldsymbol{C} = 2 \left(\lambda''(\xi) - \frac{\lambda'(\xi)}{\xi} \right) \boldsymbol{e}_\xi \otimes \boldsymbol{e}_\xi + \left(\lambda''(\xi) + (n+1) \frac{\lambda'(\xi)}{\xi} \right) \mathbf{1}, \tag{3.13}$$

where n is the number of dimensions of Ω. Comparing $\boldsymbol{C}$ to (2.78) implies that, for two- and three-dimensional bodies, particles exert forces on each other already in the

undeformed state, because

$$\hat{f}_0(\xi) = \hat{f}(\xi, \xi) = \xi\lambda''(\xi) + (n+1)\lambda'(\xi).$$

It is shown in the appendix A.13 that the forces balance each other inside the body. Close to the boundary, however, they may cause deformations and the formation of a boundary layers. In the context of chains of discrete particles, similar boundary layers were discussed by Charlotte and Truskinovsky [18]. For one-dimensional bodies, $\hat{f}_0(\xi) = 0$.

For one-, two-, and three-dimensional bodies, the stiffness of pairs in the reference configuration is

$$\frac{\partial \hat{f}}{\partial r}(\xi, \xi) = 3\lambda''(\xi) + (n-1)\frac{\lambda'(\xi)}{\xi}.$$

3.2.4 Atomistics

Peridynamic theory can be formulated such that it describes the dynamics of an atomistic system governed by a two-body potential $\hat{\phi}(r)$, e.g., a Lennard-Jones 12-6 potential as shown in figure 3-1. Consider a system of discrete numbered particles with an assigned index j. A particle j assumes the position $\boldsymbol{x}_j$ in the reference configuration. Current positions are denoted by $\boldsymbol{y}_j(t) = \boldsymbol{y}(\boldsymbol{x}_j, t)$.

For the special purposes of this section, the mass density field ρ_0, the pair-wise force $\boldsymbol{f}$ and the external forces $\boldsymbol{b}$ are allowed to assume the form of a three dimensional Dirac delta function distribution[2] $\delta(\boldsymbol{x})$. Each particles has a finite mass m_j, therefore the density field is such that masses are concentrated on points $\boldsymbol{x}_j$

$$\rho_0(\boldsymbol{x}) = \sum_j m_j \; \delta(\boldsymbol{x} - \boldsymbol{x}_j).$$

The interaction forces and external forces can only act on and between points $\boldsymbol{x}_j$ and

[2]for properties see appendix B

$\boldsymbol{x}_k$, i.e.,

$$\hat{f}(r, \boldsymbol{x}', \boldsymbol{x}) = \sum_{j,k} \delta(\boldsymbol{x} - \boldsymbol{x}_j)\delta(\boldsymbol{x}' - \boldsymbol{x}_k)\frac{d\hat{\phi}}{dr}(r) \tag{3.14}$$

with $r = |\boldsymbol{y}(\boldsymbol{x}', t) - \boldsymbol{y}(\boldsymbol{x}, t)|$, and

$$\boldsymbol{b}(\boldsymbol{x}, t) = \sum_j \boldsymbol{b}_k(t)\ \delta(\boldsymbol{x} - \boldsymbol{x}_j).$$

As the physical dimension of the Dirac delta function distribution in three dimensions is[3] $[\delta] = 1/L^3$, it follows that $[\rho_0] = M/L^3$, $[f] = F/L^6$ and $[b] = F/L^3$, where M, F and L denote the physical dimensions of mass, force and length, respectively.

With this, the peridynamic equation of motion (2.14) reads

$$\sum_j \delta(\boldsymbol{x} - \boldsymbol{x}_j) \left[m_k \ddot{\boldsymbol{y}}(\boldsymbol{x}, t) - \int_\Omega dV' \sum_k \delta(\boldsymbol{x}' - \boldsymbol{x}_k)\frac{d\hat{\phi}}{dr}(r)\, \boldsymbol{e}_r - \boldsymbol{b}(\boldsymbol{x}, t) \right] = \boldsymbol{0}. \tag{3.15}$$

Equation (3.15) has to be satisfied in the sense of generalized functions: multiplying by an arbitrary vector field $\boldsymbol{v}(\boldsymbol{x})$ and integrating over Ω yields

$$\boldsymbol{v}(\boldsymbol{x}_j) \cdot \left[m_j \ddot{\boldsymbol{y}}_j(t) - \sum_k \frac{d\hat{\phi}}{dr}\left(|\boldsymbol{y}_k(t) - \boldsymbol{y}_j(t)|\right) \boldsymbol{e}_r - \boldsymbol{b}_j(t) \right] = \boldsymbol{0} \qquad \forall \boldsymbol{x}_j.$$

and, due the arbitrariness of $\boldsymbol{v}$,

$$m_j \ddot{\boldsymbol{y}}_j = \sum_k \frac{d\hat{\phi}}{dr}\left(|\boldsymbol{y}_k - \boldsymbol{y}_j|\right) \boldsymbol{e}_r + \boldsymbol{b}_j. \tag{3.16}$$

Expression (3.16) is the well-known equation of motion for particle systems, frequently used in atomistic simulations.

All constitutive information of atomistic systems that are modeled with (3.16) is *included* in the peridynamic framework. From a conceptual point of view, this makes it possible to use peridynamic theory as a multi-scale model, as it can be applied on the macro- *and* on the micro-scale, unlike local theories. If used in the form

[3] See appendix B.

of (3.15), however, the peridynamic equation of motion inherits from the discrete version (3.16) its complex structure and the difficulties to find solutions: analytical solutions exist only for rare cases, and numerical simulations require a very fine spatial resolution of the body and consequently, for macroscopic problems, an intractable number of degrees of freedom. Therefore, (3.15) has to be considered rather a basis for approximations than a substitute model. An obvious strategy to develop an approximate method is to relax the Dirac delta function distribution and to use instead less concentrated scalar functions that assume delta function properties in the limit. This is not further pursued here and left to future research.

A useful result of this section is the insight provided by (3.14): the equivalence of a special peridynamic continuum and the atomistic system was established with a force law that is heterogeneous and includes positions of particles in the reference configuration. Seen from the continuum description, the discrete atomistic system has therefore aspects of heterogeneity in that it assumes the body to be lumped to particles, and it preserves information from the reference state by letting each discrete particle remain distinct from other particles. This is one of the reasons why a structure-less force law as (2.43) is not useful for modeling discrete systems, as will be shown in section 3.2.5.

3.2.5 Consequences for Structure-less Materials

Despite the appealing similarity to an atomistic force law, the constitutive relation of a structure-less material as in (2.43) does not represent the physics of interacting atoms for the following reasons:

Consider a structure-less continuum with a homogeneous mass density field in its reference state. As every continuum point has arbitrarily close neighbors, the interaction energy of two homogeneous parts of a structure-less body does not change under shear motion. Consequently, the body does not resist shearing and behaves like a fluid.

If a body is heterogeneous and resists shear deformation, it is not clear how it could be ensured that the mass is clustered in appropriate entities. In addition, it was not

possible to introduce a control parameter that can be used to make the structure-less material assume properties of an atomistic system (or any other relevant system) in the limit when the control parameter goes to zero; therefore, it cannot be used as an approximation medium, either.

Finally, even if a structure-less force law could represent the behavior of a solid, it could not, in general, be set equal to an atomistic interaction force. If the associated potential $\hat{\phi}(r)$ grows as fast or faster than $1/r^n$ for $r \to 0$ (like the Lennard-Jones 12-6 potential), where n is the number of dimensions of the body, the energy of any finite piece of material is unbounded. This is the case because any continuum particle has a neighbor that is arbitrarily close. Tricks to prevent the energy from blowing up, like excluding the immediate neighborhood of particles from the energy integral, cannot be justified.

Structure-less materials may find applications in modeling fluids with surface tension.

3.3 Linear Elastic Behavior of Different Models

3.3.1 Role of Dispersion Relations

The different models are compared again. This time however, with a focus on the ability to approximate the behavior of a body with microstructure, for which a chain of discrete particles will serve as a representative example[4]. The peridynamic continuum can exactly reproduce even the non-linear behavior, however, only if its mass is concentrated on points. This is impractical for modeling purposes. Therefore the peridynamic continuum that is used for comparison is homogeneous.

All elastic constitutive properties and the distribution of inertia in a body are contained in its dispersion relation. Dispersion relations can be computed for all mechanical systems of current interest – whether discrete or continuous, local or non-local. Therefore, they are the ideal tool to compare or match linear elastic behavior.

[4]Atomistic dispersion in bodies was confirmed by experiments, e.g., by Wallis [71, page 57].

Consider a one-dimensional homogeneous body, long enough that boundary effects can be ignored, consisting of a linear elastic material. The equation of motion can typically be written as

$$\rho_0 \ddot{u}(x,t) = A[u](x,t) + b(x,t), \tag{3.17}$$

where A is a general *interaction operator* that carries the constitutive information of the material. A is a linear integral or differential operator, or a sum; A will be defined for various models subsequently and is summarized in table 3.1.

There are examples of one-dimensional bodies for which the equation of motion is different. This may be the case if the continuum has internal degrees of freedom with inertia[5]. Kunin [48] calls them *media with complex structure*. They are excluded here.

The *one-dimensional acoustic tensor* is defined by $M\bar{u} = -\mathcal{F}\{A[u]\}$, where $\mathcal{F}$ denotes the Fourier transform operation[6] with respect to the spatial coordinate x. The values of $M(k)$ are also given in table 3.1. The acoustic tensor defines the dispersion relation:

$$\rho_0 \omega^2(k) = M(k). \tag{3.18}$$

Taking the Fourier transform of (3.17) yields,

$$\rho_0 \ddot{\bar{u}}(k,t) + M(k)\bar{u}(k,t) = \bar{b}(k,t), \tag{3.19}$$

or in the static case

$$\bar{u}(k) = \frac{\bar{b}(k)}{M(k)}. \tag{3.20}$$

Now consider two problem statements for an unknown displacement field, each formulated with a different model. Let the body force field and the initial displacements and velocities (in the dynamic case) be the same. Despite possible differences in the model, the solution will be the same, if the acoustic tensors and therefore the dispersion relations are identical. In other words: the dynamic and static behavior of an

[5] See, e.g., Graff [38, page 121]. A one-dimensional bar with Poisson's contraction has the equation of motion $\rho_0 \ddot{u} + \alpha \ddot{u}_{xx} = E u_{xx}$.

[6] For definition see appendix B.

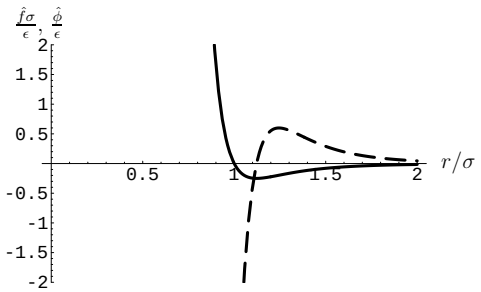

Figure 3-1: Lennard-Jones 12-6 potential $\hat{\phi}$ (solid line) as given in (3.21) and associated force $\hat{f}$ (dashed line).

atomistic system is identical with the behavior of a different model system (that is possibly continuous) if the dispersion relations are the same.

Most of the following results are general and independent of the choice of the interaction potential for the discrete system. For numerical values in plots, the Lennard-Jones 12-6 potential is chosen. It is frequently used in atomistic simulations, in particular for studies that aim at understanding the qualitative behavior of a body rather than deriving exact material values. The Lennard-Jones potential reads

$$\hat{\phi}_{LJ}(r) = \epsilon \left[\left(\frac{\sigma}{r}\right)^{12} - \left(\frac{\sigma}{r}\right)^{6} \right], \tag{3.21}$$

where σ is the distance of two particles at which they have a zero energy, and $\epsilon = 4\epsilon_0$, with ϵ_0 being the depth of the energy minimum. σ is on the order of Ångstrom; for Argon, $\sigma = 3.4 \times 10^{-10} m$ and $\epsilon_0 = 1.656 \times 10^{-21} J$. The values are taken from Allen and Tildesley [6, chap. 1.3].

3.3.2 Discrete System

Let the discrete system consist of particles j at positions in the reference configuration $x_j = ja$, then let $u_j(t) = u(x_j, t)$, $b_j(t) = b(x_j, t)$ and $\rho_0 = m/a$, where $a = 1.1193\sigma$ is the distance of particles at which the chain is stress free. The functions u and b are undefined for all $x \notin \bigcup_j \{x_j\}$. The interaction operator A is obtained by lineariz-

ing (3.16),

$$(Au)_j = \sum_{n \neq j} \frac{1}{a} \frac{d^2\phi}{dr^2}(|n-j|a)\ [u(x_n,t) - u(x_j,t)].$$

The acoustic tensor reads

$$M_*(k) = \sum_{n=1}^{\infty} 2(1-\cos k\, na)\, \frac{1}{a} \frac{d^2\phi}{dr^2}(na). \tag{3.22}$$

The corresponding dispersion curve $\omega(k)$ is shown in the figures 3-2 and 4-1 as dashed line. Note that ω is periodic and bounded. Boundedness implies that phase speeds of waves, defined as

$$v_{ph}(k) = \frac{\omega(k)}{k},$$

approach zero for large wavenumbers.

3.3.3 Classical Local Elasticity

The interaction operator and the acoustic tensor for a linear elastic local material read

$$A = E\frac{\partial^2}{\partial x^2} \qquad\qquad M(k) = Ek^2.$$

E was chosen such that the curvatures of M and M_* match, i.e., their Young's Modulus matches,

$$E = \sum_{n=1}^{\infty} n^2 a \frac{d^2\phi}{dr^2}(na).$$

The dispersion curve is a straight line that goes to infinity when $k \to \infty$ as shown in figure 3-2, therefore the phase speed is a constant. The agreement with the atomistic dispersion relation is limited to small wave numbers k.

3.3.4 Strain Gradient Model

The details of the general strain gradient formulation can be found in Rogula [58, sec. IV]. For the purposes of this section, the interaction operator A can be expressed by

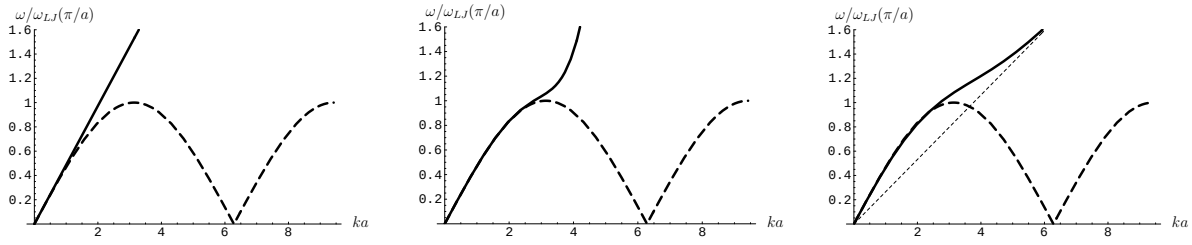

Figure 3-2: Dispersion relations ω/ω_0 for different models. *Solid lines:* (a) Classical elasticity. (b) Strain-gradient model. (c) Non-local integral-type model with strain. *Dashed lines:* Discrete system with a Lennard-Jones 12-6 potential given by (3.21). $\omega_0 = \omega_{LJ}(\pi/a)$, where ω_{LJ} is computed with (3.21).

a polynomial P as

$$A = P(\frac{\partial}{\partial x}) \qquad\qquad P(s) = Es^2 \prod_{j=1}^{n} \left(1 - (l_j s)^2\right)$$

where l_k are generalized *internal lengths* that may be complex and have to be such that the roots of P occur in mutually conjugate pairs, and are not purely imaginary. This is required to make sure that the acoustic tensor

$$M(k) = -P(-ik) = Ek^2 \prod_{j=1}^{n} \left(1 + (l_j k)^2\right)$$

does not assume negative values; negative values signify the loss of stability.

In the special case of $n = 1$, classical local elasticity is recovered and no internal length is included in the model. For $n > 1$, internal lengths can be chosen so as to approximate a system with microstructure. An approximation of n-th order involves n internal lengths. Figure 3-2 shows the dispersion curve for three internal lengths chosen such that $M^{(j)}(0) = M_*^{(j)}(0)$ for $j = 4, 6, 8$. Note that $M(k)$ and, thus, $\omega(k)$ always grow polynomially with k. For a n-th order model, ω grows with k^{n+1}, when $k \to \infty$. Although the agreement with the dispersion curve of the discrete system is better than it is in the case of a local material, ω will always be unbounded, (and therefore, prevent discontinuous solutions due to discontinuous forces, as will be shown later). In addition, the phase speed v_{ph} of waves grows with k^n.

3.3.5 Integral-type Model with Strain Field

The interaction operator of a one-dimensional version of a non-local integral-type model like in (3.11) reads

$$Au = c_0 \frac{\partial^2 u}{\partial x^2}(x,t) + \frac{\partial}{\partial x} \int_{-\infty}^{+\infty} dx' \; c(x'-x) \frac{\partial u}{\partial x}(x',t),$$

where c_0 is the local stiffness modulus and $c(\xi)$ is a stiffness kernel. If $c_0 = 0$, then the integral model is a special linear peridynamic model. For this section it is assumed that $c_0 \neq 0$ and the peridynamic model is treated separately. The acoustic tensor reads

$$M(k) = (c_0 + \bar{c}(k))k^2 = c_0 k^2 + \int_0^{\infty} d\xi \; \cos k\xi \; c(\xi) \; k^2$$

If $c(\xi)$ is continuous, then $\bar{c}(k)$ goes to zero for large k. This implies that the dispersion curve grows linearly, i.e., $\omega = O(k)$, and $v_{ph} = O(1)$ for $k \to \infty$. Figure 3-2 shows the dispersion relation for the special choice of

$$c(\xi) = \frac{E - c_0}{l} \sqrt{2/\pi} \; e^{-2(\xi/l)^2} \tag{3.23}$$

and $l = a$.

3.3.6 Peridynamic Continuum

In the linear peridynamic case, the interaction operator is derived from (2.77) and reads for the one-dimensional inviscid case

$$Au = \int_{-\infty}^{+\infty} dx' \; C(x'-x)[u(x',t) - u(x,t)]$$

with the acoustic tensor

$$M(k) = \bar{C}(0) - \bar{C}(k) = \int_0^{\infty} d\xi \; 2(1 - \cos k\xi) C(\xi). \tag{3.24}$$

model	$A[u]$	$M(k)$	$\omega(k)$, $k \to \infty$
discrete	$\sum_{n \neq j} \frac{d^2\phi}{a\, dr^2}\ (u_n - u_j)$	$\sum_{n=1}^{\infty} 2(1-\cos k\, na)\, \frac{1}{a}\frac{d^2\phi}{dr^2}(na)$	$O^*(1)$
local	$E\frac{\partial^2 u}{\partial x^2}$	Ek^2	$O(k)$
strain-gradient	$P(\frac{\partial}{\partial x})u$	$-P(-ik)$	$O(k^n)$
integral-type	$c_0\frac{\partial^2 u}{\partial x^2} + \frac{\partial}{\partial x}\int dx'\ c\frac{\partial u}{\partial x}$	$(c_0 + \bar{c}(k))k^2$	$O(k)$
peridynamic	$\int dx'\ C(u'-u)$	$\int_0^{\infty} d\xi\ 2(1-\cos k\xi)\, C(\xi)$	$O^*(1)$

Table 3.1: Operator A and acoustic tensor $M(k)$. $i^2 = -1$. *Remark on third column:* In the case of a discrete and a peridynamic system, $\omega(k) = O^*(1)$ means that $\exists \Omega(k) \geq |\omega(k)|,\ \Omega(k) = O(1)$.

The Fourier Transform $\bar{C}$ goes to zero for large k, as C is required to be continuous. Therefore, $M(k) \to M_\infty = \bar{C}(0)$. This implies that the dispersion curve stays bounded, and phase speeds go to zero, like in the discrete case. For particular choices of C and M see section 4.1.

3.3.7 Dispersion Relations and Local Stiffness

Classical local and certain non-local continuum models[7] have dispersion curves $\omega(k)$ that grow at least linearly with k. Phase speeds $v_{ph} = \omega/k$ either grow (like in strain gradient theory) or approach a constant value (like in local theory or the classical integral-type theory). A consequence of this is that displacement fields stay continuous even when a singular force field is applied. For example, let $b(x) = \delta(x)$, where δ is the delta function distribution. Then $\bar{b}(k) = 1$ and

$$\bar{u}(k) = \frac{1}{M(k)} = \frac{1}{\rho\omega^2(k)} = O(1/k^n) \tag{3.25}$$

with $n \geq 2$. As $\bar{u}$ goes to zero faster than $1/|k|$, u is continuous.

In contrast, in peridynamic theory $M(k) = O(1)$, and phase speeds go to zero, *like in the discrete system.* Under the influence of a singular force,

$$\bar{u}(k) = \frac{1}{M(k)} = \frac{1}{\rho\omega^2(k)} = O(1), \tag{3.26}$$

[7]Media with complex structure are excluded, as mentioned in section 3.3.1. The subsequent statements are for systems with $M(k) = \rho_0\omega^2(k)$.

implying that the displacement field is singular. In fact, u will be just as continuous or smooth as b. The ability to resist concentrated deformations is called *local stiffness*. A system has local stiffness, if the dispersion curve is unbounded for $k \to \infty$.

In summary, bodies in classical non-local and local theories resist concentrated deformations. In a dynamic setting, concentrated waves (with large k) can always propagate at phase speeds that are at least of order one with respect to the wave number. Peridynamic theory does not provide local stiffness. Displacement discontinuities may form. The higher the degree of localization of a deformation, the slower are the associated wave speeds. Displacement discontinuities cannot move at all, which was also shown in section 2.2.1.

3.3.8 Role of Brillouin Zone

In an atomistic system, the interval $B = [-\pi/a, \pi/a]$ is called *Brillouin zone*. It was pointed out by Kunin [48] that the displacements u_n on lattice sites $x_n = na$ may be uniquely represented by the values of the Fourier Transform $\bar{u}(k)$ in the Brillouin zone; outside B, $\bar{u}$ may be set to zero without loss of information[8], i.e., $u \in \mathcal{U}$ with

$$\mathcal{U} = \{u(x) \mid \bar{u}(k) = 0, \;\; |k| > k_B\}$$

For problems of type (3.17) this can be done consistently, if all other prescribed fields involved, like the body force b, or initial positions or displacements underly the same restriction; for discrete systems, where forces and initial conditions can only be applied to particles on lattice sites, this is easily realized. All fields lose their physical meaning between lattice sites, and the dispersion relation is significant only on the Brillouin zone. The formalization of this approach is called the *quasicontinuum method*, see Kunin [48] and Rogula [58], not to be confused with the *numerical quasicontinuum method*, presented by Miller and Tadmor in [52], which is different, but also used in

[8]This can be shown by considering a mode with an arbitrary wave number $k = k_B + j2\pi/a$, where $k_B \in B$ and j is an integer. The displacements, associated with this mode read $u(x) = \bar{u}(k)\cos kx$. Using $\cos(k_B ja + 2\pi j) = \cos k_B ja \;\; \cos 2\pi j - \sin k_B ja \;\; \sin 2\pi j = \cos k_B ja$, the displacements on lattice sites are $u(ja) = \bar{u}(k)\cos kja = \bar{u}(k)\cos k_B ja$. Therefore, the displacements due to mode k can be made part of mode k_B.

the context of multi-scale modeling.

The quasicontinuum method is not formally adopted here for the continuum theories of interest. A restriction of the Fourier Transform of external force fields seems inconvenient for a model that shall be applicable on a macroscopic scale. Instead, the motivation of the quasicontinuum method is used to interpret solutions in view of the microstructure of the system. Oscillatory parts of the displacement field with a wave number $k > l/\pi$, where l is the internal length of the microstructure, should not be considered as physically meaningful. This is particularly important for the interpretation of discontinuities: discontinuous displacement fields have a slowly decaying Fourier spectrum, i.e., their discontinuity is represented by large values of their Fourier Transforms for large values of k. The physically sensible part, however, is only defined on the Brillouin zone.

Chapter 4

Force Laws

4.1 Linear Atomistic-peridynamic Force Law

A peridynamic force law for a homogeneous body can be derived from atomistic dispersion relations. If the dispersion relations of the linearized atomistic system and the peridynamic continuum agree in the Brillouin zone, then the linear elastic behavior of both systems will be exactly the same under physically sensible loading. In addition, the peridynamic continuum serves as an approximation of the atomistic system for small deformations. A similar approach was used by Eringen [26] in the context of classical integral-type non-local elasticity.

Homogeneity of the force law is important to make analytical tools like continuous Fourier Transforms applicable. In contrast, the force law (3.14), that provided an exact match with the atomistic system, is typically solved with classical methods of molecular dynamics.

The behavior of a discrete system with given acoustic tensor $M_*(k)$ shall be approximated. Let the spacing of the particles be a, i.e., the width of the Brillouin zone is π/a. The acoustic tensor of the continuous medium is defined as

$$M(k) = \begin{cases} M_*(k) & 0 \leq k \leq \pi/a \\ M_*(\pi/a) & \pi/a < k \end{cases} \tag{4.1}$$

For a peridynamic continuum, (3.24) and (2.83) imply that

$$\bar{C}(k) = \begin{cases} M_*(\pi/a) - M_*(k) & 0 \le k \le \pi/a \\ 0 & \pi/a < k \end{cases}$$

and

$$C(\xi) = \frac{1}{\pi} \int_0^{\pi/a} dk \ \cos k\xi \ \left[M_*(\pi/a) - M_*(k) \right].$$

If the discrete system has a pair potential $\hat{\phi}$, then $M_*(k)$ is given by (3.22), and the peridynamic stiffness distribution reads

$$C_a(\xi) = \sum_{n=1}^{\infty} \left[S(n - \xi/a) + S(n + \xi/a) - 2\cos n\pi \ S(\xi/a) \right] \ \frac{1}{a^2} \frac{d^2\hat{\phi}}{dr^2}(na) \tag{4.2}$$

with

$$S(\alpha) = \frac{\sin \pi\alpha}{\pi\alpha}. \tag{4.3}$$

The *linear atomistic-peridynamic force law* is defined with (4.2) as

$$\hat{f}(r, \xi) = C_a(\xi)(r - \xi).$$

C_a has the property

$$C_a(ja) = \lim_{\xi \to ja} C(\xi) = \frac{1}{a^2} \frac{d^2\hat{\phi}}{dr^2}(ja) \qquad j = 1, 2, ..., \tag{4.4}$$

i.e., that the stiffness distribution assumes the value of the atomic stiffness distribution $\hat{\phi}''$ on lattice sites ja.

Figure 4-1 shows the corresponding peridynamic stiffness distribution and the second order derivative of ϕ_{LJ}, representing the stiffness of an atomic bond for a given distance. According to (4.4), they are the same on lattice sites. Off the lattice sites, the curves are very different, although they represent the stiffness of two systems that behave exactly the same (for $ka < \pi$), as shown by the dispersion relations.

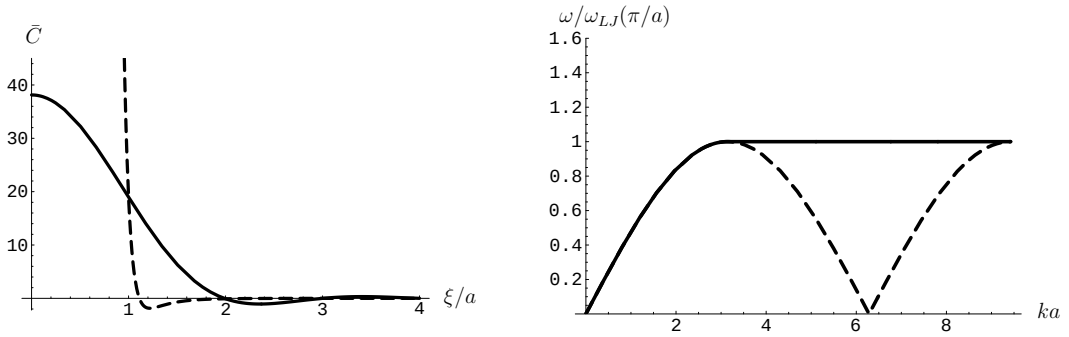

(a) (b)

Figure 4-1: Comparison of a peridynamic continuum (solid lines) and a discrete system (dashed line) with a Lennard-Jones 12-6 potential given by (3.21): (a) Stiffness distribution $\bar{C}(\bar{\xi}) = a^4 C_a(\xi)/\epsilon$ from (4.2) and the atomistic stiffness $\bar{\phi}''(\bar{\xi}) = a^2\hat{\phi}''(\xi)/\epsilon$. (b) Dispersion relations $\omega(k)/\omega_{LJ}(\pi/a)$.

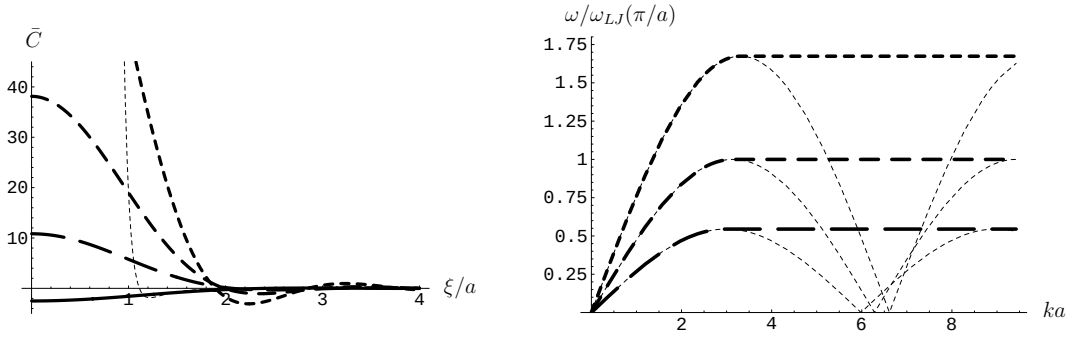

(a) (b)

Figure 4-2: Stiffness distributions and dispersion curves for $\lambda = 0.9,\ 1.0,\ 1.05,\ 1.2$ (length of dashes increases with λ): (a) $\bar{C}(\bar{\xi}) = a^4 C_a(\xi)/\epsilon$. (b) $\omega(k)/\omega_{LJ}(\pi/a)$. *Thick Lines:* Peridynamic continuum. *Thin Lines:* Discrete system with Lennard-Jones 12-6 potential given by (3.21).

4.2 General Atomistic-peridynamic Force Law

The derivation of a linear atomistic-peridynamic force law of section 4.1 can be extended to general (non-linear) behavior. Key idea is that rather than matching one dispersion relation in the reference configuration, the dispersion relations of the peridynamic continuum and the discrete system are required to be the same for all states of homogeneous deformations, denoted by the stretch value $\lambda = y'(x)$. Due to the non-linearity, the dispersion curves change with λ, as shown in figure 4-2. In particular, the acoustic tensor may assume negative values above a critical deformation, representing instability and the loss of cohesion.

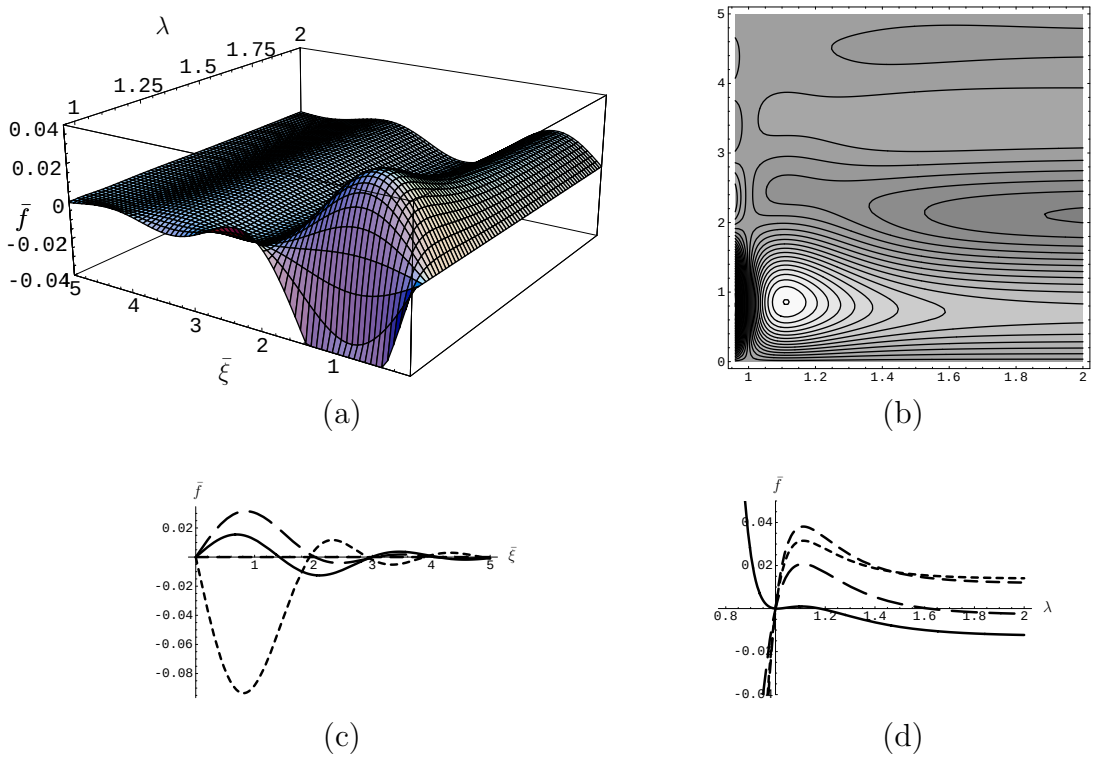

Figure 4-3: Atomistic-peridynamic force law $\bar{f}_a(\lambda, \bar{\xi})$. (c) $\lambda = 0.95,\ 1.0,\ 1.05,\ 2.0$. The length of dashes increases with λ. (d) $\bar{\xi} = 0.5,\ 1.0,\ 1.5,\ 2.0$. The length of dashes increases with $\bar{\xi}$. Note that the interval of λ in plots (a) and (b) is limited to $[0.9, 2]$.

With the definition of C_a in (4.2), the *general atomistic-peridynamic force law* for a homogeneous body is defined by

$$\frac{\partial \hat{f}_a}{\partial r}(r, \xi) = C_{\lambda a}(\xi)$$

where the reference distance[1] a was replaced by λa (with $\lambda = r/\xi$). Integration yields

$$\hat{f}_a(r, \xi) = \hat{f}_0(\xi) + \xi \int_1^{\lambda} d\tau\ C_{a\tau}(\xi), \tag{4.5}$$

where $\hat{f}_0$ is an arbitrary reference force which can be set to zero – or chosen to reproduce boundary effects of atomistic systems, as discussed by Charlotte and Truskinovsky [18]. With (4.2) and (4.3), the force law reads

[1]The reference configuration was defined as the state at which the chain is stress-free.

$$\hat{f}_a(r,\xi) = \sum_{n=1}^{\infty} \xi \int_1^{\lambda} d\tau \left\{ \left[S\left(n - \frac{\xi}{\tau a}\right) + S\left(n + \frac{\xi}{\tau a}\right) \right.\right. \\ \left.\left. -2\cos n\pi \; S\left(\frac{\xi}{\tau a}\right) \right] \; \frac{1}{\tau^2 a^2} \frac{d^2\hat{\phi}}{dr^2}(n\tau a) \right\}. \tag{4.6}$$

The force $\hat{f}_a$ is plotted in figure 4-3.

Several characteristic features of the purely atomistic force law shown in figure $3-1$ can be identified: upon compression, when $\lambda < 1$, the force becomes large and repulsive, shown as dark region in the contour plot of figure 4-3. Under extension, the force reaches a tensile maximum, shown as light regions in the contour plot of figure 4-3, and then decreases to zero. The decrease of the force is associated with a negative bond stiffness, shown in figure 4-2 for $\lambda = 1.2$.

In contrast to the purely atomistic force $\hat{f} = \partial\hat{\phi}/\partial r$, however, $\hat{f}_a$ lets some bonds attract each other under compression or repel each other under under extension. These forces can be thought of as compensation for the lack of discreteness in the peridynamic continuum.

The peridynamic model represents the underlying discrete system exactly if the stretch λ does not vary along the body. It is therefore an approximation of a non-linear discrete systems for $0 < |\lambda'(x)| \ll 1/a$.

In particular, bulk properties are exactly reproduced. The tangential Young's Modulus reads

$$E(\lambda) = \int_0^{\infty} d\xi \; C_{\lambda a}(\xi)\xi^2, \tag{4.7}$$

as the slopes of the dispersions curves of the discrete and the peridynamic medium match exactly. Furthermore, the stress reads with (4.5) and (4.7)

$$\hat{\sigma}_0(\lambda) = \int_0^{\infty} d\xi \; \hat{f}_a(r,\xi)\xi = \int_1^{\lambda} d\tau \; E(\tau).$$

The general atomistic-peridynamic force law makes peridynamic theory applicable to the analysis of micro-mechanic processes, like phase boundary propagation or dislocation motion. The major advantage is that standard analysis tools for homogeneous

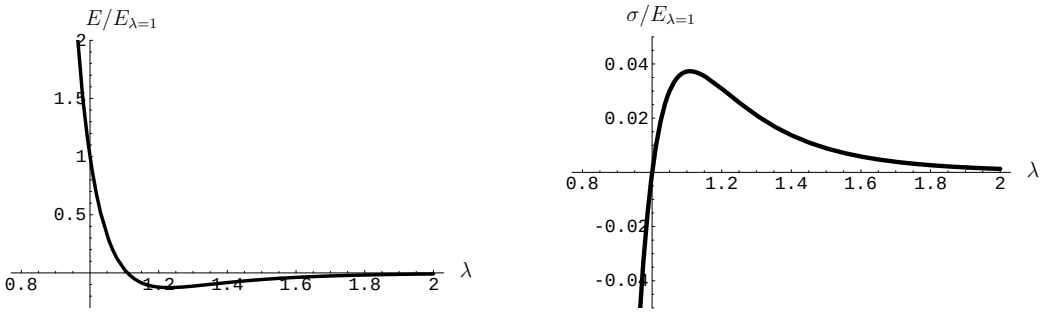

(a) (b)

Figure 4-4: Bulk properties of a peridynamic continuum with $\hat{f} = \hat{f}_a$, and the discrete system with a Lennard-Jones 12-6 potential given by (3.21): (a) Young's Modulus $E(\lambda)/E(\lambda = 1)$. (b) Stress $\sigma(\lambda)/E(\lambda = 1)$.

bodies like Fourier Transforms can be used. Due to the nonlinearities, however, this has to be combined with other assumptions or techniques, e.g., a perturbation approach for the small quantity $|u''(x)a|$.

Numerical simulations with Finite Elements also profit from the homogeneity of the peridynamic continuum. There are *no interfaces* between the macroscopic regions and the regions where atomistic details are considered.

4.3 Force Law for Heterogeneous Materials

Linear peridynamic theory can be used as a statistical model of heterogeneous media. A heterogeneous medium could be a metal consisting of grains, or concrete containing stiff aggregate pieces in a soft matrix, or a composite material. A statistical approach to elasticity of heterogeneous media that can be recast into peridynamic theory was presented by Kröner [47] and in more detail by Kunin [49]. For recent work in the context of elastic deformation of composite materials, see Drugan and Willis [24]. The essential ideas shall be summarized:

The body of interest consists of a heterogeneous linear elastic material that is macroscopically homogeneous and is in equilibrium. Locally, the body satisfies

$$\text{Div}\, \boldsymbol{\sigma}(\boldsymbol{x}) = \mathbf{0} \qquad \boldsymbol{\sigma}(\boldsymbol{x}) = \boldsymbol{\mathcal{C}}(\boldsymbol{x})\boldsymbol{\varepsilon}(\boldsymbol{x}) \tag{4.8}$$

where $\boldsymbol{\mathcal{C}}$ is the fourth order stiffness tensor representing the heterogeneity of the body through its dependence on $\boldsymbol{x}$. Rather than resolving $\boldsymbol{\sigma}$, $\boldsymbol{\mathcal{C}}$, and $\boldsymbol{\varepsilon}$ in detail, they are considered as random variables with an assigned distribution functions. The exact shapes of the distribution functions are not of importance, however, they help isolate the quantities that are relevant: the *average values* $\bar{\boldsymbol{\sigma}}$, $\bar{\boldsymbol{\mathcal{C}}}$ and $\bar{\boldsymbol{\varepsilon}}$, and the *correlation functions* of the random variable $\boldsymbol{\mathcal{C}}$.

The average or expectation values are the macroscopic quantities of primary interest. Average refers to *ensemble average*, this being a distribution weighted average of possible values of the random variable. The ensemble average is not to be confused with a volume average. Macroscopic homogeneity of the material properties means that the tensor $\bar{\boldsymbol{\mathcal{C}}}$ is constant.

The correlation functions of the random variable $\boldsymbol{c}$ represent its randomness and heterogeneity. They are by Kröner [47] referred to as functions in order to emphasize that their value depends on one or more locations $\boldsymbol{x}$. *Auto-correlation functions* only represent the distribution of a random variable at one location $\boldsymbol{x}$, whereas the *cross-correlation functions* expresses how the distribution of a random variable at point $\boldsymbol{x}$ may be related to another random variable at point $\boldsymbol{x}'$. Knowing all correlations of a random variable provides a complete statistical description, i.e., the exact distribution function. The first and second order correlation functions can be used as an approximation.

The problem statement in a statistical setting is: Find the average functions $\bar{\boldsymbol{\sigma}}(\boldsymbol{x})$ and $\bar{\boldsymbol{\varepsilon}}(\boldsymbol{x})$ that satisfy the average of (4.8). Following Kröner [47, pages 103–107], this is the case when sufficiently far away from the boundary

$$\operatorname{div} \bar{\boldsymbol{\sigma}}(\boldsymbol{x}) = \boldsymbol{0} \qquad \bar{\boldsymbol{\sigma}}(\boldsymbol{x}) = \bar{\boldsymbol{\mathcal{C}}}\, \bar{\boldsymbol{\varepsilon}}(\boldsymbol{x}) + \int_{\Omega} dV'\, \boldsymbol{c}(\boldsymbol{x} - \boldsymbol{x}')\, \bar{\boldsymbol{\varepsilon}}(\boldsymbol{x}'). \tag{4.9}$$

The forth-order tensor $\boldsymbol{c}$ is the non-local kernel of the integral equation. $\boldsymbol{c}$ contains correlation functions of the stiffness tensor $\boldsymbol{\mathcal{C}}$ and is therefore the measure of heterogeneity or randomness of variation of material properties. The range of $\boldsymbol{c}$ is on the order of the *correlation length* l_c, a length scale that can be derived from the joint dis-

tribution functions of several values of $\boldsymbol{\mathcal{C}}$ at different locations. The correlation length offers an important physical explanation: if the distance between two points $\boldsymbol{x}_1$ and $\boldsymbol{x}_2$ is less that l, their elastic properties are statistically connected. If the separation between $\boldsymbol{x}_1$ and $\boldsymbol{x}_2$ is sufficiently larger than l, the effective stiffness values at these locations are independent. Consider for example the case when l_c represents the size of a grain: two particles within the same grain share elastic properties, in particular the spatial orientation of their anisotropic environment. Two particles from different grains, however, have constitutive properties that are not necessarily related and may have for example environments with different spatial orientation.

Another insight provides the notion of *perfect disorder*: perfect disorder is the state in which stiffness properties are statistically independent everywhere. This is the case when the correlation length $l_c \to 0$. From a macroscopic point of view, the material becomes local.

The most important difference between (4.9) and peridynamic theory is the presence of a local stiffness term $\bar{\boldsymbol{\mathcal{C}}}$ that survived the averaging process. Local stiffness cannot be provided in the peridynamic framework. However, as local stiffness is a modeling abstraction for the action of atomic short range forces, these forces can be represented in peridynamic theory by letting

$$\bar{\boldsymbol{\sigma}}(\boldsymbol{x}) = \int_{\Omega} dV' \ \left(\bar{\boldsymbol{\mathcal{C}}}\, d_a(|\boldsymbol{x}' - \boldsymbol{x}|) + \ \boldsymbol{c}(\boldsymbol{x} - \boldsymbol{x}')\right) \ \bar{\boldsymbol{\varepsilon}}(\boldsymbol{x}'), \tag{4.10}$$

where d_a is a function that approaches a three dimensional Dirac delta function distribution for $a \to 0$, see appendix B. The result is a continuum with *two internal lengths*: the correlation length of macroscopic heterogeneities l_c, and the atomic length a, with $a \ll l_c$.

Using the results of section 3.2.3, a heterogeneous material with constitutive relation (4.10) can be represented by a peridynamic continuum, with these two internal lengths (provided that $\nu = 1/4$). In this context, the peridynamic model can be seen as *theory of ensemble averages*.

Applications of the non-local approach (4.9) are not limited to elastic deformation.

Material models with strain softening require constitutive relations with an internal length. Certain heterogeneous materials, like concrete, undergo distributed cracking with a macroscopically large fracture process zone. The size of this zone is measured by the internal length.

Early extensions of non-local integral-type theories to inelastic deformation resulted in the definition of an "imbricate continuum" with "broad-range stresses", see Bažant [10], where all quantities, the stress and the internal damage variables are non-local integral-type averages. The non-local continuum was later refined to a model, where, for computational efficiency, *only those quantities that are responsible for failure are non-local*, see Pijaudier-Cabot and Bažant [56]. This philosophy is fundamentally different from the peridynamic approach where all quantities are non-local to avoid special treatment of defects. Jirásek and Marfia [44] also proposed a model that, like in peridynamic theory, models the evolution of damage as driven by the displacement field. However, the elastic response of the material is still local. For a recent survey of non-local integral-type theories applied to plasticity and damage of heterogeneous materials, see Bažant and Jirásek [12].

4.4 Force Law with Resolution Length

Only certain features of a microstructure are important for the macroscopic behavior of a body. Therefore, as expressed by Ruiz et al. [60], the microstructure may be "buried" in a (macroscopic) constitutive relation. This is typically done by eliminating internal lengths from constitutive relations, like in local theories.

However, not having an internal length may make a model unphysical on the macroscale. This is the case when crack propagation is modeled in local theories without an additional constitutive law for the crack tip, that adds an internal length.

Peridynamic theory was designed to avoid special treatment of microstructural details like crack tips. This is possible, because the force law contains an internal length. The internal length can be chosen to be small in order to model micromechanical details more accurately than classical local theory does. For the purpose of

numerical simulations, however, where the fine spatial resolutions of microscopic details is expensive, it is advantageous to provide a constitutive model with an internal length l that is *not* microscopically small, but rather on the order of the distance of discretization points (see section 5.3.2), i.e.,

$$a \ll l \ll L \qquad a \sim 10^{-10}m \qquad L \sim 1m,$$

where L represents the macroscopic dimensions of the body of interest. The key idea of a *peridynamic force law with resolution length* is to equip a continuum with an internal length l_r that can be made much larger than the characteristic length of the microstructure (e.g., the atomic length a) such that numerical simulations are less expensive. At the same time, certain macroscopic properties have to be correctly reproduced. This always includes Young's Modulus and poses a restriction on $C = \partial\hat{f}/\partial r$ in the reference configuration[2]. In the context of fracture, the energy that is necessary to form a new surface has to be correctly reproduced, see chapter 6.

Having an internal length larger than the internal length of the microstructure eliminates the ability to simulate its details. However, important advantages are preserved: first, the continuum has a well-defined surface energy that is embedded in the constitutive relation (which is not the case for local theories). Second, the resolution length is still small compared to a characteristic macroscopic length, therefore, this approach reproduces bulk behavior correctly. Third and most importantly, the theory is still applicable on and off defects.

The force law with resolution length has multi-scale properties: If the resolution length is $l_r = a$, the microstructure is represented in the sense of sections 4.1 and 4.2. If $l_r > a$, the simulation results have to be looked at with a coarse view. It is true for both cases, $l_r > a$ and $l_r = a$, that *phenomena with a characteristic length smaller than l_r have no physical meaning.*

Considering (4.13), it is clear that a large resolution length l will make the width of the Brillouin zone small and, thus, decrease phase speeds of waves with wave

[2]Depending the dimensions and the deformation of the body, either (2.71), (2.93), (2.95), (2.97) or (2.99) have to be satisfied.

lengths smaller than $2l$ significantly. Small Brillouin zones are typical in numerical simulations of macroscopic mechanical bodies.

Furthermore, the stiffness of modes with wave number outside the Brillouin zone is decreased and, therefore, the resistance against the formation of (elastic) discontinuities becomes smaller.

The force law with resolution length and the force law for heterogeneous materials that results from (4.10) may both have interaction lengths of macroscopic order, i.e., several orders of magnitude larger than atomistic lengths. The latter, however, has an additional small internal length, associated with the distance of atoms.

4.5 Definition of the Elastic Internal Length

The structure of (3.1) expresses how a given pair-wise force law scales with the internal length. Upon doubling l and keeping E, λ and $\bar{\xi}$ fixed, the force changes by a factor of $1/2^{n+1}$, where n is the dimension of Ω. It does not, however, provide information about how two different force laws $\bar{f}_1$ and $\bar{f}_2$ compare for the same internal length. In this section, the length scale is fixed, and then interpreted in section 4.6.

The internal length shall represent the interaction range of forces. The spatial distribution of interaction forces may be characterized for small deformations by the stiffness distribution and its associated *stiffness moments*,

$$M_j = \int_0^\infty d\xi \; C(\xi) \frac{\xi^j}{j!}. \tag{4.11}$$

The internal length l associated with elastic deformation is then defined for one-dimensional bodies as

$$l = 2\sqrt{\frac{M_2}{M_0}}. \tag{4.12}$$

For two- and three-dimensional body, equation (4.12) is applied to moments of the one-dimensional stiffness distribution that is derived from the higher dimensional stiffness distribution for one-dimensional plane-strain deformation. For the conversion formulae of stiffness moments see the sections on plane deformation 2.8.6 and one-

1d	$l = \sqrt{4M_2/M_0}$
1d anti-plane shear	$l = \sqrt{12M_2/M_0}$
2d plane-strain	$l = \sqrt{9M_3/M_1}$
2d anti-plane shear	$l = \sqrt{18M_3/M_1}$
3d	$l = \sqrt{\frac{72}{5}M_4/M_2}$

Table 4.1: Definitions of elastic internal lengths

dimensional plane deformations 2.8.7. The definitions of the respective lengths are listed in table 4.1. A list of stiffness distributions with explicit dependence on l is given in the appendix C.

4.6 Interpretations of Internal Lengths

Elastic Internal Lengths.

1. The elastic internal length l is the *radius of inertia of the stiffness distribution* C.

2. l can be interpreted as *particle distance* a in a discrete system with similar behavior. To see this, consider a linear atomistic-peridynamic force law with associated stiffness distribution (4.2). The stiffness moments read

$$2M_0 = M(\infty) = M_*(\pi/a) = \sum_{n=1}^{\infty} 2(1-\cos n\pi)\frac{1}{a}\frac{d^2\hat{\phi}}{dr^2}(na) \approx \frac{4}{a}\frac{d^2\hat{\phi}}{dr^2}(a)$$

and

$$2M_2 = E = \sum_{n=1}^{\infty} n^2 a \frac{d^2\hat{\phi}}{dr^2}(na) \approx a\frac{d^2\hat{\phi}}{dr^2}(a),$$

thus, the internal length is in good approximation $l \approx a$.

3. Another meaning for l can be found by making use of $\omega'(0) = \sqrt{E/\rho_0}$, expression (4.1) and $\omega_\infty \approx \omega_{max}$:

$$l \approx \frac{\omega_{max}}{\omega'(0)}. \tag{4.13}$$

Therefore, if two force laws have the same internal length l, they have approximately the same limit on frequencies of waves which can propagate. The

quantity π/l may therefore be seen as the *width of a peridynamic Brillouin zone*.

4. l may be the *correlation length* l_c of a statistical heterogeneous material, see section 4.3.

5. l can be interpreted as a *resolution length* l_r as explained in detail in section 4.4.

6. In addition, the internal length l is a measure of the material's *compliance to form discontinuities* as shown in section 5.2.

Inelastic Internal Lengths.

1. A peridynamic force law with link failure, as defined in section 6.2, has a strength limit that depends on the choice of the internal length and the surface energy. $l/2$ is approximately the length of the flaw in an infinite body (in local theory) that has the same strength limit as a peridynamic body with the force law defined in section 6.2.

2. Finally, if l is the characteristic length in a failure process, then, noting that failure occurs in peridynamic theory as failure of bonds, the internal length l is a measure of the *size of the fracture process zone*, described in Fineberg and Marder [30].

4.7 Interpretation of Displacement Discontinuities

A peridynamic continuum does not provide local stiffness. This leads to the formation of discontinuities in the presence of discontinuous force fields as shown in section 3.3.7. Displacements discontinuities may also appear at interfaces of regions with prescribed displacements Ω_u as explained in section 2.5.3 or computed in section 5.2.3. Certain displacement discontinuities have to be interpreted in a non-conventional way for two reasons:

First, unlike in classical continuum theory, a displacement discontinuity does not signify a loss of material cohesion. Due to the long-range character of non-local interaction forces, a body may keep its strength even in the presence of a gap.

Second, displacement fields carry information that may not be physically meaningful, e.g., a displacement discontinuity. The physically meaningful information of a displacement function is completely contained in the Brillouin zone of its Fourier Transform. The magnitude of a discontinuity, however, is included in its Fourier Transform at infinity.

4.8 Application of Boundary Conditions

Displacement discontinuities may affect the deformation of the entire body. This is the case, for example, if boundary regions are deformed such that the formation of a displacement discontinuity relaxes the rest of the body[3]. If the the internal length is a physical quantity like the atomistic length a, this effect is part of the physically justified response of the system. However, if l is a resolution length without a physical meaning, discontinuities at interfaces have to be avoided. As resolution lengths are typically large, the compliance to form discontinuities is high. This makes it even more important that boundary conditions are applied appropriately: the region Ω_u (where displacements are prescribed) has to have a width of at least l. And ideally, the deformation gradient on Ω_u is close to the expected deformation gradient on the other side of the interface.

4.9 Interpretation of a Peridynamic Continuum

The nature of a peridynamic continuum is best understood by the action of its forces: with an internal length *on the atomistic scale*, the force law may be chosen such that the peridynamic continuum reproduces the behavior of an atomistic system, as described in section 4.1 and 4.2. The continuum can then be thought of as a result of smearing, i.e., homogeneously distributing, atoms over the reference configuration. An atom is represented by an infinity of peridynamic continuum particles. Continuum

[3]Imagine a bar that is pulled apart on both ends. If the region where displacements are prescribed is smaller than the internal length, large displacement discontinuities form at the interfaces as shown in section 5.2.4 and the middle region relaxes.

particles, in the sense of Truesdell and Noll [69], are by definition, infinitesimally small in terms of mass and volume, and, thus, smaller than an atom or any other finite part of the body. The force between two atoms is represented by a volume integral of peridynamic forces.

With an internal length *on the macroscopic scale*, a peridynamic force acts between distant clusters of material. Then, the peridynamic force may have two different meanings:

First, the clusters may be part of a heterogeneous compound, e.g., aggregate piece in concrete, or a grain in metal. In the homogenized continuum, long-range forces let the clusters interact, as described in section 4.3. The peridynamic theory then becomes a theory of ensemble averages, and its forces can be understood as generalized forces associated with the stochastic correlation length of material properties.

Second, for homogeneous materials, the length scale is made large for approximation purposes. In this case, peridynamic forces represent diffusely distributed material interaction. The length is is not a physical parameter, but rather a resolution length of the model. If the resolution length is large, only bulk properties are correctly reproduced. If it is reduced to the internal length of the underlying microstructure, it captures microstructural details.

In summary, the peridynamic continuum is a pure modeling concept. Peridynamic forces have no direct analogue in classical physics and can only be defined by their effective behavior.

Chapter 5

Solution Techniques

5.1 Introduction

In peridynamic theory, exact analytical solutions or solution methods are only known for certain classes of problems:

1. Problems for one-dimensional infinitely large bodies with an arbitrary linear elastic force law. For static solutions see Silling et al. [64], for dynamic solutions see Weckner and Abeyaratne [72]. Solutions are obtained by Fourier Transforms. Extensions to two- and three-dimensional bodies are possible.

2. Problems for one-dimensional infinitely large bodies with a particular non-linear force law. Static and steady-state solutions are obtained by making kinematic assumptions and turning the non-linear problem into a linear problem.

3. Problems for one-dimensional finite bodies and a linear-elastic force law with special stiffness distributions, e.g., the *Lalesco-Piccard*-type kernel, as given in Tricomi [67, page 162].

4. Kunin [48, page 66] suggests an analytical method that is applicable to one-dimensional semi-infinite bodies (with one boundary) with arbitrary linear elastic force law. The method is based on the *Wiener-Hopf Technique* that can be used to solve linear integral equations with a difference kernel on a semi-infinite

domain. The method is not convenient and may be too difficult to use in two or three dimensions.

The solutions to most problems may only be approximated. Non-numerical approximation techniques for integral equations are scarce and cumbersome. Some are described in Tricomi [67], e.g., the classical *Neumann iteration*. However, the resulting series converges either very slowly, or it does not converge at all for the problems of interest.

A perturbation-type method for peridynamic problems is presented in section 5.2. It is applied to a finite body with an arbitrary linear elastic force law. Extensions to non-linear problems are possible. Numerical approximation is possible by the collocation or the Ritz method. Both are presented in section 5.3.

5.2 Perturbation-type Analysis

5.2.1 Problem

In this section, the deformation of a one-dimensional linear elastic peridynamic body is analyzed. Special focus lies on displacement discontinuities which emerge at interfaces between regions with prescribed displacements Ω_u and the rest of the body Ω_b. A method is presented that describes the discontinuities correctly. It does not resolve, however, fine boundary layer deformations, that usually decay exponentially fast.

Consider a one-dimensional non-local bar occupying the region $\Omega = [-L, L]$. A body force $b(x) = b_*(x)$ is applied to the bar on $\Omega_b = [-L, 0]$, the displacement is prescribed as $u(x) = u_*(x)$ on $\Omega_u = (0, L]$ (see also figure 5-1). The material is assumed to be linear elastic, thus the pair-wise interaction force reads

$$\hat{f}(r, \xi) = C(\xi)(r - \xi). \tag{5.1}$$

where $C = \partial \hat{f} / \partial r$ is the one-dimensional stiffness distribution with an internal

length l. From (2.73) and (3.1) follows that $C(\xi)$ satisfies

$$C(\xi) = \frac{E}{l^3}\bar{C}(\frac{\xi}{l}) \qquad C(\xi) = C(-\xi) \qquad \int_0^\infty C(\xi)\xi^2 d\xi = E. \tag{5.2}$$

Further assume that $C(\xi) \to 0$ sufficiently fast as $|\xi| \to \infty$.

Assume that the external body force b_* is at least N-times differentiable on Ω_b and that u_* is sufficiently differentiable at $x = 0+$. With the known functions u_* and b_* the problem statement reads: Find $u(x)$ on $\Omega_b = [-L, 0]$ such that

$$\left.\begin{array}{ll} -L \le x \le 0: & \int_{-L}^{L} dx'\, C(x'-x)[u(x') - u(x)] + b_*(x) = 0 \\ 0 < x \le L: & u(x) = u_*(x) \end{array}\right\}. \tag{5.3}$$

Length Scales. Non-dimensional quantities are introduced,

$$\bar{x} = x/L \qquad \lambda = l/L \qquad \bar{u}(\bar{x}) = u(x)/L \qquad \bar{b}^* = \frac{L}{E} b_*(x),$$

representing the magnitude of quantities measured on the *macroscopic length scale*. For the following analysis, they will be used exclusively and the bars are dropped for conciseness. The problem statement reads in non-dimensional form

$$\left.\begin{array}{ll} -1 \le x \le 0: & \frac{1}{\lambda}\int_{-1}^{1} dx'\, C(\frac{x'-x}{\lambda})[u(x') - u(x)] + \lambda^2 b_*(x) = 0 \\ 0 < x \le 1: & u(x) = u_*(x) \end{array}\right\} \tag{5.4}$$

The integral sums up forces exerted on particles x by particles x' from the region of prescribed external force load ($-1 \le x \le 0$) and the region of prescribed displacements ($0 < x \le 1$). Splitting the interaction integral and putting all the known functions on the right hand side yields

$$\left[\int_{-1}^{1} C(\frac{x'-x}{\lambda})\frac{dx'}{\lambda}\right] u(x) - \int_{-1}^{0} C(\frac{x'-x}{\lambda})u(x')\frac{dx'}{\lambda}$$
$$= \lambda^2 b_*(x) + \int_0^1 C(\frac{x'-x}{\lambda})u_*(x')\frac{dx'}{\lambda} \tag{5.5}$$

which has to hold for $-1 \leq x \leq 0$. The structure of the integral equation motivates the definition of two *boundary length scales*, for the right and the left boundary:

$$y = \frac{1+x}{\lambda} \qquad z = \frac{x}{\lambda}.$$

In addition, the corresponding displacement fields v and u are defined as

$$v(y) = v(\frac{1+x}{\lambda}) = u(x) \qquad w(z) = w(\frac{x}{\lambda}) = u(x)$$

The equilibrium condition expressed with respect to y reads

$$\left[\int_0^{\frac{2}{\lambda}} C(y'-y)dy'\right] v(y) - \int_0^{\frac{1}{\lambda}} C(y'-y)v(y')dy' = \lambda^2 b_*(-1+\lambda y) + \int_{\frac{1}{\lambda}}^{\frac{2}{\lambda}} C(y'-y)u_*(-1+\lambda y')dy' \qquad (5.6)$$

and for z

$$\left[\int_{-\frac{1}{\lambda}}^{\frac{1}{\lambda}} C(z'-z)dz'\right] w(z) - \int_{-\frac{1}{\lambda}}^{0} C(z'-z)w(z')dz' = \lambda^2 b_*(\lambda z) + \int_0^{\frac{1}{\lambda}} C(z'-z)u_*(\lambda z')dz'. \qquad (5.7)$$

All three equilibrium conditions (5.5), (5.6) and (5.7) are equivalent for $\lambda > 0$. However, they will be different in the limit when $\lambda \to 0$.

5.2.2 Approximation Method

Approximation techniques should make use of the fact that λ is small. The obvious approach, Taylor-expanding the kernel in (5.5) with respect to λ and then setting $u = u_0 + \lambda u_1 + \lambda^2 u_2 + ...$ is not sufficient. The stiffness distributions are often not analytic for $\lambda = 0$ and therefore not Taylor-expandable. And even if they are, this approach only gives another set of Fredholm-type integral equations, one for each function u_k, and does not simplify the problem. Therefore, additional simplifications

have to be made.

From an Integral Equation to an ODE of infinite order. Using the expansion

$$u(x') = u(x) + u'(x)(x'-x) + u''(x)\frac{(x'-x)^2}{2!} + ... \tag{5.8}$$

and the definitions of the *stiffness functions* C_k^b and C_k^u

$$\begin{aligned} N_k(s) &= \int_0^s C(\zeta)\frac{\zeta^k}{k!}d\zeta \\ C_k^b(x,\lambda) &= N_k(\frac{-x}{\lambda}) - N_k(\frac{-1-x}{\lambda}) \qquad (5.9) \\ C_k^u(x,\lambda) &= N_k(\frac{1-x}{\lambda}) - N_k(\frac{-x}{\lambda}) \qquad (5.10) \end{aligned}$$

the equilibrium condition can be expressed on the respective length scale as

$$\begin{aligned} C_0^u(x,\lambda)u(x) - \sum_{k=1}^{\infty}\lambda^k C_k^b(x,\lambda)u^{(k)}(x) & \\ = \lambda^2 b_*(x) + \int_0^1 C(\frac{x'-x}{\lambda})u_*(x')\frac{dx'}{\lambda} & \qquad (5.11) \\ C_0^u(-1+\lambda y,\lambda)v(y) - \sum_{k=1}^{\infty} C_k^b(-1+\lambda y,\lambda)v^{(k)}(y) & \\ = \lambda^2 b_*(-1+\lambda y) + \int_{\frac{1}{\lambda}}^{\frac{2}{\lambda}} C(y'-y)u_*(-1+\lambda y')dy' & \qquad (5.12) \\ C_0^u(\lambda z,\lambda)w(z) - \sum_{k=1}^{\infty} C_k^b(\lambda z,\lambda)w^{(k)}(z) & \\ = \lambda^2 b_*(\lambda z) + \int_0^{\frac{1}{\lambda}} C(z'-z)u_*(\lambda z')dz'. & \qquad (5.13) \end{aligned}$$

If the expansion is valid (requiring u to be sufficiently smooth), and integration and summation can be exchanged, then each of these equations are equivalent to the integral-type equilibrium condition.

Interior and Boundary Regions. Depending on the location, either λ, y or z are small and dominate the character of the solution. In the interior, λ is the dominating

small quantity; close to boundaries, however, y and z approach zero and for any $\lambda > 0$, there will be region for which $|y| < \lambda$ or $|z| < \lambda$ and λ does not dominate. The *left boundary region* is defined as $\{x| -1 < x < -1 + \lambda\}$, the *interior region* as $\{x| -1 + \lambda < x < -\lambda\}$ and the *right boundary region* as $\{x| -\lambda < x < 0\}$.

Comment on Wiener-Hopf Technique for Boundary Regions. A zero-th order solution is obtained by letting $\lambda \to 0$. Equations (5.6) and (5.7) turn into integral equations with difference kernels, defined on semi-infinite domains. They can be solved by applying the Wiener-Hopf technique[1]. Higher order solutions are obtained by appropriate iteration. This technique resolves the fine structure of boundary layers, however, a different and simpler approach is used here. It ignores details of boundary layers, but approximates nevertheless the interface discontinuities and deformation energies sufficiently well.

Reducing the Order of Equilibrium Condition in Differential Form. With decreasing λ, the stiffness distribution localizes. Thus, as a good approximation, higher order terms in the expansion (5.8) of $u(x')$ can be neglected. For further analysis, whenever the equilibrium condition is used in differential form, only terms up to order N are considered:

$$C_0^u(x,\lambda)u(x) - \sum_{k=1}^{N} \lambda^k C_k^b(x,\lambda)u^{(k)}(x) = \lambda^2 b_*(x) + \int_0^1 C(\frac{x'-x}{\lambda})u_*(x')\frac{dx'}{\lambda} \qquad (5.14)$$

The equations (5.12) and (5.13) are truncated in the same manner. N is the *order of integral approximation.*

Note that $N \geq 2$ is necessary for the reduced ODE to satisfy the boundary and interface conditions that will occur.

[1]The Wiener-Hopf technique was applied to the resolution of similar boundary layers in the context of fluid mechanics by Choi et al. [20].

Approximation of Stiffness Functions. The expressions (5.9) and (5.10) are rewritten in terms of y and z,

$$\begin{aligned} C_k^b(-1+\lambda y,\lambda) &= N_k(\frac{1}{\lambda}-y)-N_k(-y) \\ C_k^u(-1+\lambda y,\lambda) &= N_k(\frac{2}{\lambda}-y)-N_k(\frac{1}{\lambda}-y) \end{aligned}$$

and

$$\begin{aligned} C_k^b(\lambda z,\lambda) &= N_k(-z)-N_k(-\frac{1}{\lambda}-z) \\ C_k^u(\lambda z,\lambda) &= N_k(\frac{1}{\lambda}-z)-N_k(-z). \end{aligned}$$

The functions N_k can be approximated for small and large arguments. Assume that

$$\lim_{\zeta\to 0} C^{(A)}(\zeta)\zeta = 0 \qquad \lim_{\zeta\to\infty} C^{(A)}(\zeta)\zeta^{2M+1} = 0 \qquad \forall A = 0,1,2,..,M$$

The latter can be easily satisfied by requiring that C is strictly zero beyond some critical value of ζ. This critical value is a *horizon*. These restrictions can be relaxed, however, then the algebra becomes more complicated.

The approximations of N_k are defined as Taylor-expansions for small and for large s:

$$\begin{aligned} |s|<1: \qquad & N_k(s) = N_k^{small}(s) + o(s^{M+1}) \\ & N_k^{small}(s) = \sum_{B=k}^{M} \binom{B}{k} \frac{s^{B+1}}{(B+1)!} C^{(B-k)}(0) \\ |s|\geq 1: \qquad & N_k(s) \approx N_k^{big}(s) \\ & N_k^{big} = \left(\frac{s}{|s|}\right)^k N_k \end{aligned} \tag{5.15}$$

with

$$N_k = N_k(\infty) = \int_0^\infty C(\zeta)\frac{\zeta^k}{k!}d\zeta.$$

The $\approx$-sign in (5.15) accounts for the fact that $N_k(\frac{1}{\varepsilon})$ is not analytic in ε at $\varepsilon = 0$. If

this is the case, $N_k(\zeta)$ cannot be approximated arbitrarily well for large ζ by increasing the expansion order M.

The different length scales were introduced to distinguish between the quantities that are small and dominate. On the *left boundary region*

$$-1 < x < -1 + \lambda \quad \Rightarrow \quad 0 < y < 1$$

the approximations for the stiffness functions read

$$\begin{aligned} C_k^b(-1+\lambda y, \lambda) &\approx C_{k,y}^b(y) = N_k^{big}(\frac{1}{\lambda} - y) - N_k^{small}(-y) \\ C_k^u(-1+\lambda y, \lambda) &\approx C_{k,y}^u(y) = N_k^{big}(\frac{2}{\lambda} - y) - N_k^{big}(\frac{1}{\lambda} - y) \end{aligned}$$

in particular

$$\begin{aligned} C_{0,y}^b(y) &= +N_0 + yC(0) + \frac{y^3}{6}C''(0) + \frac{y^5}{120}C^{(4)}(0) + ... \\ C_{1,y}^b(y) &= +N_1 - \frac{y^2}{2}C(0) - \frac{y^4}{8}C''(0) + ... \\ C_{2,y}^b(y) &= +N_2 + \frac{y^3}{6}C(0) + \frac{y^5}{20}C''(0) + ... \\ &... \\ C_{k,y}^u(y) &= 0 \qquad \forall k \end{aligned}$$

on the *interior region*

$$-1 + \lambda < x < -\lambda$$

$$\begin{aligned} C_k^b(x, \lambda) &\approx C_{k,x}^b(x) = N_k^{big}(-\frac{x}{\lambda}) - N_k^{big}(\frac{-1-x}{\lambda}) \\ C_k^u(x, \lambda) &\approx C_{k,x}^u(x) = N_k^{big}(\frac{1-x}{\lambda}) - N_k^{big}(-\frac{x}{\lambda}) \end{aligned}$$

in particular

$$\begin{aligned} C^b_{k,x}(x) &= \begin{cases} 2N_k & k=0,2,4,... \\ 0 & k=1,3,5,... \end{cases} \\ C^u_{k,x}(x) &= 0 \qquad\qquad \forall k \end{aligned}$$

and on the *right boundary region*

$$-\lambda < x < 0 \quad \Rightarrow \quad -1 < z < 0$$

$$\begin{aligned} C^b_k(\lambda z, \lambda) &\approx C^b_{k,z}(z) = N^{small}_k(-z) - N^{big}_k(-\frac{1}{\lambda} - z) \\ C^u_k(\lambda z, \lambda) &\approx C^u_{k,z}(z) = N^{big}_k(\frac{1}{\lambda} - z) - N^{small}_k(-z). \end{aligned}$$

in particular

$$\begin{aligned} C^b_{0,z}(z) &= +N_0 - zC(0) - \frac{z^3}{6}C''(0) - \frac{z^5}{120}C^{(4)}(0) + ... \\ C^b_{1,z}(z) &= -N_1 + \frac{z^2}{2}C(0) + \frac{z^4}{8}C''(0) + ... \\ C^b_{2,z}(z) &= +N_2 - \frac{z^3}{6}C(0) - \frac{z^5}{20}C''(0) + ... \\ &... \\ C^u_{0,z}(z) &= +N_0 + zC(0) + \frac{z^3}{6}C''(0) + \frac{z^5}{120}C^{(4)}(0) + ... \\ C^u_{1,z}(z) &= +N_1 - \frac{z^2}{2}C(0) - \frac{z^4}{8}C''(0) + ... \\ C^u_{2,z}(z) &= +N_2 + \frac{z^3}{6}C(0) + \frac{z^5}{20}C''(0) + ... \\ &... \end{aligned}$$

Left Hand Side of (5.14)**.** Let on the free region of the body $-1 < x < 0$,

$$u(x) = u_0(x) + \lambda u_1(x) + \lambda^2 u_2(x) + ..., \tag{5.16}$$

then the left hand side of the reduced ODE (5.14) can be rewritten as

$$\begin{aligned} C_0^u u_0 &+ \lambda \left[C_0^u u_1 - C_1^b u_0'\right] \\ &+ \lambda^2 \left[C_0^u u_2 - C_1^b u_1' - C_2^b u_0''\right] \\ &+ \lambda^3 \left[C_0^u u_3 - C_1^b u_2' - C_2^b u_1'' - C_3^b u_0'''\right] \\ &\quad ... \end{aligned}$$

Right Hand Side of (5.14)**.** The integral in the right hand side of the equilibrium condition (5.14) can be expanded in λ or x using the previously defined stiffness functions $C_k^u(x,\lambda)$. First, the prescribed displacements u_* are approximated as

$$u_*(x) = u_*(0) + x u_*'(0) + \frac{x^2}{2} u_*''(0) + ... \tag{5.17}$$

then

$$\begin{aligned} \int_0^1 C(\frac{x'-x}{\lambda}) u_*(x') \frac{dx'}{\lambda} &\approx \lambda^2 b_*(x) + \sum_{A=0}^{M} \lambda^A C_A^u(x,\lambda) \sum_{B=A}^{M} \frac{x^{B-A}}{(B-A)!} u_*^{(B)}(0) \\ &= C_0^u(x,\lambda)\left[u_*(0) + x u_*'(0) + ...\right] \\ &\quad + \lambda\, C_1^u(x,\lambda)\left[u_*'(0) + x u_*''(0) + ...\right] \\ &\quad + \lambda^2\, b_*(x) + \lambda^2\, C_2^u(x,\lambda)\left[u_*''(0) + x u_*'''(0) + ...\right] \\ &\quad + ... \end{aligned}$$

Construction of Approximate Solution. An approximate solution of the form (5.16) is obtained by requiring that coefficients of λ vanish in the equilibrium condition. A hierarchy of ODEs is obtained:

$$\begin{aligned} C_0^u(x,\lambda) u_0(x) &= C_0^u(x,\lambda)\left[u_*(0) + x u_*'(0) + ...\right] \\ C_0^u(x,\lambda) u_1(x) - C_1^b(x,\lambda) u_0'(x) &= C_1^u(x,\lambda)\left[u_*'(0) + x u_*''(0) + ...\right] \\ C_0^u(x,\lambda) u_2(x) - C_1^b(x,\lambda) u_1'(x) - C_2^b(x,\lambda) u_0''(x) &= b_*(x) + C_2^u(x,\lambda)\left[u_*''(0) + x u_*'''(0) + ...\right] \\ &\quad ... \end{aligned}$$

The stiffness functions are approximated by setting λ to zero. This is equivalent to neglecting terms that are of order $e^{-1/\lambda}$. Letting $\lambda \to 0$ has to be done separately for the left boundary, the interior region and the right boundary. The resulting expressions on the boundaries are *boundary conditions* in the classical sense for the the functions u_k. On the left boundary at $x = -1$:

$$\begin{aligned} 0 &= 0 \\ u_0'(-1) &= 0 \\ N_1 u_1'(-1) - N_2 u_0''(-1) &= 0 \\ &\ldots \end{aligned}$$

On the interior region $-1 < x < 0$:

$$\begin{aligned} 0 &= 0 \\ 0 &= 0 \\ -2N_2 u_0''(x) &= b_*(x) \\ -2N_2 u_1''(x) &= 0 \\ -2N_2 u_2''(x) - N_4 u_0'''(x) &= 0 \\ &\ldots \end{aligned}$$

On the right boundary $x = 0$:

$$\begin{aligned} u_0(0) &= u_*(0) \\ N_0 u_1(0) + N_1 u_0'(0) &= N_1 u_*'(0) \\ N_0 u_2(0) + N_1 u_1'(0) - N_2 u_0''(0) &= b_*(0) + N_2 u_*''(0) \\ &\ldots \end{aligned}$$

Each function u_k of the perturbation solution is the solution to a well-posed boundary-value problem. For u_0

$$\left.\begin{aligned} 2N_2 u_0''(x) + b_*(x) &= 0 \\ u_0'(-1) &= 0 \\ u_0(0) &= u_*(0) \end{aligned}\right\}, \tag{5.18}$$

for u_1

$$\left.\begin{aligned} u_1''(x) &= 0 \\ u_1'(-1) &= \tfrac{N_2}{N_1} u_0''(-1) \\ u_1(0) &= \tfrac{N_1}{N_0}(u_*'(0) - u_0'(0)) \end{aligned}\right\}, \tag{5.19}$$

and for u_2

$$\left.\begin{aligned} 2N_2 u_2''(x) + 2N_4 u_0''''(x) &= 0 \\ u_2'(-1) &= \tfrac{N_2 u_1''(-1) - N_3 u_0'''(-1)}{N_1} \\ u_2(0) &= \tfrac{N_2}{N_0}(u_*''(0) + u_0''(0)) - \tfrac{N_1}{N_0} u_1'(0) + \tfrac{b_*(0)}{N_2} \end{aligned}\right\}. \tag{5.20}$$

The zero-th order solution satisfies the equilibrium condition of local theory with zero-stress conditions on the left boundary, $u'(-1) = 0$, and the requirement for the displacement field to be continuous on the right boundary, $u(0) = u_*(0)$.

5.2.3 Example I: Discontinuity at Interface

If $b_*(x) = 0$, the approximate solution reads

$$u_0(x) = u_*(0) \qquad u_1(x) = \frac{N_1}{N_0} u_*'(0) \qquad u_2(x) = \frac{N_2}{N_0} u_*''(0). \tag{5.21}$$

Even if external forces are absent, a displacement discontinuity may form at the interface of Ω_u and Ω_b. The displacement discontinuity is due to long range forces and the prescribed deformation u_* on Ω_u. A first order estimate of its magnitude is given by

$$[[u]](0) = \lambda \frac{N_1}{N_0} u_*'(0) + o(\lambda^2).$$

For vanishing internal length l, when $\lambda = 0$, the displacement discontinuity $[[u]](0)$ goes to zero. For a fixed value of λ, N_0/N_1 is a measure of the resistance against

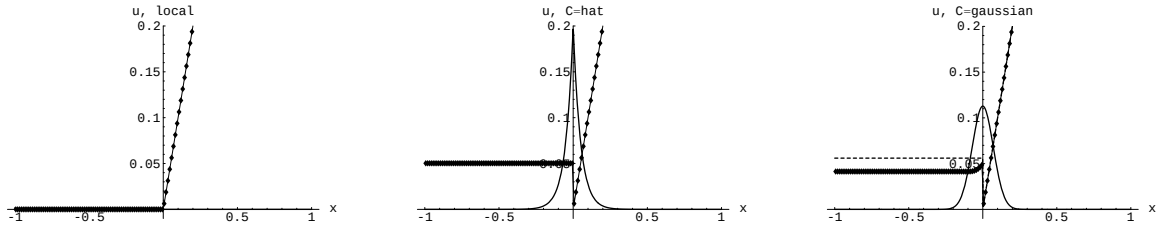

(a) (b) (c)

Figure 5-1: Solutions to problem (5.4) for $b_*(x) = 0$ and $u_*(x) = x$. Exact solutions (lines with dots) and first order approximations (thin dashed lines, or not visible because covered by exact solution): (a) Local solution with $\lambda = 0$. (b) and (c) Peridynamic solution with $\lambda = 0.1$. Stiffness distributions C (thin solid lines, not to scale) are defined in table 5.1.

	$C(\zeta)$	N_0	N_1	$[[u]]_{\text{approx.}}$	$[[u]]_{\text{simulation}}$
(b)	$4e^{-2\lvert\zeta\rvert}$	2	1	0.05	0.05
(c)	$\frac{4}{\sqrt{\pi}}e^{-\zeta^2}$	2	1.128	0.056	0.05

Table 5.1: Stiffness distributions and magnitudes of displacement discontinuities at $x = 0$ for $\lambda = 0.1$ when $b_*(x) = 0$ and $u_*(x) = x$.

forming a displacement discontinuity.

Figure 5-1 shows three exact solutions[2] of the problem (5.4): for a local material (i.e., a solution in the limit, when $\lambda \to 0$), and two different peridynamic materials for $\lambda = 0.1$. The displacements on Ω_u are prescribed as $u_*(x) = x$. The approximated and the exact magnitude of the displacement discontinuities at $x = 0$ agree well according to table 5.1. The strain of the approximate solution (5.21) is constant along Ω_b – even upon increasing the order of approximation. Fine boundary layers like in figure 5-1(c) cannot be captured with this method, due to the fact that order $e^{-1/\lambda}$ terms where set to zero, as in (5.15).

Interface Energy. The energy analysis of a propagating crack in chapter 6 requires an expression for the *interface energy*. The interface energy is the integral of energies of all links crossing the point $x = 0$,

$$W_{ub} = \int_{-1}^{0} dx' \int_{0}^{1} dx \; \frac{1}{2\lambda^3} C(\frac{x' - x}{\lambda}) \left[u(x') - u_*(x)\right]^2 . \tag{5.22}$$

[2] i.e., numerical solutions with sufficiently fine spatial resolution

For the solution given by (5.21) and $u(x) = u_0(x) + \lambda u_1(x) + \lambda^2 u_2(x) + ...$, the interface energy reads

$$W_{ub} = \lambda (u'_*(0))^2 \left[2N_3 - 2N_2 \frac{N_1}{N_0} + N_1 \left(\frac{N_1}{N_0} \right)^2 \right] + o(\lambda^2). \tag{5.23}$$

For the derivation see appendix A.14.

5.2.4 Example II: Two Interfaces

Consider a one-dimensional bar both ends of which are displaced. No additional external forces act on the body. If the deformation is (anti)symmetric, the results of the previous section can be applied under slightly modified conditions. Let the the body be $\Omega = [-3, 1]$ with regions of prescribed displacements $\Omega_{u,l} = [-3, -2)$ and $\Omega_{u,r} = (0, 1]$. The prescribed displacements are anti-symmetric with respect to $x = -1$, i.e., $u_*(x + 1) = -u_*(-x - 1)$. Therefore the deformation on $\Omega_b = [-2, 0]$ is anti-symmetric with $u(x + 1) = -u(-x - 1)$. The problem can be treated like problem (5.3), replacing the left boundary conditions in the ODEs for modes (5.18), (5.19), etc., by $u_k(-1) = 0$. With this, the first modes of the solution read

$$\begin{aligned} u_0(x) &= u_*(0)(1 + x) \\ u_1(x) &= \frac{N_1}{N_0}[u'_*(0) - u_*(0)](1 + x) \\ u_2(x) &= \left(\frac{N_2}{N_0} u''_*(0) - (\frac{N_1}{N_0})^2 [u'_*(0) - u_*(0)] \right) (1 + x). \end{aligned} \tag{5.24}$$

The displacement discontinuities at the interfaces of Ω_u and Ω_b are

$$-[[u]](-2) = [[u]](0) = \lambda \frac{N_1}{N_0} [u_*(0) - u'_*(0)] + o(\lambda^2).$$

The solution for a rigid body deformation of Ω_u, i.e., $u_*(x) = -1$, $x \in \Omega_{u,l}$ and $u_*(x) = 1$, $x \in \Omega_{u,r}$, is shown in figure 5-2(a). The larger the internal length, the bigger the displacement discontinuity, the more relaxes the body on the interior region.

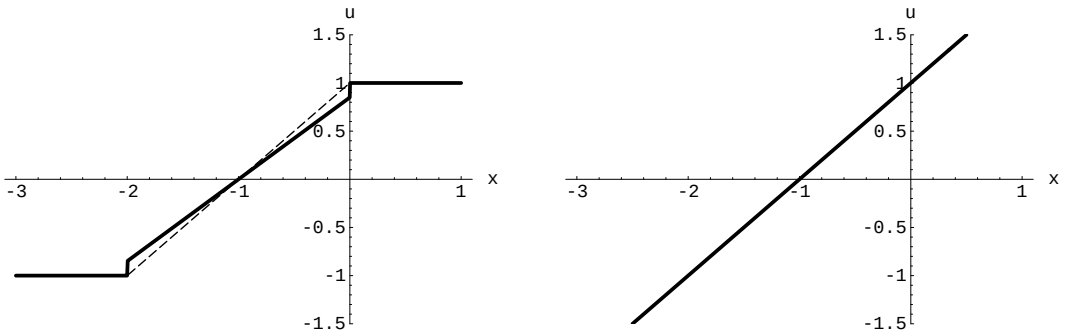

(a) (b)

Figure 5-2: Approximate solution (5.24) for different boundary conditions. *Dashed Line:* zeroth-order solution (= local solution). *Solid Line:* First order solution (a) $u_*(\Omega_{u,l}) = -1$, $u_*(\Omega_{u,r}) = 1$. (b) $u_*(x) = 1 + x$ on $\Omega_{u,l}$ and $\Omega_{u,r}$. Zeroth-order and first-order solution are identical. (a)+(b) $b_*(x) = 0$ and $\lambda = 0.2$. The stiffness distribution C is given in table 5.1(b).

If on the other hand $u_*(0) = u'_*(0) = 1$, i.e., the strain on Ω_u equals the elongation of the body, the first order corrections terms disappear. In the case when $u_*(x) = 1+x$, the local and the peridynamic solution are identical, see figure 5-2(b).

Interface and Bulk Energy. The interface energy as defined in (5.22) reads for the solution (5.24)

$$W_{ub} = \frac{N_1^3}{N_0^2}(u_*(0) - u'_*(0))^2 + 2\frac{N_1 N_2}{N_0}(u_*(0)^2 - [u'_*(0)]^2) \\ +N_3(u_*(0)^2 + u_*(0)u'_*(0) + [u'_*(0)]^2) + o(\lambda^2). \qquad (5.25)$$

The *bulk energy* is the integral of energies of all links within Ω_b,

$$W_{bb} = \int_{-2}^{0} dx' \int_{-2}^{0} dx \ \frac{1}{2\lambda^3} C(\frac{x' - x}{\lambda}) \left[u(x') - u_*(x)\right]^2,$$

and reads for the displacement field (5.24)

$$W_{bb}^{II} = 2N_2 u_*^2(0) + \lambda \left[4\frac{N_2 N_1}{N_0}\left(u'_*(0) - u_*(0)\right) u_*(0) - 3N_3 u_*^2(0)\right]. \qquad (5.26)$$

For the derivation see appendix A.14.

5.2.5 Summary

The method describes interface discontinuities and provides a good estimate of their magnitude. It relates the moments N_i of the stiffness distribution to higher order corrections of the solution. The results of the method will be applied in section 6.4.3.

The method *cannot* resolve the fine deformation structure of a boundary layer. While a displacement discontinuity is of order[3] λ, boundary layer effects disappear exponentially fast when $\lambda \to 0$; therefore a different kind of analysis would be necessary, like the Wiener-Hopf method.

No error bounds are derived. However, the method is justified by comparing solutions with results from numerical simulations.

5.3 Numerical Methods

5.3.1 Cutoff in the Reference Configuration

A large range of interaction forces makes numerical simulations expensive. As interaction forces typically decay with the distance of particles, it is justified to limit the range of interaction of a particle to its immediate neighborhood. If this is done in the reference configuration, the deformation has to remain small. The range limit is called *cutoff radius* h_c and is defined by the equation

$$\int_{B(h_c)} dV_\xi \; \xi^{n+1} C(\xi) = 0.99 \times \int_{\mathbb{R}^n} dV_\xi \; \xi^{n+1} C(\xi) \tag{5.27}$$

where $B(h_c)$ is a ball with radius h_c, and $C(\xi)$ is the stiffness distribution in the reference configuration. The number of dimensions of the body is denoted by n.

The cut-off radius is defined such that Young's Modulus in the reference configuration is not changed by more than 1%. Values of h_c are tabulated with stiffness distributions in the appendix C.

[3] provided that $u'_*(0) \neq 0$

5.3.2 Collocation Method

For an approximate solution $\tilde{\boldsymbol{u}}(\boldsymbol{x},t)$, the *collocation method* requires the equation of motion in (2.52) (or the equilibrium condition in (2.54) for static problems) to be satisfied only on discrete points $\boldsymbol{x}_i$ (see Bathe [9]). The discrete points $\boldsymbol{x}_i$ are called *collocation points*. Let $\boldsymbol{u}_i(t) = \tilde{\boldsymbol{u}}(\boldsymbol{x}_i,t)$, $\rho_{0i} = \rho_0(\boldsymbol{x}_i)$, $\boldsymbol{b}_i^{int}(t) = \int_\Omega dV'\, \boldsymbol{f}(\boldsymbol{x}',\boldsymbol{x}_i,t)$, and $\boldsymbol{b}_i(t) = \boldsymbol{b}(\boldsymbol{x}_i,t)$, then the equation of motion for the approximate solution reads

$$\rho_{0i}\ddot{\tilde{\boldsymbol{u}}}_i(t) = \boldsymbol{b}_i^{int}(t) + \boldsymbol{b}_i(t). \tag{5.28}$$

The integral of the interaction force $\boldsymbol{b}_i^{int}$ can be approximated by a discrete sum. Each collocation point represents a discrete volume element, and the forces between them sum up to

$$\boldsymbol{b}_i^{int} \approx \sum_{j,\, j\neq i} \Delta V_j\ \boldsymbol{f}(\boldsymbol{x}_j,\boldsymbol{x}_i,t) = \sum_{j,\, j\neq i} \Delta V_j\ \hat{f}[r_{ij},\boldsymbol{x}_j,\boldsymbol{x}_i]_t \boldsymbol{e}_{ij} = \boldsymbol{b}_i^{int}[\boldsymbol{u}_k]_t. \tag{5.29}$$

The interaction force $\boldsymbol{b}_i^{int}[\boldsymbol{u}_k]_t$ depends only on the displacement histories of collocation points. As, in addition, the equation of motion describes only the motion of collocation points $\boldsymbol{x}_i$, the formulation does not include values of $\tilde{\boldsymbol{u}}(\boldsymbol{x},t)$ for $\boldsymbol{x} \notin \{\boldsymbol{x}_i\}$.

The complete problem statement for the discrete approximation $\boldsymbol{u}_i$ of (2.52) reads, with the given fields of initial displacements $\boldsymbol{u}_0(\boldsymbol{x})$ on Ω_b, initial velocities $\dot{\boldsymbol{u}}_0(\boldsymbol{x})$ on Ω_b, external forces $\boldsymbol{b}_*(\boldsymbol{x},t)$ on Ω_b and boundary displacements $\boldsymbol{u}_*(\boldsymbol{x},t)$ on Ω_u:

$$\left.\begin{aligned} &\boldsymbol{x}_i \in \Omega_b: \quad \rho_{0i}\ddot{\boldsymbol{u}}_i(t) = \boldsymbol{b}_i^{int}[\boldsymbol{u}_k]_t + \boldsymbol{b}_i(t) \\ &\boldsymbol{x}_i \in \Omega_b: \quad \boldsymbol{u}_i(0) = \boldsymbol{u}_0(\boldsymbol{x}_i), \quad \dot{\boldsymbol{u}}_i(0) = \dot{\boldsymbol{u}}_0(\boldsymbol{x}_i) \\ &\boldsymbol{x}_i \in \Omega_u: \quad \boldsymbol{u}_i(t) = \boldsymbol{u}_*(\boldsymbol{x}_i,t) \end{aligned}\right\} \tag{5.30}$$

Distribution of Collocation Points. For small deformations, the sum in (5.29) can be limited to collocation points that lie within the range of the cutoff radius.

For the approximation (5.29) to be good, collocation points have to be densely distributed, such that the pair-wise force does not vary significantly along a discrete volume element. The denser the collocation points, the smaller the represented vol-

ume elements, and the better the approximation.

This means for elastic force laws of type (3.1) that the distance of collocation points h has to be significantly smaller than the cutoff radius of the stiffness distribution as defined in (5.27). For most stiffness distributions it is sufficient[4] that

$$h \approx h_c/3. \tag{5.31}$$

The cutoff radius is usually $l < h_c < 4l$ (see appendix C). Therefore, *the distance of collocation points should not be larger than the internal length.*

Interpolation of Strains. Methods that are used for strain interpolations in atomistic systems may be used to compute strains for irregular distributions of collocation points. The method by Horstemeyer and Baskes [42] is recommended.

Applicability. The collocation method is not well suited for simulations of bodies with an internal length on the atomistic scale. As h would have to be on the order of the distance of atoms, the collocation would make simulations as computationally expensive as molecular dynamics.

For bodies with large internal lengths, however, the method provides several advantages. In particular, if a force law with resolution length is adopted, the internal length l may be large allowing for coarse computational grids. The advantages are:

- The implementation is simple.
- No meshing is required.
- Interpolation between collocation points is not necessary (however possible).
- The non-local forces acting on one collocation point are summed up by a single integral (as opposed to a double integral in FEM).

As peridynamic theory is valid on and off strain and displacement discontinuities, defects like cracks may emerge and propagate without special treatment, in particular

[4]Sufficient means here that Young's Modulus is integrated with an error of up to 5%.

without reorganization of discretization points.

5.3.3 Ritz and FE Method

The Ritz method is the basis of the method of Finite Elements. It assumes an approximate solution of the form

$$\tilde{\boldsymbol{u}}(\boldsymbol{x},t) = \sum_{i=1}^{n} \boldsymbol{u}_i(t)\phi_i(\boldsymbol{x}) \tag{5.32}$$

where $\phi_i(\boldsymbol{x})$ are *trial functions* and $\boldsymbol{u}_i$ are (vector-valued) factors that are to be determined by the approximation method. In the context of Finite Elements, the trial functions are such that the vectors $\boldsymbol{u}_i$ are the displacements of the *nodes* $\boldsymbol{x}_i$. Then the trial functions satisfy particular conditions and are called *shape functions*. For details see Bathe [9] or Belytschko et al. [13].

The approximate solution $\tilde{\boldsymbol{u}}$ has to satisfy a relaxed version of the variational problem statement (2.53): it is less strict, because the set of arbitrary test functions $\boldsymbol{v}(\boldsymbol{x})$ is restricted to vector fields with trial functions $\phi_i(\boldsymbol{x})$ as components.

For the problem statement of the Ritz approximation of (2.53), let the initial displacements $\boldsymbol{u}_0(\boldsymbol{x})$ be given on Ω_b, initial velocities $\dot{\boldsymbol{u}}_0(\boldsymbol{x})$ on Ω_b, external forces $\boldsymbol{b}_*(\boldsymbol{x},t)$ on Ω_b and boundary displacements $\boldsymbol{u}_*(\boldsymbol{x},t)$ on Ω_u. The *global mass matrix* M is defined as

$$M_{ij} = \int_\Omega dV\ \rho_0(\boldsymbol{x})\phi_i(\boldsymbol{x})\phi_j(\boldsymbol{x}),$$

the *vectors of external forces* as

$$\boldsymbol{B}_i(t) = \int_\Omega dV\ \phi_i(\boldsymbol{x})\boldsymbol{b}_*(\boldsymbol{x},t),$$

and the *vectors of interaction forces* as

$$\boldsymbol{B}_i^{int}[\tilde{\boldsymbol{u}}]_t = -\frac{1}{2}\int_\Omega dV \int_\Omega dV'\ \ \hat{f}[\tilde{r},\boldsymbol{x}',\boldsymbol{x}]_t \boldsymbol{e}_r[\phi_i(\boldsymbol{x}') - \phi_i(\boldsymbol{x})].$$

Assuming the definition[5] $D_{ij} = \int_\Omega dV\ \phi_i(\boldsymbol{x})\phi_j(\boldsymbol{x})$, the *vectors of initial displacements* are given by

$$\sum_j D_{ij}\boldsymbol{u}_{0j} = \int_\Omega dV\ \phi_i(\boldsymbol{x})\boldsymbol{u}_0(\boldsymbol{x})$$

and the *vectors of initial velocities* by

$$\sum_j D_{ij}\boldsymbol{v}_{0j} = \int_\Omega dV\ \phi_i(\boldsymbol{x})\boldsymbol{v}_0(\boldsymbol{x}).$$

Then the $\boldsymbol{u}_i(t)$ have to satisfy

$$\left.\begin{aligned} \textstyle\sum_j M_{ij}\ddot{\boldsymbol{u}}_j(t) &= \boldsymbol{B}_i^{int}[\tilde{\boldsymbol{u}}]_t + \boldsymbol{B}_i(t) \\ \boldsymbol{u}_i(0) &= \boldsymbol{u}_{0i} \\ \dot{\boldsymbol{u}}_i(0) &= \boldsymbol{v}_{0i} \\ \boldsymbol{x} \in \Omega_b : \qquad \tilde{\boldsymbol{u}}(\boldsymbol{x},t) &= \textstyle\sum_{i=1}^n \boldsymbol{u}_i(t)\phi_i(\boldsymbol{x}) \\ \boldsymbol{x} \in \Omega_u : \qquad \tilde{\boldsymbol{u}}(\boldsymbol{x},t) &= \boldsymbol{u}_*(\boldsymbol{x},t) \end{aligned}\right\} \tag{5.33}$$

Elements. The body may be clustered into discrete and disjoint regions, defined by lines that connect nodes. These regions are called *elements*. Due to (5.32), elements are restricted in their deformation. Elements can be made large where little spatial variation of the deformation is expected. Large elements reduce the number of degrees of freedoms of large regions significantly. This is what makes the method efficient and faster than molecular dynamics.

If atomistic details are important, elements can be reduced in size down to the atomistic scale. Using an atomistic-peridynamic force law, the dynamics of an atomistic system is then approximated as described in section b4.1.

Applicability. The Ritz or Finite Element Method may be used with the atomistic-peridynamic force law (i.e., a three-dimensional version of (4.5)). This combination is a multi-scale model, as there are no restrictions on the element size h. If h is on the order of a (atom distance), then it approximates the dynamics of atoms. If h is

[5]Typically, D_{ij} is the identity matrix.

View of Theory	macroscopic model	multi-scale model
Force Law	force law with resolution length	atomistic-peridynamic
Approximation method	Collocation	Ritz / FEM
Restrictions on l	$l > h$ (bad for micro-scale)	none
Advantages	no mesh required, force is single a integral	large elements possible, exact boundary geometries

Table 5.2: Views of the theory and appropriate approximation methods

macroscopically large, i.e., $h \gg a$, an element is practically a local continuum. As both regimes are formulated in continuum theory, there is no interface between an atomistic and a continuum region. The Finite Element mesh has to follow critical regions like crack tips. This may make it necessary to remesh, i.e., to resize and reorganize elements.

The disadvantage of this approach is due to the element mesh. Creating regular meshes is expensive and often difficult to do, in particular in three dimensions. The necessity of remeshing can be circumvented by using a mesh that is fine enough – or a force law with large resolution length. The multi-scale modeling capabilities are then reduced to reproducing certain macroscopic quantities, such as the surface energy (see chapter 6). In this case, however, the collocation method should be preferred for its simplicity.

5.3.4 Time Integration

For time integration, the explicit central difference method is advantageous. It requires minimum storage space and is fast for small time steps. No iterations are required as in implicit methods. The method is described in detail in Belytschko et al. [13] and Bathe [9]. When using the Finite Element Method, the size of the critical stable time step may be derived from the stiffest element of the body. Using the element-free collocation method, an algorithm based on Gershgorin's Theorem can be used.

For static problems, the dynamic approximation method may be used in combination with a force law with viscosity. The viscosity dissipates kinetic or elastic energy and the system evolves towards equilibrium.

Chapter 6

Brittle Fracture

6.1 Basic Concepts

6.1.1 Particle Separation

In peridynamic theory, material failure is modeled with a force law that has a deformation threshold, beyond which a pair of particles does not interact. This critical deformation will be referred to as *point of separation*.

If the separation is reversible, the pair may regain its cohesive strength whenever the distance between the particles is decreased. A peridynamic force law with this feature would model, for example, decohesion in a perfect atomistic system. Bonds in a crystal lattice are recovered when atoms are brought back together.

If a pair of particles ceases to interact permanently, the link of the pair has *failed*. Link failure is a particular kind of *damage*[1] and is irreversible. Force laws with link failure are preferred for the simulation of macroscopic bodies, as separation processes on the macroscale are usually not reversible.

The minimum energy necessary to separate a pair is called *pair-wise separation energy* and is denoted by w_s. It is a work integral

$$w_s = w_s(\boldsymbol{x}', \boldsymbol{x}) = \int_{\boldsymbol{\xi}}^{\boldsymbol{r}_s} d\boldsymbol{r} \cdot \boldsymbol{f} \tag{6.1}$$

[1] Damage could also increase gradually for each link before complete failure.

taken along the path that yields the smallest possible value to get from $\boldsymbol{\xi}$ to $\boldsymbol{r}_s$ (e.g., for a viscous material along a path with vanishing velocity). $\boldsymbol{r}_s$ denotes the point of separation. The pair-wise separation energy is a constitutive quantity, that can be extracted from the force law. If the body is homogeneous and isotropic, then the separation energy can be written as $w_s = \hat{w}_s(\xi)$.

6.1.2 Strength

The macroscopic strength of a peridynamic continuum depends on the strength of its pairs. Strength limits may be defined with the first Piola-Kirchhoff stress (2.61). For example, the tensile strength is defined as

$$\sigma_{ts} = \max_{\lambda_m} \{(\hat{\boldsymbol{\sigma}}_0(\boldsymbol{F}))_{11}\} \tag{6.2}$$

for

$$\boldsymbol{F} = \begin{pmatrix} \lambda_m & 0 & 0 \\ 0 & 1 & 0 \\ 0 & 0 & 1 \end{pmatrix},$$

where the macroscopic stretch λ_m is the controlled deformation parameter.

6.1.3 Surface Energy

The *surface energy* of a body is defined (in the context of this theory) as the minimum amount of work that is necessary to create a new body surface. The surface energy per unit area in the reference configuration is denoted by $2\gamma_s$ (the factor 2 accounts for the fact that, in a separation process, surfaces are created in pairs).

In peridynamic theory, the surface energy is an integral of separation energies. In particular, the *specific surface energy* at a point $\boldsymbol{x}$ associated with the creation of a surface element $d\boldsymbol{A}$ is defined as the integral of the separation energies of all links going through $d\boldsymbol{A}$. This integral can be conveniently evaluated in a body that is homogeneous and isotropic, i.e., $w_s = \hat{w}_s(\xi)$, at a point that is sufficiently far away from the boundaries. Assume a body is separated along the plane $z = 0$ to form an

upper part $\Omega_1 = \{(x, y, z)|\ z \geq 0\} \cap \Omega$ and a lower part $\Omega_2 = \{(x, y, z)|\ z < 0\} \cap \Omega$.

Then the specific surface energy associated with the point $(\hat{x}, \hat{y}, 0)$, located on the crack surface, can be written as the integral of all pair-wise separation energies of the pairs with points on a line $(\hat{x}, \hat{y}, -h) \in \Omega_+$ where $h > 0$, and all points $(x', y', z') \in \Omega_+$. The specific surface energy per unit area reads

$$\int_0^\infty dh \int_h^\infty d\xi\ A(h, \xi)\hat{w}_s(\xi) \tag{6.3}$$

where $A(h, \xi)$ is the surface area of a sphere about the point $(\hat{x}, \hat{y}, -h)$ with radius ξ intersected by Ω_+, i.e., $A(h, \xi) = 2\pi\xi^2(1 - h/\xi)$. Evaluating expression (6.3) yields the three-dimensional specific surface energy

$$2\gamma_s = \pi \int_0^\infty d\xi\ \xi^3\hat{w}_s(\xi).$$

The two-dimensional specific surface energy is derived similarly and reads

$$2\gamma_s = 2 \int_0^\infty d\xi\ \xi^2\hat{w}_s(\xi). \tag{6.4}$$

Finally, the one-dimensional specific surface energy is

$$2\gamma_s = \int_0^\infty d\xi\ \xi\hat{w}_s(\xi).$$

6.1.4 Cracks

A *crack* in the context of peridynamic theory is defined as a surface[2] across which particles practically do not interact. This is the case when the separation energies of links crossing that surface is close to the surface energy, indicating that the remaining cohesive energy is negligible.

The crack surface lies *in the reference configuration* to avoid geometrical ambiguities due to the deformation of the body. The exact location of the crack tip is defined

[2]In a two-dimensional body, a crack is a line. In a one-dimensional body, a crack is a point. The dimensions of a body are the dimension of the reference configuration Ω.

in section 6.4.4 where numerical simulation results are presented.

6.2 Example

In this section, a force-law with resolution length is presented that can be used to model brittle material failure in two dimensions. Plastic material behavior is not considered. The force law defined in section 2.4.4 is adopted for homogeneous and isotropic bodies under plane strain conditions[3]. The link failure criterion assumes the special form

$$\kappa(\lambda_{\max}, \xi) = \lambda_{\max} - \lambda_c,$$

where λ_c is the critical link stretch. The critical link strain is defined as $\varepsilon_c = \lambda_c - 1$. The Helmholtz free energy reads

$$\psi = \hat{\psi}(r, \lambda_{\max}, \xi) = \begin{cases} \frac{1}{2} C(\xi)(r-\xi)^2 & \lambda_{\max} \leq \lambda_c \\ 0 & \lambda_{\max} > \lambda_c \end{cases}, \tag{6.5}$$

with the associated force law

$$f = \hat{f}(r, \lambda_{\max}, \xi) = \begin{cases} C(\xi)(r-\xi) & \lambda_{\max} \leq \lambda_c \\ 0 & \lambda_{\max} > \lambda_c \end{cases}, \tag{6.6}$$

and the evolution law

$$\lambda_{\max} = \max_{\tau \leq t} \left\{ \frac{r(\tau)}{\xi} \right\}. \tag{6.7}$$

Stress-strain Relation and Strength. Assume a homogeneous one-dimensional deformation

$$\boldsymbol{F} = \begin{pmatrix} \lambda_m & 0 \\ 0 & 1 \end{pmatrix},$$

with macroscopic stretch λ_m. The vector $\boldsymbol{\xi}$ is expressed with polar coordinates, i.e.,

$$\boldsymbol{\xi} = \xi \, (\cos\phi, \, \sin\phi).$$

[3] See section 2.8.6.

As the deformation is homogeneous, the relative distance vector of each link reads

$$\boldsymbol{r} = \boldsymbol{F}\boldsymbol{\xi} = \xi\ (\lambda_m \cos\phi,\ \sin\phi).$$

The link stretch λ_{nl} is

$$\lambda_{nl}(\phi) = \frac{r}{\xi} = \sqrt{\lambda_m^2 \cos^2\phi + \sin^2\phi}.$$

and the unit vector of $\boldsymbol{r}$ reads

$$\boldsymbol{e}_r = \boldsymbol{r}/r = \frac{1}{\lambda_{nl}(\phi)}\ (\lambda_m \cos\phi,\ \sin\phi),$$

The first Piola-Kirchhoff stress (2.61) reads in two dimensions

$$\boldsymbol{\sigma}_0 = \int_0^\infty \xi d\xi \int_0^\pi d\phi\ f\ \boldsymbol{e}_r \otimes \boldsymbol{\xi}$$

where f is given by (6.6). A link fails, if it is deformed beyond λ_c. Assume that λ_m can only grow. Then, the integral with respect to ϕ can be taken from ϕ_c to $\pi/2$, with

$$\lambda_{nl}(\phi_c) = \lambda_c \quad \Rightarrow \quad \phi_c(\lambda_m) = \begin{cases} 0 & \lambda_m \le \lambda_c \\ \arccos\sqrt{\frac{\lambda_c^2-1}{\lambda_m^2-1}} & \lambda_m > \lambda_c \end{cases}, \tag{6.8}$$

and the first Piola-Kirchhoff stress reads

$$\hat{\boldsymbol{\sigma}}_0(\lambda_m) = \left[\int_0^\infty d\xi\ \xi^3 C(\xi)\right]\ 2\int_{\phi_c(\lambda_m)}^{\pi/2} d\phi\ \frac{\lambda_{nl}(\phi)-1}{\lambda_{nl}(\phi)} \begin{pmatrix} \lambda_m \cos^2\phi & 0 \\ 0 & \sin^2\phi \end{pmatrix}.$$

The off-diagonal terms vanish for symmetry reasons. The integral over the stiffness distribution can be evaluated separately, using (2.93). The stress components read in

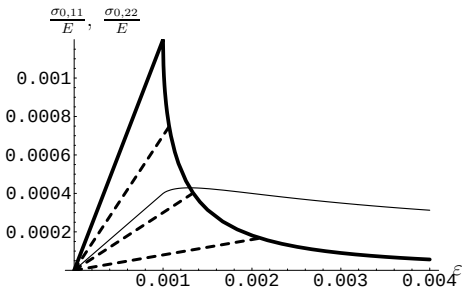

Figure 6-1: Stress-strain relation for material with force law (6.6) and $\varepsilon_c = 0.001$. The strain is $\varepsilon = \lambda - 1$. *Thick lines:* $\sigma_{0,11}/E$. Solid lines for loading, dashed lines for unloading. *Thin line:* $\sigma_{0,22}/E$ for loading only.

non-dimensional form

$$\begin{aligned} \frac{\hat{\sigma}_{0,11}(\lambda_m)}{E} &= \frac{32}{5\pi} \int_{\phi_c(\lambda_m)}^{\pi/2} d\phi \ \frac{\lambda_{nl}(\phi) - 1}{\lambda_{nl}(\phi)} \ \lambda_m \cos^2 \phi \\ \frac{\hat{\sigma}_{0,22}(\lambda_m)}{E} &= \frac{32}{5\pi} \int_{\phi_c(\lambda_m)}^{\pi/2} d\phi \ \frac{\lambda_{nl}(\phi) - 1}{\lambda_{nl}(\phi)} \ \sin^2 \phi. \end{aligned}$$

They are shown in figure 6-1 for a critical link strain of $\varepsilon_c = 0.001$. Also shown are the unloading paths for $\sigma_{0,11}$. As no plasticity mechanism is included, the stress-strain relation shows no permanent deformation after unloading.

The tensile strength in uniaxial extension can be identified as

$$\sigma_{ts} = \hat{\sigma}_{0,11}(\lambda_c) \approx 1.2E \, \varepsilon_c. \tag{6.9}$$

The $\approx$-sign accounts for the fact that the stress-strain relation is only in very good approximation linear.

Surface Energy. The force law is elastic until links fail. Therefore, the separation energy is *independent* of the deformation path to the point of separation, and independent of the deformation velocity. The pair-wise separation energy of (6.6) integrates to

$$\hat{w}_s(\xi) = \frac{1}{2} C(\xi) \xi^2 \varepsilon_c^2$$

yielding with (6.4)

$$2\gamma_s = \left[\int_0^\infty d\xi\ C(\xi)\xi^4\right]\ \varepsilon_c^2,$$

or with the fourth order non-dimensional stiffness moment[4]

$$2\gamma_s = 24N_4\ El\ \varepsilon_c^2. \tag{6.10}$$

Scaling. For the particular choice of a force law like (6.6), the constitutive model includes only one internal length l. It relates the tensile strength, the surface energy and the critical strain by

$$\frac{2\gamma_s E}{\sigma_{ts}^2 l} = \frac{50}{3}N_4 = \text{const.} \tag{6.11}$$

For a typical stiffness distribution[5],

$$\frac{2\gamma_s E}{\sigma_{ts}^2 l} \approx 1. \tag{6.12}$$

Internal Flaws. A similar expression is given in Anderson [7, page 37]

$$\frac{2\gamma_s E}{\sigma_f^2 c} = 1.57 \tag{6.13}$$

where σ_f is the critical stress at which a crack in an infinite medium with a length c advances. This means that *the force law* (6.6) *has approximately the same strength limit as a material with flaws of size* l.

Applicability. The shape of the force law (6.6) was not derived from microscopic properties. l is considered a resolution length that can be made large in order to simulate macroscopic behavior with the numerical collocation method presented in section 5.3.2. The stiffness distribution C and the critical link strain ε_c are chosen such that a material with the force law (6.6) has a given Young's Modulus E and a

[4]The fourth order non-dimensional stiffness moment is defined as $N_4 = \int_0^\infty d\bar{\xi}\ \bar{C}(\bar{\xi})\bar{\xi}^4/4!$, with $\bar{\xi} = \xi/l$ and (for two dimensional bodies only) $\bar{C} = l^4/E\ C$.

[5]Let, e.g., $C(\xi) = E/l^4\bar{C}(\bar{\xi})$ with $\bar{C}(\bar{\xi}) = \frac{72}{5\pi}e^{-3\bar{\xi}^2/2}$, where l has the meaning of the elastic internal length as explained in section 4.5. Then $\frac{50}{3}N_4 = 0.77$. Other stiffness distributions for plane strain are listed in table C.2

surface energy $2\gamma_s$. Then, it can be used to model crack propagation without knowing the crack path in advance.

A peridynamic model with the force law (6.6) is *not applicable* in the following cases:

1. *Cracks shorter than l.* The strength of the simulated body is at most the strength of a body with pre-cracks of size l. Therefore, bodies with cracks shorter than l cannot be simulated. The problem can be solved by using a different force law or by decreasing the size of l.

2. *Mode II cracks.* Crack formation in mode II cannot be adequately modeled. According to the force law (6.6), link failure may only occur under tension. In mode II, however, a surface is created by shearing, requiring link failure under compression.

3. *Contact.* Particles that do not interact in the reference configuration will never interact. Under large deformations, it may be necessary to model repelling forces of particles that are brought close together. This can be done either by using the atomistic-peridynamic force law (4.5) instead, or by including a repelling force in (6.6) on a phenomenological basis.

4. *Friction.* The force law (6.6) has no friction mechanism built in. Friction may play a crucial role in certain applications, like impact problems.

6.3 Griffith Criterion

Fracture under equilibrium conditions can be described by the Griffith energy balance. Griffith postulated that a crack is at a state of incipient growth if the reduction of *macroscopic potential energy* associated with a virtual crack advance is equal to the *microscopic work of separation* for the crack surface area created by the virtual crack (see Freund [34, page 4]). The macroscopic potential energy includes the elastic

energy and the potential of external work,

$$\Pi = \Psi_{el} - W_{ext}.$$

Consider a body of thickness t under plane strain conditions with a through-thickness crack of length c. The *macroscopic energy release rate* is defined as

$$\mathcal{G}(c) = -\frac{d\Pi}{dc}.$$

The work of separation consumed per unit crack length is denoted by R, also known as *material resistance to crack extension*, see Anderson [7, page 46]. The critical crack length for incipient growth satisfies the condition

$$\mathcal{G}(c) = R(c), \tag{6.14}$$

which is known as *Griffith criterion*. The classical continuum theory has typically no mechanisms built in that allow decohesion processes or the formation of a surface. This is why the material resistance to crack extension R is not included and must be added to the fracture model through equation (6.14). In brittle fracture, R is typically equal to the surface energy $2\gamma_s$ and does not change with c.

In peridynamic theory, the force law itself provides the information on how the material resists crack nucleation or growth. Links can undergo deformations that form surfaces. The work of separation to form a crack is then consumed to increase the stored elastic energy (reversible crack formation), or it is dissipated when links fail (and is then irreversibly lost). The amount of consumed energy may depend on many factors like the deformation velocity, the structure of the crack tip, etc.

R is defined in peridynamic theory as the *minimum amount of work* per unit length that needs to be expended for the nucleation or growth of a *particular crack*. R is then the integral of separation energies w_s of all links that are separated. The energy consumed during the actual process may be higher, however, the Griffith criterion will serve as a *necessary criterion for incipient growth*.

In this sense, the Griffith criterion can be applied to peridynamic theory. For consistency, the elastic energy is replaced by the Helmholtz free energy, as no elastic energy is defined for links that have failed. Therefore the total potential energy reads $\Pi = \Psi - W_{ext}$.

6.4 Incipient Crack Growth in a Strip

6.4.1 Introduction

In this section, the connection between microscopic link failure and macroscopic structural failure shall be established analytically and numerically. The chosen structure is a long strip containing a seed crack in the reference configuration. The numerical simulations are done for a peridynamic body with the material properties of glass. A force law of type (6.6) is adopted. The questions of interest are:

1. At what macroscopic deformation does link failure occur?
2. At what deformation does the strip fail?
3. What is a sensible definition of the location of a crack tip?
4. How does boundary deformation affect failure?
5. What is the influence of the internal length l?

At first, the critical deformation of incipient crack growth is computed within classical Linear Elastic Fracture Mechanics, where the Griffith criterion is added as a separate law. Then, two different analysis methods are applied to the peridynamic body, the perturbation method, presented in section 5.2, and the numerical approximation method with collocation points in section 5.3.2. No seperate law is applied; instead, the Griffith energy balance is included in the model. The results are used to verify the consistency of both methods.

6.4.2 Infinite Strip in Local Theory

Consider a strip of height $2L$, and infinite length and thickness. The upper and the lower boundary are displaced in the y-direction by u_0 and $-u_0$, respectively, and held fixed. The deformation occurs only in the x-y-plane under plane strain conditions. The material is linear elastic until it undergoes fracture. In the elastic regime, it has the Young's Modulus E and the Poisson's Ration $\nu = 1/4$. Fracture is controlled by the surface energy $2\gamma_s$.

A semi-infinite horizontal crack cuts the body in half for $x < 0$. The crack tip is at $x = 0$, $y = 0$. Far behind the crack tip, the crack lips are relaxed and contain no elastic energy. Far ahead of the crack tip, the elastic energy per unit length and thickness reads

$$\Psi''_{el} = \frac{\Delta\Psi_{el}}{t\Delta x} = \frac{6}{5} EL \left(\frac{u_0}{L}\right)^2 . \tag{6.15}$$

(The factor of $\frac{6}{5}$ is due to the plane strain conditions.) As the boundaries are held fixed, they do not do work. The total energy of the strip is therefore the total elastic energy and energy used to create a new surface.

The translational symmetry of the problem makes it very convenient to derive expressions for the change of total energy. The deformation of the crack tip region does not need to be considered. Instead the energy balance is only concerned with deformations far ahead and far behind the crack tip. If the crack grows quasi-statically[6] by an amount of Δc, the strip looses elastic energy by the amount of $\Delta c \Psi''_{el}$, i.e., $\mathcal{G} = \Psi''_{el}$. At the same time, the body needs to expend energy by the amount of $2\gamma_s \Delta c$ to extend the crack, therefore $R = 2\gamma_s$.

According to the Griffith criterion, the body is at a state of incipient crack growth if the strip does not change its energy after a crack advance by Δc, i.e., the stored elastic energy per unit length ahead of the crack tip equals the surface energy, $\mathcal{G} = 2\gamma_s$. Therefore, the critical deformation of incipient crack growth reads

$$\varepsilon_{0c} = \frac{u_0}{L} = \sqrt{\frac{2\gamma_s}{\frac{6}{5}EL}}. \tag{6.16}$$

[6] A quasi-static motion is considered to be a one-parameter family of equilibrium solutions.

Above ε_{0c}, a crack runs in an unstable manner and cause complete structural failure of the strip.

6.4.3 Perturbation Analysis of Infinite Strip

Some aspects of incipient crack growth in an infinite strip can be studied in peridynamic theory without numerical approximation. The perturbation method, presented in section 5.2 shall be used. The purpose of the analysis is to determine the critical deformation and how it changes with the internal length l. The results obtained are verified by a numerical simulation in section 6.4.4.

The problem presented in section 6.4.2 is extended by adding a region Ω_u of finite thickness to the upper and lower boundary. The thickness is chosen to be L in order to stay consistent with section 5.2. L can be made smaller without practically changing the result (provided that the internal length and thus the range of the pair-wise force is small). The displacement of region Ω_u is given by $u_*(x, y) = u_*(y)$.

The peridynamic material is linear elastic until it fails. It is assumed that no failure occurs far ahead of the crack tip. Far behind the crack tip, the two crack lips have entirely separated, there remain no links across the crack line. Furthermore, only those links fail that cross the line $y = 0$. The surface energy $2\gamma_s$ is included in the link failure criterion. The stiffness distribution and the link failure criterion need not be further specified for the subsequent analysis. The relevant information is provided by Young's Modulus and by the assumption that no failure has occurred to the right, whereas complete failure to form a crack has occurred to left.

Unlike in section 5.2, quantities are dimensional.

Energy Balance. The key argument of the preceding analysis for a local material is applied again: the region around the crack tip is considered as a black box. The energy balance only takes energies into account that enter and leave the region.

Ahead of the crack tip, the total energy is the sum of the bulk energy W_{bb}^{II} and the energy of the two interfaces $2W_{ub}^{II}$. The bulk energy of the deformed region Ω_u is not considered as it does not change along the strip. Behind the crack tip, the crack

lips are relaxed and have no bulk energy. Due to the deformation of Ω_u, however, the two interfaces have the energy $2W^I_{ub}$. The surface energy is part of the dissipated energy. The change of dissipated energy is $W'_{diss} = 2\gamma_s$ because the force law was chosen accordingly and the location where failure occurs is assumed to be limited to the crack.

The non-dimensional expressions for W^{II}_{bb}, W^{II}_{ub}, W^I_{bb} can be found in (5.25), (5.26) and (5.23), respectively. The approximation of the energy release rate reads

$$\mathcal{G} = W^{II}_{bb} + W^{II}_{ub} - W^I_{ub} = 2N_2 \left(\frac{u_0}{L}\right)^2 + \lambda\alpha \left(\frac{u_0}{L} - 2u'_0\right) \frac{u_0}{L} + o(\lambda^2), \tag{6.17}$$

with the constant α that is entirely determined by moments of the stiffness distribution

$$\alpha = \frac{1}{2} \frac{N_1^3 - 2N_0N_1N_2 - N_0^2N_3}{N_0^2}, \tag{6.18}$$

and the boundary deformations $u_0 = u_*(L)$ and $u'_0 = u'_*(L)$. Note that the stiffness moments are for one-dimensional stiffness distributions. The approximated critical deformations of incipient crack growth are stated for two different boundary deformations:

Case 1: $u'_0 = 0$. Rigid body motion. From the requirement $\mathcal{G} = 2\gamma_s$ follows the critical deformation

$$\varepsilon_{0c,1} = \frac{u_{0c,1}}{L} = \frac{\varepsilon_{0c}}{\sqrt{1 - \lambda\alpha}}. \tag{6.19}$$

where $\varepsilon_{0c} = \sqrt{\frac{2\gamma_s}{\frac{6}{5}EL}}$ is the critical deformation in local theory, and $\lambda = l/L$ is the length scale parameter.

Case 2: $u'_0 = u_0/L$. Proportional boundary deformation. The critical deformation reads

$$\varepsilon_{0c,2} = \frac{u_{0c,2}}{L} = \frac{\varepsilon_{0c}}{\sqrt{1 + \lambda\alpha}}. \tag{6.20}$$

For the stiffness distribution given in table 6.1 ($\alpha = 0.29$), the change of the critical deformation with respect to the internal length is plotted in figure 6-2. For $l = 0$ the

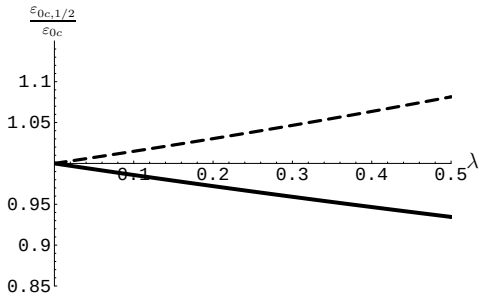

Figure 6-2: Change of the critical deformations $\varepsilon_{0c,i}/\varepsilon_{0,c}$ with increasing length scale parameter $\lambda = l/L$. *Solid Line:* Case 1 when $u_0' = 0$. *Dashed Line:* Case 2: $u_0' = u_0/L$.

result of local theory is recovered.

The critical deformation increases when the boundaries are rigidly deformed. This is due to the fact that the displacement discontinuities at the boundary interfaces ahead of the crack tip let the strip relax. The elastic energy and thus the driving force decreases. The effect increases with l.

The critical deformation decreases when the boundary regions are proportionally deformed. Crack growth is possible at lower states of deformation because the interface between Ω_u and Ω_b provide more elastic energy and thus a higher driving force.

Both effects are rather small. The size effect can be reduced to an order l^2 effect, if $u_0' = \frac{1}{2}u_0/L$. In this case, the first order term in (6.17) vanishes. Numerical verification is given in the next section. The analysis is equally applicable in anti-plane shear with different values for the stiffness moments.

6.4.4 Numerical Simulation of Finite Strip

Geometry. Consider a body as shown in figure 6-3. The body is clamped on the upper and lower boundary region Ω_u^+ and Ω_u^-, respectively. There are no external body forces. The boundary regions have the height of the cutoff radius h_c. The length in x-direction is L_x, the total height is $H = 2h_c + 2L_y$ where $2L_y$ is the height of Ω_b (the region that can move freely). $L = L_y$ is defined as the characteristic

Material properties of glass	Young's Modulus surface Energy density	$65\,GPa$ $2\gamma_s = 5\,\frac{J}{m^2}$ $\rho_0 = 2190\,\frac{kg}{m^3}$
Geometry	Horizontal length Macroscopic characteristic length (=half the height of Ω_b) Initial crack length	$L_x = 4\,m$ $L = 0.4\,m$ $c_0 = 1\,m$
Peridynamic properties	stiffness distribution (derived from 3d Gaussian, see appendix C) horizon internal length length scale parameter Poisson's ratio	$\bar{C}(\bar{\xi}) = \frac{1944\bar{\xi}\ \mathrm{erfc}\left[\frac{3\bar{\xi}}{\sqrt{5}}\right]}{25\sqrt{5\pi}}$ ∞ $l = 0.06\,m$ $\lambda = \frac{l}{L} = 0.15$ $\nu = \frac{1}{4}$
Simulation parameters	cutoff radius distance of collocation points	$h_c = 2l = 0.12\,m$ $h = \frac{1}{3}l = 0.02\,m$

Table 6.1: Properties of the simulated glass strip.

macroscopic length. The x-axis runs horizontally, the y-axis vertically, The origin lies in the center of the body.

Initial Conditions. Initially, the body is undeformed and stress-free. A seed crack is artificially created by cutting all links that cross the line $y = 0$, $x < -1$. The seed crack is *sharp*, as only those links are cut that cross the crack line. The initial crack length is c_0.

Material properties. Glass is chosen for its brittleness. The material properties and the choice of peridynamic quantities are summarized in table 6.1.

The peridynamic force law (6.6) with resolution length l and brittle link failure is adopted. The critical link strain ε_c depends on the choice of l and is obtained from (6.10) as $\varepsilon_c = \sqrt{\frac{2\gamma_s}{4!N_4 E\, l}} = 3.5 \times 10^{-5}$. The tensile strength $\sigma_{ts} = 1.2E\varepsilon_c = 2.7MPa$ significantly below the tensile strength of real glass ($\approx 200MPa$). This is a consequence of what is described in section 6.2: a body with this force law has the same strength limit as a body with internal flaws of the size of about l. As glass has a comparatively low toughness, a large l may make the resulting tensile strength

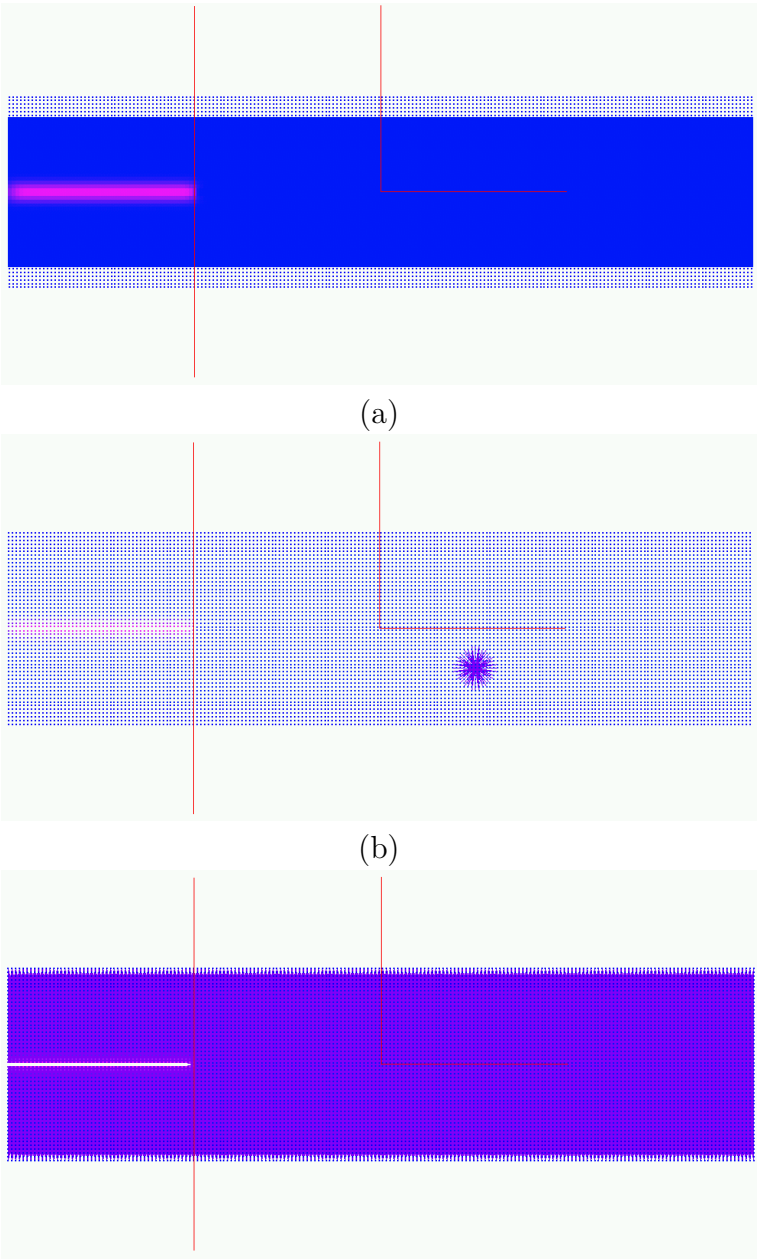

Figure 6-3: Glass Strip with initial crack. The crack tip position $c_1 = c_2$ is shown by long vertical line. Coordinate axes in the middle have the length $1m$. (a) The blue area is the region Ω_b that can move freely. Thin points lie on region Ω_u with prescribed displacements. The red region shows cumulated dissipated energy $\bar{w}_{diss}$ due to link failure. (b) Collocation points. The circular region represents the interaction range of one particle. (c) Links between collocation points cover the body densely.

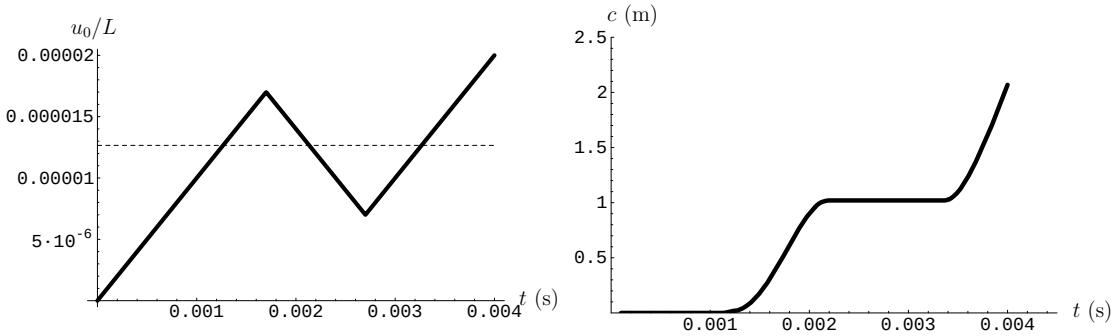

(a) (b)

Figure 6-4: (a) Motion of boundaries. (b) Motion of crack tip.

low. For the current purposes, l is chosen on the order of L ($l/L = 0.15$) to make numerical simulation with the collocation method possible. If necessary, it can be made smaller in order to recover the correct tensile strength.

Boundary Deformation and Definition of Natural Crack. To initiate crack growth, the clamped regions Ω_u are moved apart in a *rigid body motion*. Adopting the notation of section 5.2, the deformation on Ω_u is

$$u_*(x,y) = u_*(y) = \begin{cases} u_0 & (x,y) \in \Omega_u^+ \\ -u_0 & (x,y) \in \Omega_u^- \end{cases} \tag{6.21}$$

At first, the boundaries move well above the critical strain ε_{0c} (from local theory) to initiate crack growth. The crack starts propagating. Then, the load is decreased and the crack stops with its tip at $x \approx 0$. The crack at rest will be called *natural crack* because its tip was formed by an autonomous deformation process. Finally, crack propagation is initiated again. A graph of $u_0(t)/L$ is shown in figure 6-4

General Remark on Simulation. The simulation is done with explicit time integration. To ensure quasi-static conditions at the beginning of crack growth, the boundaries move at a speed that is significantly below the speed of sound, $\dot{u}_0/c_{ph} = 7 \times 10^{-6}$. Viscosity is switched on during the initial loading period and during the unloading period to damp out vibrations. When the crack is at the state of incipient growth, the viscosity is switched off.

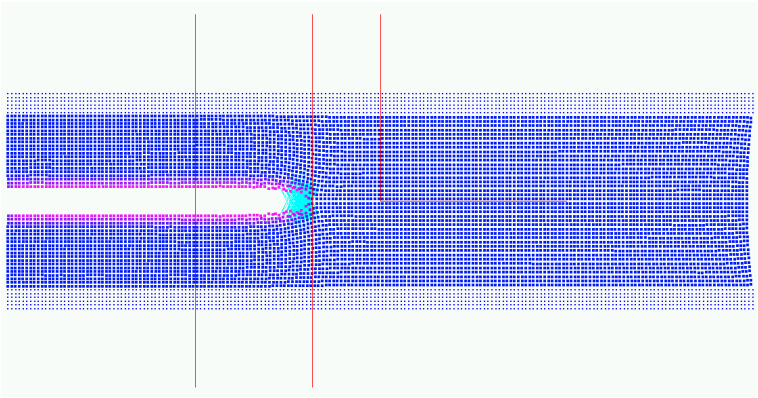

(a)

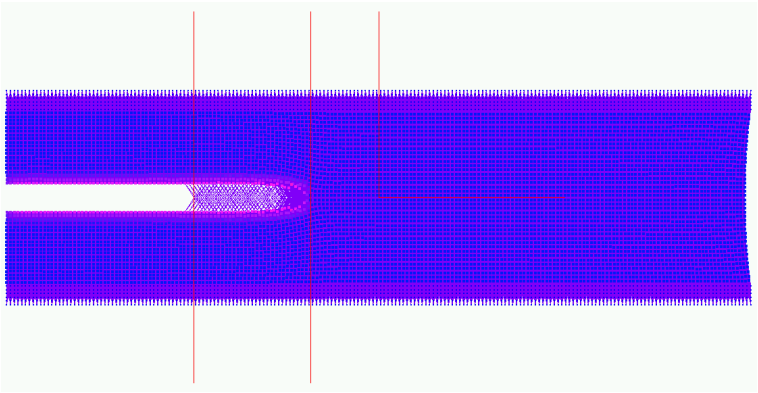

(b)

Figure 6-5: Magnified deformation of a growing crack. The left and right long vertical lines visualize the positions of c_1 and c_2, respectively. (a) Shows the fracture process zone at the crack tip, represented by all failing links during one time step. (b) Shows all links intact and the remaining links across the crack line.

Definition of the Location of a Crack Tip. Two distinct positions of a moving crack can be identified: the last point of links crossing the crack line and the first point of link failure.

Let c_1 denote the end position of the zone where cohesive forces act on the crack lips (i.e., the position in the reference configuration where the last link intact crosses the crack line). When the crack propagates, it is possible that a few links remain intact[7] as shown in figure 6-5(b) and thus c_1 does not change, although the cohesive forces and the remaining separation energy are negligible for $x > c_1$. This can be seen in figure 6-6, where the work expended to make the crack advance is shown as dissipated energy per unit surface area. Therefore, c_1 is not practical to express the location of the crack tip.

The tip of the zone of cohesive forces is denoted by c_2, defined as the farthest point in the direction of crack growth where a failed link intersects the crack line in the reference configuration, see figure 6-5. c_2 is typically closer to the point where the cohesive forces and the remaining separation energy decrease significantly in magnitude and is, therefore, called location of the crack tip.

Incipient Crack Growth. Figure 6-6 shows the change of the crack tip position c_2 with increasing deformation. The initial sharp crack starts moving at $\varepsilon_{0c,s} = 1.15 \times 10^{-5}$, the natural crack at $\varepsilon_{0c,n} = 1.39 \times 10^{-5}$. The sharp crack starts growing at a smaller boundary deformation. The proximity to the left boundary does not explain this, as it would rather increase the critical deformation.

Early incipient growth is caused by the sharpness of the crack tip. The next two paragraphs show that this does not affect the structural strength of the body.

***R*-Curve.** The change of dissipated energy with respect to the crack length can be computed by

$$\frac{dW_{diss}}{dc} = \frac{\dot{W}_{diss}}{\dot{c}} \tag{6.22}$$

[7]Links survive the crack propagation in this simulation because the deformations are controlled at the boundary and remain very small throughout the body. Links with a small angle with respect to the x-axis survive the longest.

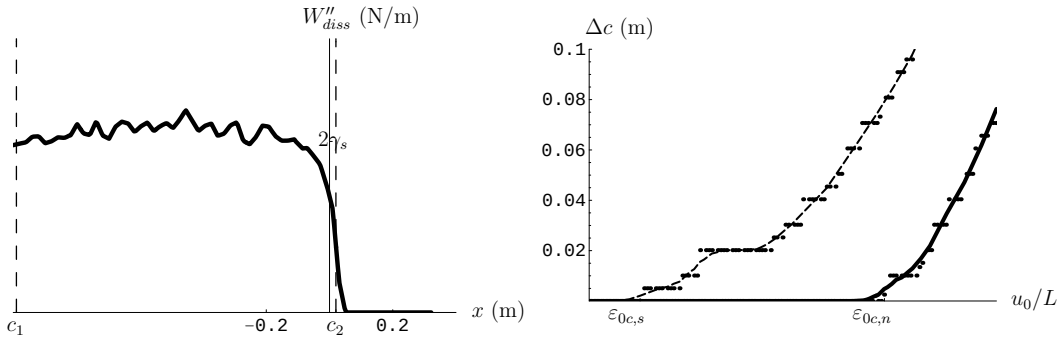

Figure 6-6: (a) Profile of dissipated energy $W''_{diss}(x) = \int dy\ w_{diss}(x,y)$ of natural crack. Crack tip position $c = c_2$ and end of cohesive zone c_1 are shown as dashed lines. (b) Filtered c. *Dashed Line:* Initial sharp crack. *Solid Line:* Natural crack. Dots represent discrete measured values.

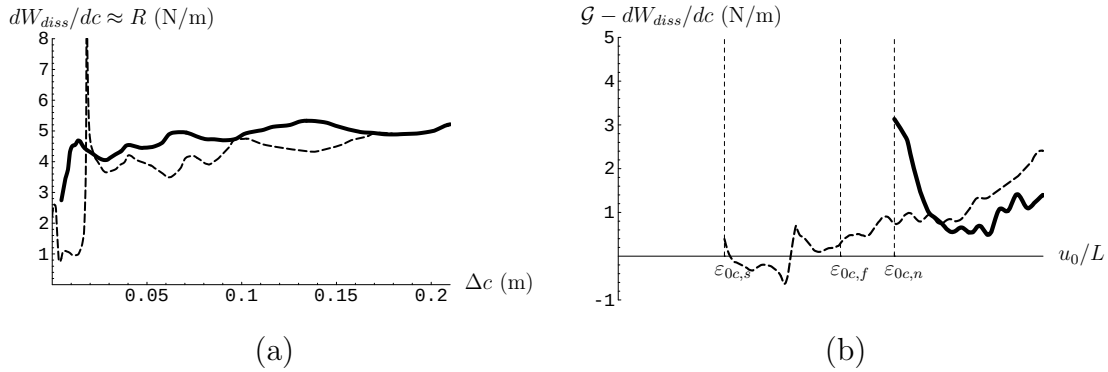

Figure 6-7: (a) Change of dissipated energy with crack extension dW_{diss}/dc vs. crack length increase. (b) Net driving force on crack tip $\mathcal{G} - dW_{diss}/dc$ vs. boundary deformation u_0/L. *Dashed Line:* Initial sharp crack. *Solid Line:* Natural crack.

where $\dot{c} = \frac{d}{dt}c_2$ denotes the crack tip velocity. The result is an expression that is independent of time and serves as an approximation of the material resistance to crack extension R. The function $c_2(t)$ is filtered, as shown in figure 6-6(b), to make it smoother for the time derivative operation. The same is done for $\dot{W}_{diss}(t)$.

A plot of dW_{diss}/dc is shown in figure 6-7. Initially, the sharp crack dissipates little energy at the onset of crack growth, whereas the natural crack starts growth at the level of almost $2\gamma_s$. The sharp crack goes then through a region of high energy dissipation with little crack growth. This is interpreted to be the formation period of a natural crack tip. For both cracks, the dissipation per crack unit extension approaches the level of macroscopic surface energy $2\gamma_s$ soon after incipient growth.

Griffith Criterion. To extract an approximation of the energy release rate $\mathcal{G}(c)$ from the simulated quantities, assume that the total Helmholtz free energy depends only on the boundary deformation u_0 and the position of the crack tip[8]. Then,

$$\frac{d}{dt}\Psi(c, u_0) = \frac{\partial \Psi}{\partial c}\dot{c} + \frac{\partial \Psi}{\partial u_0}\dot{u}_0, \tag{6.23}$$

and with $\mathcal{G} = -\partial\Psi/\partial c$,

$$\mathcal{G} = \frac{\dot{W}_{ext} - \dot{\Psi}}{\dot{c}}. \tag{6.24}$$

Knowing that the resistance to crack extension is given by the dissipated energy, the net driving force is represented by the quantity $\mathcal{G} - dW_{diss}/dc$, see plot in figure 6-7. If $\mathcal{G} - dW_{diss}/dc \approx 0$ then the crack tip is at the state of incipient growth. if $\mathcal{G} - dW_{diss}/dc > 0$, then the crack tip is past the state of incipient growth and may move. The latter is the case at $\varepsilon_{0c,s}$ for the sharp crack, and at $\varepsilon_{0c,n}$ for the natural crack. The curve of the natural crack stays well above zero and the crack may continue to grow. For the sharp crack however, the curve goes quickly down to zero, indicating a short period of stable growth. $\mathcal{G} - dW_{diss}/dc$ becomes only considerably larger than zero, when it passes the critical deformation $\varepsilon_{0c,f}$, defined in the next paragraph.

Deformation of Macroscopic Failure. The *critical deformation of macroscopic failure* $\varepsilon_{0c,f}$ is defined as the point above which a crack runs in an unstable manner, resulting in complete failure of the strip. Below this point, local failure may occur, but it stays localized and does not lead to structural failure.

The natural crack tip does not significantly change its structure while advancing. Therefore, it is assumed that, whenever a link fails, the deformation is high enough to provide a driving force that translates the crack tip entirely. If the boundaries do not move and the tip is sufficiently far from the boundary, neither the driving force nor the resistance to crack extension change, and the crack can continue growing. Therefore, $\varepsilon_{0c,f}$ can be distinctly measured as the *deformation at which the first link*

[8]The assumption is justified by the slow velocity of the boundaries and the fact that the material is rate-independent. The expression for $\mathcal{G}$ is still an approximation, because the chosen deformation path depends on the dynamics of the system.

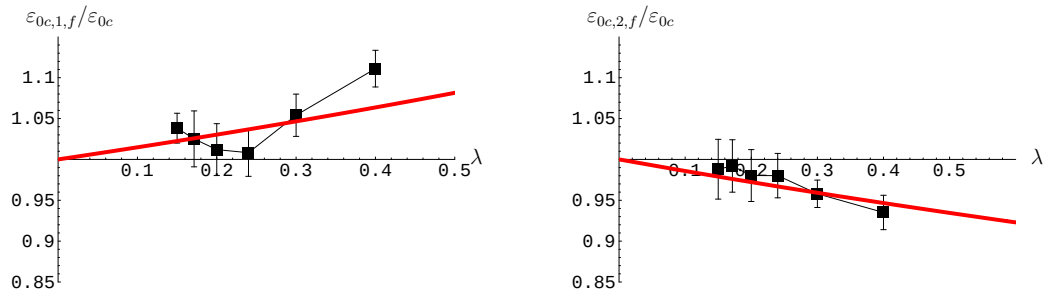

(a) (b)

Figure 6-8: Critical deformations for different λ. Results of simulation (dots) compared to perturbation analysis (lines). (a) Case 1 when $u_0' = 0$ (rigid body deformation). (b) Case 2 when $u_0' = u_0/L$ (proportional deformation).

failure occurs at a natural crack tip.

$\varepsilon_{0c,f}$ coincides roughly with the deformation at which the net driving force of a sharp crack becomes positive (see figure 6-7). For the natural crack tip, the net driving force cannot be computed at this point, as it has not started moving. In fact, $\varepsilon_{0c,f}$ is slightly smaller than $\varepsilon_{0c,n}$ (the point at which the natural crack tip starts moving) which is attributed to inertial effects in the simulation.

Size Effect. The effect of the length scale parameter on the critical deformation of macroscopic failure $\varepsilon_{0c,f}$ is simulated for bodies with varying heights L. $\varepsilon_{0c,f}$ is determined by measuring the first occurrence of link failure at a natural crack tip. The results are compared to those obtained by the perturbation analysis in section 6.4.3, representing an approximation for finite bodies. The results are shown in figure 6-8. The error bars visualize the interval of two discrete deformation values between which crack growth was observed. The results of the perturbation method and the results of the simulation are in good agreement.

The agreement becomes worse upon increasing the distance of collocation points. Coarser grids increase the critical deformation. This is effect is similar to the delay of crack propagation in crystals due to the discreteness of atoms, called *lattice trapping* (see, e.g., Bernstein and Hess [14]).

6.4.5 Summary

The results concerning the failure of a long strip are summarized.

1. The crack tip is defined as the first location where a failed link crosses the crack path, indicating the beginning of rapid loss of cohesive strength.

2. Local failure at a sharp crack does not necessarily cause structural failure.

3. Structural failure occurs at the deformation at which a natural crack starts propagating.

4. Depending on how the boundary is deformed, the point of failure may increase or decrease. A rigid boundary deformation decreases the critical deformation, as the displacement discontinuities that form at the interfaces of Ω_u and Ω_b relax the body.

5. The perturbation method and the numerical simulations produce results which are in good agreement for a sufficiently small distance of collocation points.

6. The deformation of macroscopic failure $\varepsilon_{0c,f}$ converges to the critical deformation predicted by classical linear elastic fracture mechanics.

6.5 Autonomous Growth of a Curved Crack

This section provides a short demonstration of how a crack may choose its path autonomously in a numerical simulation. The force law (6.6) is applied to the simulation of the failure of a non-symmetric strip. Figure 6-9 shows crack paths that were computed with a grid of varying coarseness. The simulation parameters are summarized in table 6.2.

In the simulation, the left and the right boundary are deformed in a rigid body motion. They are pulled apart at constant velocity. Beyond a critical deformation, the crack starts propagating at a small angle. Finally, the crack hits the vertical boundary line.

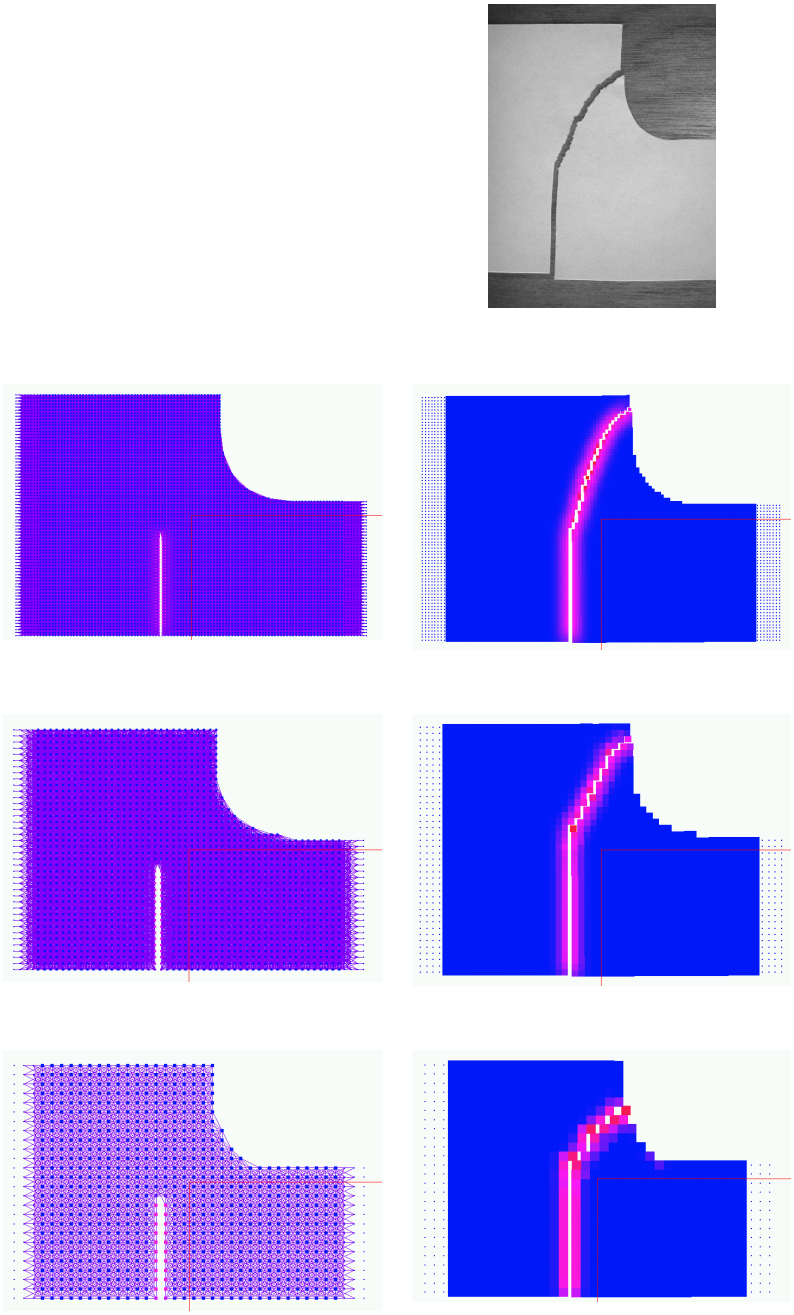

(reference configuration) (after failure)

Figure 6-9: *Row 1:* Failure of a paper strip. *Rows 2-4:* Numerical simulation of a strip with different grids. Collocation point distance $h/l = 1/4$ (row 2), $h/l = 1/2$ (row 3), $h/l = 3/4$ (row 4)

Material properties	Young's Modulus surface Energy density	$1\,GPa$ $2\gamma_s = 100\,\frac{J}{m^2}$ $\rho_0 = 300\,\frac{kg}{m^3}$
Geometry	horizontal length vertical height left vertical height right length of initial crack radius of corner horizontal distance between crack and vertical boundary	$L_x = 0.1\,m$ $L_y = 0.08\,m$ $L_y = 0.045\,m$ $c_0 = 0.035\,m$ $R = 0.02\,m$ $d = 0.02m$
Peridynamic properties	stiffness distribution (derived from 3d Gaussian, see appendix C) horizon internal length Poisson's ratio	$\bar{C}(\bar{\xi}) = \frac{1944\bar{\xi}\ \mathrm{erfc}\left[\frac{3\bar{\xi}}{\sqrt{5}}\right]}{25\sqrt{5\pi}}$ ∞ $l = 0.004\,m$ $\nu = \frac{1}{4}$
Simulation parameters	cutoff radius distance of collocation points	$h_c = 2l = 0.008\,m$ $h_{\text{fine}} = \frac{1}{4}l = 0.001\,m$ $h_{\text{medium}} = \frac{1}{2}l = 0.002\,m$ $h_{\text{coarse}} = \frac{3}{4}l = 0.003\,m$

Table 6.2: Properties of simulated strip.

Similar crack paths can be observed in a simple experiment with a sheet of paper. To obtain qualitative agreement, the pre-crack has to be cut perpendicularly to the rolling direction. The sheet may then be pulled apart by hand. The experiment serves as illustration rather than as justification of the theory. The mechanical behavior of paper is in general not sufficiently represented by an isotropic medium like the one chosen for the simulation. Its material properties depend strongly on the way it was manufactured and may be highly anisotropic. In addition, in the later stages of failure in the paper strip, when the crack is close to the boundary, out-of-plane forces are strong, which is not captured by the simulation.

The simulation pictures show that a fairly coarse grid of collocation points with $h = 3/4l$ predicts a crack path that is close to the one with a fine grid with $h = 1/4l$.

Chapter 7

Conclusions

A theoretical framework for peridynamic theory was presented. The theory can be used to model solid bodies without special treatment of discontinuity surfaces. In particular, it was shown that the global balance of linear momentum is equivalent to the local form without jump conditions, and that the local formulation of an initial boundary value problems is equivalent to the variational form without jump conditions. Solutions do not need to be continuous or smooth. Furthermore, equilibrium problems for elastic materials do not have to satisfy Weierstrass-Erdmann corner conditions to be strong extrema of the energy functional.

Chapter 3 showed that peridynamic theory formally includes local elasticity[1] for a vanishing internal length, and that it includes atomistic systems with pair-potentials in the limit when the mass of the body is concentrated into point masses.

Two classes of force laws associated with two different views of the theory were identified. First, the atomistic-peridynamic force law makes the peridynamic framework a multi-scale model. It approximates the general non-linear dynamics of an atomistic system and captures exactly the non-linear homogeneous and the linear non-homogeneous behavior of a chain of atoms. The associated internal length is on the order of $10^{-10}m$. The method of Finite Elements is best suited for numerical simulations with this force law, as the size of elements is not restricted by the internal length.

[1] This is currently restricted to materials with a Poisson's ratio of $\nu = 1/4$.

Second, the force law with resolution length creates a model that works well on the macroscale and does not require remeshing in numerical simulations. The internal length can be chosen much larger than the distance of atoms, making simulations with the collocation method less expensive than, e.g., molecular dynamics. In the context of brittle fracture, the force law includes the macroscopically relevant surface energy and Young's Modulus.

A perturbation method that is suitable for discontinuous displacements at boundaries was developed. It was then applied to crack propagation in an infinite strip. The predictions of the critical deformation for incipient crack growth are in good agreement with the numerical simulations of a peridynamic body representing a glass strip. The perturbation method and the numerical simulation reproduce the macroscopic failure criterion of Linear Elastic Fracture Mechanics. The failure of an asymmetrically pre-cracked strip was simulated. The results demonstrated that cracks may grow autonomously.

Large internal lengths may cause unphysical behavior such as the loss of local stiffness. To prevent the formation of spurious discontinuities, regions where the body is clamped (and displacements are prescribed) have to be sufficiently large. Clamped regions can themselves be deformed so as to keep the interface discontinuities small. Loads applied to the body are required to be sufficiently smooth to prevent unphysically singular deformations. Large internal lengths may pose an unphysical strength limit on the material. The force law chosen in chapter 6 imposes the tensile strength of a material with flaws of size l. All three effects become weaker upon decreasing the internal length. Good agreement with classical local theories is achieved if the internal length is sufficiently smaller than the macroscopic dimensions of the body.

Extensions. Non-local materials with pair-wise interaction have a Poisson's ratio of $\nu = 1/4$. A polar peridynamic theory with three-body interactions will allow for a free choice of ν.

Peridynamic theory is advantageous for impact modeling, as crack paths do not need to be known in advance. Key mechanisms of fracture due to impact, however,

are friction and contact. While contact was implemented with repulsive force by Silling [62], friction is still a hurdle to overcome. This is difficult, because the theory does not include surface forces.

Applying the theory as multi-scale method in combination with Finite Elements was not pursued here, because the necessity of remeshing makes this approach incompatible with the goal of this thesis. The approach is nevertheless a promising basis for future research, as it provides seamless interfaces between regions of atomistically fine and macroscopically large resolution.

Appendix A

Derivations

A.1 Global and Local Balance of Momentum

When taking time derivatives of volume integrals, special attention has to be paid to integrand that are discontinuous with respect to time or to space. Assume that the specific linear momentum $\rho_0 \dot{\boldsymbol{y}}$ is discontinuous across $S_{\rho_0 \dot{\boldsymbol{y}}}(t)$. Applying Reynold's transport theorem (see Marsden and Hughes [51, page 124]) to (2.4) yields

$$\int_{\Omega \backslash S_{\rho_0 \dot{\boldsymbol{y}}}} \rho_0 \ddot{\boldsymbol{y}} \, dV - \int_{S_{\rho_0 \dot{\boldsymbol{y}}}} [[\rho_0 \dot{\boldsymbol{y}}]] \, \dot{s} \boldsymbol{n} \cdot d\boldsymbol{A} = \int_{\Omega} \boldsymbol{b}_{tot} \, dV.$$

As $\boldsymbol{b}_{tot}$ is bounded, the integral on the right hand side can be equivalently replaced by an integral over $\Omega \backslash S_{\rho_0 \dot{\boldsymbol{y}}}$. The resulting expression is required to hold for arbitrary parts of the body $\Omega_{sub} \subset \Omega$, including arbitrary parts of the surface $S_{\rho_0 \dot{\boldsymbol{y}}}$. The local balance of linear momentum (2.6) has to hold almost everywhere on $\Omega \backslash S_{\rho_0 \dot{\boldsymbol{y}}}$, and $[[\rho_0 \dot{\boldsymbol{y}}]] \dot{s} = \boldsymbol{0}$ has to be satisfied almost everywhere on $S_{\rho_0 \dot{\boldsymbol{y}}}$.

The latter is true, if and only if $\dot{s} = 0$, as $[[\rho_0 \dot{\boldsymbol{y}}]] \neq \boldsymbol{0}$ by definition, thus, the surface $S_{\rho_0 \dot{\boldsymbol{y}}}$ does not move into its normal direction. Consequently, $\ddot{\boldsymbol{y}}$ can be defined on $S_{\rho_0 \dot{\boldsymbol{y}}}$ as limits from either side and the local balance of linear momentum can be stated for the entire body Ω. Finally, it follows the equivalence between the global

and local form,

$$\frac{d}{dt}\int_\Omega \rho_0 \dot{\boldsymbol{y}}\, dV = \int_\Omega \rho_0 \ddot{\boldsymbol{y}}\, dV = \int_\Omega \boldsymbol{b}_{tot}\, dV \quad \Leftrightarrow \quad \rho \ddot{\boldsymbol{y}} = \boldsymbol{b}_{tot}, \tag{A.1}$$

where the local form has to be satisfied almost everywhere. Any condition on a discontinuity surface can be derived from the global and local balance of momentum, as they are equivalent.

The local balance law of angular momentum (2.7), and the equivalence between the global and the local form are derived in exactly the same manner.

(2.7) also follows directly from (2.6) by simple multiplication with $\boldsymbol{y}$.

A.2 Action Equals Reaction

The pair-wise force $\boldsymbol{f}$ can be uniquely split into a symmetric and an anti-symmetric part. They are defined as

$$\begin{aligned} \boldsymbol{f}_s(\boldsymbol{x}', \boldsymbol{x}, t) &= \frac{1}{2}\left(\boldsymbol{f}(\boldsymbol{x}', \boldsymbol{x}, t) + \boldsymbol{f}(\boldsymbol{x}, \boldsymbol{x}', t)\right) \\ \boldsymbol{f}_a(\boldsymbol{x}', \boldsymbol{x}, t) &= \frac{1}{2}\left(\boldsymbol{f}(\boldsymbol{x}', \boldsymbol{x}, t) - \boldsymbol{f}(\boldsymbol{x}, \boldsymbol{x}', t)\right). \end{aligned}$$

It follows

$$\boldsymbol{f}(\boldsymbol{x}', \boldsymbol{x}, t) = \boldsymbol{f}_s(\boldsymbol{x}', \boldsymbol{x}, t) + \boldsymbol{f}_a(\boldsymbol{x}', \boldsymbol{x}, t)$$

and

$$\boldsymbol{f}_s(\boldsymbol{x}', \boldsymbol{x}, t) = \boldsymbol{f}_s(\boldsymbol{x}, \boldsymbol{x}', t) \tag{A.2}$$

$$\boldsymbol{f}_a(\boldsymbol{x}', \boldsymbol{x}, t) = -\boldsymbol{f}_a(\boldsymbol{x}, \boldsymbol{x}', t). \tag{A.3}$$

and with (2.9) and (2.11)

$$\int_\Omega dV \int_\Omega dV' \boldsymbol{f}_s + \int_\Omega dV \int_\Omega dV' \boldsymbol{f}_a = \boldsymbol{0}. \tag{A.4}$$

The right hand side of (A.4) can be shown to be equal to its negative value: Using (A.3) and changing the order of integration gives

$$\int_\Omega dV \int_\Omega dV' \boldsymbol{f}_a(\boldsymbol{x}', \boldsymbol{x}, t) = -\int_\Omega dV \int_\Omega dV' \boldsymbol{f}_a(\boldsymbol{x}, \boldsymbol{x}', t)$$
$$= -\int_\Omega dV' \int_\Omega dV \boldsymbol{f}_a(\boldsymbol{x}, \boldsymbol{x}', t) = -\int_\Omega dV \int_\Omega dV' \boldsymbol{f}_a(\boldsymbol{x}', \boldsymbol{x}, t).$$

Therefore, the double integral of $\boldsymbol{f}_a$ has to vanish and (A.4) reduces to

$$\int_\Omega dV \int_\Omega dV' \boldsymbol{f}_s = \boldsymbol{0}, \tag{A.5}$$

which has to be satisfied for arbitrary subsections of the body. In particular, (A.5) has to be satisfied on parts of the body Ω that are arbitrary environments of $\hat{\boldsymbol{x}}$ denoted by $\Omega_\varepsilon(\hat{\boldsymbol{x}}) \subset \Omega$. If $\boldsymbol{f}$ is piece-wise continuous, $\Omega_\varepsilon(\hat{\boldsymbol{x}})$ can be chosen such that $\boldsymbol{f}$ is continuous on $\Omega_\varepsilon(\hat{\boldsymbol{x}}) \times \Omega_\varepsilon(\hat{\boldsymbol{x}})$ almost everywhere. Then, by application of the mean value theorem for integrals, there exists a pair $\boldsymbol{x}_1, \boldsymbol{x}_2 \in \Omega_\varepsilon(\hat{\boldsymbol{x}})$ such that

$$\int_{\Omega_\varepsilon(\hat{x})} dV \int_{\Omega_\varepsilon(\hat{x})} dV' \boldsymbol{f}_s(\boldsymbol{x}', \boldsymbol{x}, t) = |\Omega_\varepsilon(\hat{\boldsymbol{x}})|^2 \boldsymbol{f}_s(\boldsymbol{x}_1, \boldsymbol{x}_2, t). \tag{A.6}$$

Now, assume that $\boldsymbol{f}_s(\hat{\boldsymbol{x}}, \hat{\boldsymbol{x}}, t) \neq \boldsymbol{0}$. Due to piece-wise continuity, by adjusting $\Omega_\varepsilon(\hat{\boldsymbol{x}})$, the minimum and maximum value of $\boldsymbol{f}_s$ on $\Omega_\varepsilon(\hat{\boldsymbol{x}})$ can be made arbitrarily close to $\boldsymbol{f}_s(\hat{\boldsymbol{x}}, \hat{\boldsymbol{x}}, t)$. Therefore, expression (A.6) is different from zero and (A.5) is violated. Consequently,

$$\boldsymbol{f}_s(\boldsymbol{x}, \boldsymbol{x}, t) = \boldsymbol{0} \tag{A.7}$$

Consider next two arbitrary particles $\hat{\boldsymbol{x}}$ and $\bar{\boldsymbol{x}} \neq \hat{\boldsymbol{x}}$ of Ω. Expression (A.5) reads for a certain subsection of the body that is defined to be $\Omega_\varepsilon(\hat{\boldsymbol{x}}) \cup \Omega_\varepsilon(\bar{\boldsymbol{x}})$

$$\int_{\Omega_\varepsilon(\hat{x}) \cup \Omega_\varepsilon(\bar{x})} dV \int_{\Omega_\varepsilon(\hat{x}) \cup \Omega_\varepsilon(\bar{x})} dV' \boldsymbol{f}_s = \boldsymbol{0},$$

and, using (A.2),

$$\int_{\Omega_\varepsilon(\hat{x})} dV \int_{\Omega_\varepsilon(\hat{x})} dV' \boldsymbol{f}_s + 2\int_{\Omega_\varepsilon(\hat{x})} dV \int_{\Omega_\varepsilon(\bar{x})} dV' \boldsymbol{f}_s + \int_{\Omega_\varepsilon(\bar{x})} dV \int_{\Omega_\varepsilon(\bar{x})} dV' \boldsymbol{f}_s = \boldsymbol{0}.$$

The mean value theorem implies (piece-wise continuity of $\boldsymbol{f}_s$ is assumed) that there are positions $\hat{\boldsymbol{x}}_1, \hat{\boldsymbol{x}}_2, \hat{\boldsymbol{x}}_3 \in \Omega_\varepsilon(\hat{\boldsymbol{x}})$ and $\bar{\boldsymbol{x}}_1, \bar{\boldsymbol{x}}_2, \bar{\boldsymbol{x}}_3 \in \Omega_\varepsilon(\bar{\boldsymbol{x}})$ such that the left hand side equals

$$|\Omega_\varepsilon(\hat{x})|^2 \boldsymbol{f}_s(\hat{\boldsymbol{x}}_1, \hat{\boldsymbol{x}}_2, t) + 2|\Omega_\varepsilon(\hat{x})||\Omega_\varepsilon(\bar{x})| \boldsymbol{f}_s(\hat{\boldsymbol{x}}_3, \bar{\boldsymbol{x}}_3, t) + |\Omega_\varepsilon(\bar{x})|^2 \boldsymbol{f}_s(\bar{\boldsymbol{x}}_1, \bar{\boldsymbol{x}}_2, t).$$

Let, without restriction of generality, $|\Omega_\varepsilon(\hat{\boldsymbol{x}})| = |\Omega_\varepsilon(\bar{\boldsymbol{x}})|$. Then (A.5) can be simplified to

$$2\boldsymbol{f}_s(\hat{\boldsymbol{x}}_3, \bar{\boldsymbol{x}}_3, t) = -\boldsymbol{f}_s(\hat{\boldsymbol{x}}_1, \hat{\boldsymbol{x}}_2, t) - \boldsymbol{f}_s(\bar{\boldsymbol{x}}_1, \bar{\boldsymbol{x}}_2, t).$$

Knowing that for $|\Omega_\varepsilon(\hat{\boldsymbol{x}})| \to 0$, $\hat{\boldsymbol{x}}_1, \hat{\boldsymbol{x}}_2, \hat{\boldsymbol{x}}_3 \to \hat{\boldsymbol{x}}$ and $\bar{\boldsymbol{x}}_1, \bar{\boldsymbol{x}}_2, \bar{\boldsymbol{x}}_3 \to \bar{\boldsymbol{x}}$, and using (A.7), it follows finally that

$$\boldsymbol{f}_s(\hat{\boldsymbol{x}}, \bar{\boldsymbol{x}}, t) = \boldsymbol{0} \quad \forall \hat{\boldsymbol{x}}, \bar{\boldsymbol{x}} \in \Omega.$$

Therefore,

$$\boldsymbol{f} = \boldsymbol{f}_a \quad \Rightarrow \quad \boldsymbol{f}(\boldsymbol{x}', \boldsymbol{x}, t) = -\boldsymbol{f}(\boldsymbol{x}, \boldsymbol{x}', t).$$

A.3 Pair-wise Forces are Central Forces

From (2.10) and (2.11) follows that

$$\int_\Omega dV \int_\Omega dV' \, \boldsymbol{y}(\boldsymbol{x}, t) \times \boldsymbol{f}(\boldsymbol{x}', \boldsymbol{x}, t) = \boldsymbol{0}$$

and

$$\int_\Omega dV \int_\Omega dV' \, \boldsymbol{y}(\boldsymbol{x}', t) \times \boldsymbol{f}(\boldsymbol{x}', \boldsymbol{x}, t) = \boldsymbol{0}.$$

With the definition

$$\boldsymbol{m}(\boldsymbol{x}', \boldsymbol{x}, t) = [\boldsymbol{y}(\boldsymbol{x}', t) - \boldsymbol{y}(\boldsymbol{x}, t)] \times \boldsymbol{f}(\boldsymbol{x}', \boldsymbol{x}, t),$$

the difference of the previous expressions reads

$$\int_\Omega dV \int_\Omega dV' \, \boldsymbol{m}(\boldsymbol{x}', \boldsymbol{x}, t) = \boldsymbol{0}. \tag{A.8}$$

(A.8) has to hold for Ω and all its subsections. The integrand $\boldsymbol{m}$ is a symmetric, as

$$\boldsymbol{m}(\boldsymbol{x}', \boldsymbol{x}, t) = \boldsymbol{m}(\boldsymbol{x}, \boldsymbol{x}', t).$$

Therefore, expression (A.8) is equivalent to (A.5), where the integrand had to vanish. Finally,

$$\boldsymbol{m} = (\boldsymbol{y}' - \boldsymbol{y}) \times \boldsymbol{f} = \boldsymbol{0} \quad \Rightarrow \quad (\boldsymbol{y}' - \boldsymbol{y}) \parallel \boldsymbol{f} \quad \Rightarrow \quad \boldsymbol{f} \parallel \boldsymbol{e}_r.$$

A.4 Global Power Balance

Multiplying the local balance of linear momentum (2.6) by the velocity $\dot{\boldsymbol{y}}$ and integrating over the body yields

$$\int_\Omega \rho_0 \frac{\partial}{\partial t}(\dot{\boldsymbol{y}} \cdot \dot{\boldsymbol{y}}) \, dV = \int_\Omega \boldsymbol{b}_{int} \cdot \dot{\boldsymbol{y}} \, dV + \int_\Omega \boldsymbol{b} \cdot \dot{\boldsymbol{y}} \, dV. \tag{A.9}$$

Next, in order to find the time derivative of the total kinetic energy (2.16), assume the field of kinetic energy density $\frac{1}{2}\rho_0 \dot{\boldsymbol{y}} \cdot \dot{\boldsymbol{y}}$ is discontinuous on $S_{\rho_0 \dot{\boldsymbol{y}}^2}(t)$ and continuous anywhere else, therefore,

$$\frac{d}{dt}E = \int_{\Omega \setminus S_{\rho_0 \dot{\boldsymbol{y}}^2}} \rho_0 \frac{\partial}{\partial t}(\dot{\boldsymbol{y}} \cdot \dot{\boldsymbol{y}}) dV - \int_{S_{\rho_0 \dot{\boldsymbol{y}}^2}} [[\frac{1}{2}\rho_0 \dot{\boldsymbol{y}} \cdot \dot{\boldsymbol{y}}]] \dot{s} \boldsymbol{n} \cdot d\boldsymbol{A}. \tag{A.10}$$

It is known from section 2.2.1 that the field of specific linear momentum $\rho_0 \dot{\boldsymbol{y}}$ is continuous except on surfaces $S_{\rho_0 \dot{\boldsymbol{y}}}$ that do not move. If $[[\rho_0]] = \boldsymbol{0}$, then $[[\dot{\boldsymbol{y}}]] = \boldsymbol{0}$, and $[[\dot{\boldsymbol{y}} \cdot \dot{\boldsymbol{y}}]] = 0$, implying that $[[\rho_0 \dot{\boldsymbol{y}} \cdot \dot{\boldsymbol{y}}]] = 0$ except on surfaces that cannot move. The normal speed $\dot{s}$ associated with $S_{\rho_0 \dot{\boldsymbol{y}}^2}$ is therefore zero. If $[[\rho_0]] \neq \boldsymbol{0}$, assume that there is a discontinuity surface $S_{\rho_0 \dot{\boldsymbol{y}}^2}$ that necessarily has to overlap with S_{ρ_0} across which the density is discontinuous. As the density field does not depend on time, S_{ρ_0}

does not move, and, therefore $S_{\rho_0 \dot{\boldsymbol{y}}^2}$ is fixed, too, and $\dot{s} = 0$. For any field of kinetic energy density that is compatible with the balance of momentum, the time derivative of the total kinetic energy reads

$$\frac{d}{dt}E = \int_\Omega \rho_0 \frac{\partial}{\partial t}(\dot{\boldsymbol{y}} \cdot \dot{\boldsymbol{y}}) dV. \tag{A.11}$$

From this and (A.9) follows immediately (2.15).

A.5 Internal Work Rate

This section shows that the expressions (2.17) and (2.20) are equal. First, note that

$$\dot{r} = \frac{d}{dt}|r| = \boldsymbol{e}_r \cdot \dot{\boldsymbol{r}} \quad \Rightarrow \quad f\dot{r} = \boldsymbol{f} \cdot \dot{\boldsymbol{r}} = \boldsymbol{f} \cdot [\dot{\boldsymbol{y}}(\boldsymbol{x}', t) - \dot{\boldsymbol{y}}(\boldsymbol{x}, t)]$$

The next steps start from (2.20) and involve changing order of integration, renaming integration variables and making use of (2.12) and finally (2.11):

$$\begin{aligned}
& \int_\Omega dV \, \frac{1}{2} \int_\Omega dV' \boldsymbol{f}(\boldsymbol{x}', \boldsymbol{x}, t) \cdot [\dot{\boldsymbol{y}}(\boldsymbol{x}', t) - \dot{\boldsymbol{y}}(\boldsymbol{x}, t)] \\
= \; & \frac{1}{2} \int_\Omega dV \int_\Omega dV' \, \boldsymbol{f}(\boldsymbol{x}', \boldsymbol{x}, t) \cdot \dot{\boldsymbol{y}}(\boldsymbol{x}', t) - \frac{1}{2} \int_\Omega dV \int_\Omega dV' \, \boldsymbol{f}(\boldsymbol{x}', \boldsymbol{x}, t) \cdot \dot{\boldsymbol{y}}(\boldsymbol{x}, t) \\
= \; & \frac{1}{2} \int_\Omega dV' \, \dot{\boldsymbol{y}}(\boldsymbol{x}', t) \cdot \int_\Omega dV \boldsymbol{f}(\boldsymbol{x}', \boldsymbol{x}, t) - \frac{1}{2} \int_\Omega dV \, \dot{\boldsymbol{y}}(\boldsymbol{x}, t) \cdot \int_\Omega dV' \boldsymbol{f}(\boldsymbol{x}', \boldsymbol{x}, t) \\
= \; & -\int_\Omega dV \, \dot{\boldsymbol{y}}(\boldsymbol{x}, t) \cdot \left[\int_\Omega dV' \boldsymbol{f}(\boldsymbol{x}', \boldsymbol{x}, t) \right] = -\int_\Omega dV \, \dot{\boldsymbol{y}} \cdot \boldsymbol{b}_{int}.
\end{aligned}$$

A.6 First Time Derivative of Elastic Energy

When taking the time derivative of the total elastic energy (2.23), special attention has to be paid again to the continuity of the integrands, this being the pair-wise elastic energy $\psi_{el}(\boldsymbol{x}', \boldsymbol{x}, t)$ and the elastic energy density $\bar{\psi}_{el}(\boldsymbol{x}, t)$.

Consider the pair-wise elastic energy $\psi_{el}(\boldsymbol{x}', \boldsymbol{x}, t) = \hat{\psi}_{el}(r, \boldsymbol{x}', \boldsymbol{x})$. It is important to carefully distinguish field function and constitutive function. From (2.39) follows that $\hat{\psi}_{el}$ is the integral of $\hat{f}_{el}$, which is assumed to be bounded. Therefore, $\hat{\psi}_{el}$ is

continuous in in r; with respect to $\boldsymbol{x}'$ or $\boldsymbol{x}$, $\hat{\psi}_{el}$ may only be piece-wise continuous. Therefore, necessary for $\psi_{el}(\boldsymbol{x}', \boldsymbol{x}, t)$ to be discontinuous with respect to $\boldsymbol{x}'$ or $\boldsymbol{x}$ is that either r is discontinuous or the body is discontinuously non-homogeneous. The latter case can be be ignored for the purpose of this analysis, as such a discontinuity cannot move with time, and, therefore, it does not affect time derivatives of ψ_{el} and $\bar{\psi}_{el}$. Without restriction of generality, it is henceforth assumed that the body is not discontinuously non-homogeneous.

If $r = |\boldsymbol{y}(\boldsymbol{x}', t) - \boldsymbol{y}(\boldsymbol{x}, t)|$ is discontinuous with respect to $\boldsymbol{x}$ for a fixed $\boldsymbol{x}'$, then $\boldsymbol{y}$ is discontinuous at $\boldsymbol{x}$. With the definition of the jump operator acting on $\psi_{el}(\boldsymbol{x}', \boldsymbol{x}, t)$

$$[[\psi_{el}]]_{x_1}(\boldsymbol{x}_2, \boldsymbol{n}, t) = \lim_{\varepsilon \to 0} \left[\psi_{el}(\boldsymbol{x}_1, \boldsymbol{x}_2 + \varepsilon \boldsymbol{n}, t) - \psi_{el}(\boldsymbol{x}_1, \boldsymbol{x}_2 - \varepsilon \boldsymbol{n}, t)\right],$$

the connection between $[[\psi_{el}]]$ and $[[\boldsymbol{y}]]$ can be expressed as

$$[[\psi_{el}]]_{x'}(\boldsymbol{x}, \boldsymbol{n}, t) \neq 0 \quad \Rightarrow \quad [[\boldsymbol{y}]](\boldsymbol{x}, \boldsymbol{n}, t) \neq \boldsymbol{0}. \tag{A.12}$$

Discontinuities in $\bar{\psi}_{el}$ and ψ_{el} are connected by:

$$\begin{aligned}
[[\bar{\psi}_{el}]](\boldsymbol{x}, \boldsymbol{n}, t) &= \lim_{\varepsilon \to 0} \left[\bar{\psi}_{el}(\boldsymbol{x} + \varepsilon \boldsymbol{n}, t) - \bar{\psi}_{el}(\boldsymbol{x} - \varepsilon \boldsymbol{n}, t)\right] \\
&= \lim_{\varepsilon \to 0} \int_{\Omega} dV' \, \frac{1}{2} \left[\psi_{el}(\boldsymbol{x}', \boldsymbol{x} + \varepsilon \boldsymbol{n}, t) - \psi_{el}(\boldsymbol{x}', \boldsymbol{x} - \varepsilon \boldsymbol{n}, t)\right] \\
&= \int_{\Omega} dV' \, \frac{1}{2} \lim_{\varepsilon \to 0} \left[\psi_{el}(\boldsymbol{x}', \boldsymbol{x} + \varepsilon \boldsymbol{n}, t) - \psi_{el}(\boldsymbol{x}', \boldsymbol{x} - \varepsilon \boldsymbol{n}, t)\right] \\
&= \int_{\Omega} dV' \, \frac{1}{2} [[\psi_{el}]]_{x'}(\boldsymbol{x}, \boldsymbol{n}, t).
\end{aligned} \tag{A.13}$$

Switching the limit operation and the integral was possible, because ψ_{el} is bounded and piecewise continuous, thus, it is integrable and limits exist everywhere. (A.13) implies that the elastic energy density $\bar{\psi}_{el}$ is spatially discontinuous in and at $\boldsymbol{x}$ only if the pair-wise elastic energy ψ_{el} is discontinuous in and at $\boldsymbol{x}$ for many different but fixed $\boldsymbol{x}'$. This implies together with (A.12) that

$$[[\bar{\psi}_{el}]] \neq \boldsymbol{0} \quad \Rightarrow \quad [[\boldsymbol{y}]] \neq \boldsymbol{0}$$

or in terms of discontinuity surfaces

$$S_{\bar{\psi}_{el}} \subseteq S_{\boldsymbol{y}}.$$

If the motions $\boldsymbol{y}(\boldsymbol{x},t)$ obey the balance of linear momentum, discontinuities in $\boldsymbol{y}$ cannot propagate according to section 2.2.1. It follows that

$$\frac{d}{dt}\Psi_{el} = \frac{1}{2}\int_{\Omega} dV \int_{\Omega} dV' \, \frac{\partial \hat{\psi}_{el}}{\partial r}\dot{r}. \tag{A.14}$$

To explore the energy landscape of deformations, it is useful to view $\boldsymbol{y}(\boldsymbol{x},t)$ as a family of fields of positions rather than an actual motion that satisfies the balance of linear momentum. In this case, $\boldsymbol{y}(\boldsymbol{x},t)$ may have moving discontinuities, and t is just a parameter. Assume that $\bar{\psi}_{el}$ is discontinuous on $S_{\bar{\psi}_{el}}$. Rather than $S_{\bar{\psi}_{el}}$, the possibly larger surface $S_{\boldsymbol{y}}$ is considered as discontinuity surface. The time derivative reads

$$\frac{d}{dt}\Psi_{el} = \int_{\Omega\backslash S_{\boldsymbol{y}}} dV \frac{\partial}{\partial t}\bar{\psi}_{el}(\boldsymbol{x},t) - \int_{S_{\boldsymbol{y}}} d\boldsymbol{A}\cdot\dot{s}\boldsymbol{n}[[\bar{\psi}_{el}]].$$

Replacing $S_{\bar{\psi}_{el}}$ by $S_{\boldsymbol{y}}$ was justified, because, first, it does not change the value of the volume integral, and, second, in the case that $\boldsymbol{x} \in S_{\boldsymbol{y}}\backslash S_{\bar{\psi}_{el}}$, then $[[\bar{\psi}_{el}]] = 0$, i.e., the surface integral remains unchanged. Using the the definition of $\bar{\psi}_{el}$ (2.22),

$$\frac{\partial}{\partial t}\bar{\psi}_{el}(\boldsymbol{x},t) = \frac{1}{2}\int_{\Omega\backslash S_{\boldsymbol{y}}} dV' \, f_{el}\dot{r} - \frac{1}{2}\int_{S_{\boldsymbol{y}}} d\boldsymbol{A}'\cdot\dot{s}\boldsymbol{n}[[\psi_{el}]]_x(\boldsymbol{x}',\boldsymbol{n},t)$$

and therefore by renaming the variables $\boldsymbol{x}$ and $\boldsymbol{x}'$,

$$\begin{aligned}
&\int_{\Omega\backslash S_{\boldsymbol{y}}} dV \, \frac{\partial}{\partial t}\bar{\psi}_{el}(\boldsymbol{x},t) = \int_{\Omega\backslash S_{\boldsymbol{y}}} dV' \, \frac{\partial}{\partial t}\bar{\psi}_{el}(\boldsymbol{x}',t) \\
= \;& \frac{1}{2}\int_{\Omega\backslash S_{\boldsymbol{y}}} dV' \int_{\Omega\backslash S_{\boldsymbol{y}}} dV \, f_{el}\dot{r} - \frac{1}{2}\int_{\Omega\backslash S_{\boldsymbol{y}}} dV' \int_{S_{\boldsymbol{y}}} d\boldsymbol{A}\cdot\dot{s}\boldsymbol{n}[[\psi_{el}]]_{x'}(\boldsymbol{x},\boldsymbol{n},t).
\end{aligned}$$

In the last term, the order of integration can be exchanged (as the integrand is bounded) which yields expression (A.13). Putting everything together and integrating

over Ω rather than $\Omega \backslash S_{\boldsymbol{y}}$, the time derivative of the elastic energy finally reads

$$\frac{d}{dt}\Psi_{el} = \frac{1}{2}\int_{\Omega} dV \int_{\Omega} dV'\ f_{el}\dot{r} - 2\int_{S_{\boldsymbol{y}}} d\boldsymbol{A}\cdot\dot{s}\boldsymbol{n}[[\bar{\psi}_{el}]]. \tag{A.15}$$

A.7 Stationarity of Potential Energy

Let $\Delta\boldsymbol{u} = \Delta\boldsymbol{u}(\boldsymbol{x},\varepsilon)$ be a one parameter family of admissible incremental deformations with the properties that

- $\Delta\boldsymbol{u}(\boldsymbol{x},0) = \boldsymbol{0}$,
- $\Delta\boldsymbol{u}(\boldsymbol{x},\varepsilon) = \boldsymbol{0}$ for $\boldsymbol{x}\in\Omega_u$, and
- $\Delta\boldsymbol{u}$ is piece-wise continuous in $\boldsymbol{x}$ and continuous in ε, i.e., discontinuities in $\boldsymbol{x}$ do not move with ε.

Discontinuities in $\boldsymbol{x}$ represent cracks, that are not allowed to move in their normal direction, however, their crack lip distance may increase. Surfaces where $\Delta\boldsymbol{u}$ is continuous but non-smooth represent phase boundaries in the classical sense, and they are allowed to form and to move. Consequently, $\delta\boldsymbol{u}(\boldsymbol{x}) = \frac{\partial}{\partial\varepsilon}\Delta\boldsymbol{u}(\boldsymbol{x},\varepsilon)|_{\varepsilon=0}$ is well defined and bounded. Also, $\delta\boldsymbol{u}(\boldsymbol{x}) = \boldsymbol{0}$ if $\boldsymbol{x}\in\Omega_u$.

The stationarity of (2.56) at $\boldsymbol{u} = \boldsymbol{u}(\boldsymbol{x})$ with respect to these increments $\Delta\boldsymbol{u}$ is established when the variation of Π vanishes for all $\delta\boldsymbol{u}$, i.e.,

$$\delta\Pi[\boldsymbol{u}] = \frac{d}{d\varepsilon}\Pi[\boldsymbol{u}(\boldsymbol{x}) + \Delta\boldsymbol{u}(\boldsymbol{x},\varepsilon)]\Big|_{\varepsilon=0} = 0 \qquad \forall\delta\boldsymbol{u}. \tag{A.16}$$

The definition $\boldsymbol{u}(\boldsymbol{x},t) = \boldsymbol{u}(\boldsymbol{x}) + \Delta\boldsymbol{u}(\boldsymbol{x},t)$ (implying that $\dot{\boldsymbol{u}}(\boldsymbol{x},0) = \delta\boldsymbol{u}(\boldsymbol{x})$) shows that the variation is essentially a time derivative. For fixed $S_{\boldsymbol{y}}$, the time derivative of Ψ_{el} is given by (A.14). As the material is assumed to be elastic, $\partial\hat{\psi}_{el}/\partial r = f$. Then the variation of Π reads

$$\delta\Pi[\boldsymbol{u}] = \frac{1}{2}\int_{\Omega} dV \int_{\Omega} dV'\ \boldsymbol{f}(\boldsymbol{x}',\boldsymbol{x})\cdot[\delta\boldsymbol{u}(\boldsymbol{x}') - \delta\boldsymbol{u}(\boldsymbol{x})] - \int_{\Omega}\boldsymbol{b}_*(\boldsymbol{x})\cdot\delta\boldsymbol{u}(\boldsymbol{x})$$

Rearrangements similar to those in section A.5 yield

$$\delta\Pi[\boldsymbol{u}] = -\int_{\Omega_b} dV \;\; \delta\boldsymbol{u}(\boldsymbol{x}) \cdot \left[\int_{\Omega} dV' \; \boldsymbol{f}(\boldsymbol{x}', \boldsymbol{x}) + \boldsymbol{b}_*(\boldsymbol{x})\right]. \tag{A.17}$$

Stationarity requires (A.16) to hold for all $\delta\boldsymbol{u}$, or equivalently that the integrand in (A.17) vanishes on Ω_b almost everywhere, i.e., that the equilibrium condition be satisfied.

A.8 Waves

P-Waves. $\bar{\boldsymbol{u}} \parallel \boldsymbol{k}$ is a solution to (2.81), if $\boldsymbol{k}$ is an eigenvector of $\boldsymbol{M}$ given by (2.85). This can be established by showing that $\boldsymbol{M}\boldsymbol{k}$ is parallel to $\boldsymbol{k}$. Define the unit vector $\boldsymbol{e}_k = \boldsymbol{k}/k$ and a unit vector $\boldsymbol{e}_s$ that is arbitrary, but orthogonal to $\boldsymbol{e}_k$, i.e., $\boldsymbol{e}_s \cdot \boldsymbol{e}_k = 0$. The dot product of $\boldsymbol{M}\boldsymbol{e}_k$ and $\boldsymbol{e}_s$

$$\boldsymbol{e}_s \cdot \boldsymbol{M}\boldsymbol{e}_k = \int_{\mathbb{R}^3} dV_\xi \; (1 - \cos \boldsymbol{k} \cdot \boldsymbol{\xi}) \; C(\xi) \; (\boldsymbol{e}_s \cdot \boldsymbol{e}_\xi)(\boldsymbol{e}_\xi \cdot \boldsymbol{e}_k) = 0 \tag{A.18}$$

vanishes, as for any $\boldsymbol{\xi}$, there exists another $\boldsymbol{\xi}^*$ for which the integrand has the same absolute value with opposite sign[1]. This implies that $\boldsymbol{M}\boldsymbol{k}$ is orthogonal to any vector that is orthogonal to $\boldsymbol{k}$ itself; therefore, $\boldsymbol{M}\boldsymbol{k} \parallel \boldsymbol{k}$. The eigenvalue associated with $\boldsymbol{k}$ reads

$$\rho\omega^2(k) = \boldsymbol{e}_k \cdot \boldsymbol{M}\boldsymbol{e}_k = \int_{\mathbb{R}^3} dV_\xi \; (1 - \cos \boldsymbol{k} \cdot \boldsymbol{\xi}) \; C(\xi) \; (\boldsymbol{e}_\xi \cdot \boldsymbol{e}_k)^2.$$

As $\boldsymbol{k}$ appears only in the dot product with $\boldsymbol{\xi}$, and the integral with respect to $\boldsymbol{\xi}$ is taken over the entire space $\mathbb{R}^3$, the eigenvalue does not depend on the orientation of $\boldsymbol{k}$ and can be expressed by (2.86).

S-Waves. All $\bar{\boldsymbol{u}}$ with $\bar{\boldsymbol{u}} \cdot \boldsymbol{k} = 0$ are solutions to (2.81), if every $\boldsymbol{e}_s$ is is an eigenvector of $\boldsymbol{M}$. It is already established that $\boldsymbol{M}\boldsymbol{e}_s$ is orthogonal to $\boldsymbol{e}_k$. If $\boldsymbol{M}\boldsymbol{e}_s$ is also

[1] e.g., when $\boldsymbol{\xi}^* = (2\boldsymbol{e}_k \otimes \boldsymbol{e}_k - \boldsymbol{1})\, \boldsymbol{\xi}$

orthogonal to $(\boldsymbol{e}_k \times \boldsymbol{e}_s)$, then $\boldsymbol{M}\boldsymbol{e}_s \parallel \boldsymbol{e}_s$ and $\boldsymbol{e}_s$ is an eigenvector:

$$(\boldsymbol{e}_k \times \boldsymbol{e}_s) \cdot \boldsymbol{M}\boldsymbol{e}_s = \int_{\mathbb{R}^3} dV_\xi \, (1 - \cos \boldsymbol{k} \cdot \boldsymbol{\xi}) \, C(\xi) \, (\boldsymbol{e}_k \times \boldsymbol{e}_s) \cdot \boldsymbol{e}_\xi \, (\boldsymbol{e}_\xi \cdot \boldsymbol{e}_k) = 0.$$

Again, for every $\boldsymbol{\xi}$ there exists another $\boldsymbol{\xi}^*$ for which the integrand has the same absolute value with opposite sign[2]. The eigenvalue associated with $\boldsymbol{e}_s$ reads

$$\rho\omega^2(k) = \boldsymbol{e}_s \cdot \boldsymbol{M}\boldsymbol{e}_s = \int_{\mathbb{R}^3} dV_\xi \, (1 - \cos \boldsymbol{k} \cdot \boldsymbol{\xi}) \, C(\xi) \, (\boldsymbol{e}_\xi \cdot \boldsymbol{e}_s)^2,$$

which is independent of the orientation of $\boldsymbol{k}$ for the same reason as above, and can, therefore, be expressed as (2.87).

Phase Speeds at $k = 0$. The phase speed of a wave is defined as $c_{ph}(k) = \omega(k)/k$, therefore, $c_{ph}(0) = \omega'(0)$. $\rho\omega^2(k)$ is given by (2.86) and (2.87). To avoid inverting these expressions and taking the derivative of the square root, the phase speed is more conveniently computed by making use of

$$\frac{d}{dk}\omega^2(k) = 2\omega'(k)\,\omega(k) \quad \Rightarrow \quad \omega'(k) = \frac{\frac{d}{dk}\omega^2(k)}{2\omega(k)} \quad \rightarrow \quad \frac{\frac{d^2}{dk^2}\omega^2(k)}{2\omega'(k)}$$
$$\Rightarrow \quad [\omega'(0)]^2 = \frac{1}{2}\lim_{k\to 0}\frac{d^2}{dk^2}\omega^2(k) = c_{ph}^2(0);$$

then the phase speed at $k = 0$ is for P-waves

$$\rho c_{ph;P}^2(0) = \lim_{k\to 0}\left[\frac{d^2}{dk^2}\,\boldsymbol{e}_k \cdot \boldsymbol{M}\boldsymbol{e}_k\right] = \int_{\mathbb{R}^3} dV_\xi \, (\boldsymbol{e}_\xi \cdot \boldsymbol{e}_1)^4 \, \xi^2 C(\xi),$$

and for S-waves

$$\rho c_{ph;S}^2(0) = \lim_{k\to 0}\left[\frac{d^2}{dk^2}\,\boldsymbol{e}_s \cdot \boldsymbol{M}\boldsymbol{e}_s\right] = \int_{\mathbb{R}^3} dV_\xi \, (\boldsymbol{e}_\xi \cdot \boldsymbol{e}_1)^2 (\boldsymbol{e}_\xi \cdot \boldsymbol{e}_2)^2 \, \xi^2 C(\xi).$$

Integration with respect to the angles of spherical coordinates yields the expressions (2.88) and (2.89) for one, two and three dimensions.

[2] e.g., when $\boldsymbol{e}_t = \boldsymbol{e}_k \times \boldsymbol{e}_s$ and $\boldsymbol{\xi}^* = (2\boldsymbol{e}_t \otimes \boldsymbol{e}_t - \mathbf{1})\,\boldsymbol{\xi}$

A.9 Infinitesimal Stability

Let the incremental deformation $\Delta\boldsymbol{u}(\boldsymbol{x},\varepsilon)$, defined in section A.7, be smooth with respect to ε, meaning that the motion of a non-smoothness, like a moving phase boundary (in the classical sense) is excluded from the stability analysis. This, however, constitutes practically no restriction, as these motions are incompatible with the conservation of linear momentum, see section 2.2.1 – even if the energy is not a minimum in this direction, the system cannot evolve towards an unstable trajectory in this direction anyway.

The potential energy is at a relative minimum if the first order variation (A.16) vanishes, and the second order variation

$$\begin{aligned}\delta^2\Pi[\boldsymbol{u}] &= \frac{d^2}{d\varepsilon^2}\Pi[\boldsymbol{u}(\boldsymbol{x})+\Delta\boldsymbol{u}(\boldsymbol{x},\varepsilon)]\Big|_{\varepsilon=0} \\ &= \frac{1}{2}\int_\Omega dV\int_\Omega dV'\,[\delta\boldsymbol{u}(\boldsymbol{x}')-\delta\boldsymbol{u}(\boldsymbol{x})]\cdot\boldsymbol{C}[\delta\boldsymbol{u}(\boldsymbol{x}')-\delta\boldsymbol{u}(\boldsymbol{x})] \qquad \text{(A.19)}\end{aligned}$$

is greater than zero for all $\delta\boldsymbol{u}$. This is the case if and only if the eigenvalue problem

$$\int_\Omega dV'\,\boldsymbol{C}[\boldsymbol{v}(\boldsymbol{x}')-\boldsymbol{v}(\boldsymbol{x})]+\beta\boldsymbol{v}(\boldsymbol{x})=\boldsymbol{0} \qquad \boldsymbol{x}\in\Omega_b \qquad \text{(A.20)}$$

has only positive eigenvalues β associated with eigenvectors $\boldsymbol{v}(\boldsymbol{x})$, with $\boldsymbol{v}(\boldsymbol{x})=\boldsymbol{0}$ if $\boldsymbol{x}\in\Omega_u$. The condition (A.20) can be derived following Silling [61]: As $\boldsymbol{C}$ is bounded, the variation (A.19) must have a direction of minimum growth. A direction is expressed by a unit vector with

$$\int_{\Omega_b} dV\;\boldsymbol{v}\cdot\boldsymbol{v}=1. \qquad \text{(A.21)}$$

Taking the functional derivative of (A.19) with respect to $\delta\boldsymbol{u}$ and with $\boldsymbol{v}$ as variational increment yields (A.20) with β as Lagrangian multiplier for the constraint (A.21).

A.10 Small Scale Stability

Stability of Pairs and Small Scale Stability. A sum of positive definite tensors is also positive definite. The integral value $\boldsymbol{M}$ in (2.91) is a limit of sums. If the integrand of (2.91) is positive definite for all $\boldsymbol{\xi}$, then $\boldsymbol{M}$ is positive definite. Each value of $\boldsymbol{\xi}$ represents a particular pair, thus, if all pairs are stable small scale stability follows.

A sum of tensors can only be not positive definite if at least one of the elements of the sum is not positive definite. (This statement is easily proofed by exclusion of the contrary.) Therefore, $\boldsymbol{M}$ can only be not positive definite if the integrand is not positive definite for some values of $\boldsymbol{\xi}$. Therefore, small scale instability requires necessarily the instability of some pairs.

Stability of Pairs. A pair $\boldsymbol{\xi}$ is stable (unstable or neutrally stable) if the integrand of (2.91) is (is not) positive definite. The factor $(1 - \cos \boldsymbol{k} \cdot \boldsymbol{\xi})$ can be ignored as far as statements about the stability of pairs are concerned: the factor is either positive, i.e., it preserves the sign of the remaining expression, or it is zero on an interval of values for $\boldsymbol{k}$ that has a zero measure, i.e., the remaining expression does not make a contribution to the integral.

Multiplying the remaining part of the integrand twice by an arbitrary unit vector $\boldsymbol{e}$ yields

$$\boldsymbol{e} \cdot \left[\frac{\partial \hat{f}}{\partial r} \boldsymbol{e}_r \otimes \boldsymbol{e}_r + \frac{\hat{f}}{r} (\mathbf{1} - \boldsymbol{e}_r \otimes \boldsymbol{e}_r) \right] \boldsymbol{e} = \left(\frac{\partial \hat{f}}{\partial r} - \frac{\hat{f}}{r} \right) \cos^2 \phi + \frac{\hat{f}}{r}, \tag{A.22}$$

where $\cos \phi = \boldsymbol{e} \cdot \boldsymbol{e}_r$, and $\phi \in [0, 2\pi)$ is an arbitrary angle having absorbed the arbitrariness of $\boldsymbol{e}$. The expression $\cos^2 \phi$ assumes all values on the interval $[0, 1]$. Therefore, (A.22) may assume values between $\frac{\partial \hat{f}}{\partial r}$ and $\frac{\hat{f}}{r}$. A pair is stable, if (A.22) is positive for all ϕ. This is the case when

$$\frac{\partial \hat{f}}{\partial r} > 0 \qquad \text{and} \qquad \frac{\hat{f}}{r} > 0.$$

In turn, the pair is not stable (i.e., unstable or neutrally stable) if

$$\frac{\partial \hat{f}}{\partial r} \leq \frac{\hat{f}}{r} \qquad \text{or} \qquad \frac{\hat{f}}{r} \leq 0.$$

A.11 Transition to Strain Gradient Model

This section shows how the peridynamic interaction force term can be expressed in the form of (3.2), provided that the displacement field and the force law are sufficiently smooth. It will be convenient, to write the interaction force with (3.1) as

$$\boldsymbol{f} = \frac{E}{l^{n+1}} \bar{f}\left(\lambda, \bar{\xi}\right) \boldsymbol{e}_r = \frac{E}{l^{n+1}} \bar{\boldsymbol{f}}\left(\boldsymbol{\lambda}, \bar{\xi}\right)$$

where $\boldsymbol{\lambda} = \boldsymbol{r}/\xi$, and n is the number of dimensions of Ω. Provided that the deformation is sufficiently smooth, $\boldsymbol{y}$ can be expanded in a Taylor series at $\boldsymbol{x}$ with

$$\boldsymbol{y}(\boldsymbol{x}', t) = \boldsymbol{y}(\boldsymbol{x}, t) + \frac{\partial \boldsymbol{y}}{\partial x_j}(\boldsymbol{x}, t)\xi_j + \frac{\partial^2 \boldsymbol{y}}{\partial x_j \partial x_k}(\boldsymbol{x}, t)\frac{\xi_j \xi_k}{2} + ...$$

or with $\boldsymbol{F} = \partial \boldsymbol{y}/\partial \boldsymbol{x}$, $\bar{\boldsymbol{\xi}} = \boldsymbol{\xi}/l$, $\boldsymbol{e}_\xi = \boldsymbol{e}_\xi/\xi$ and $e_j = (\boldsymbol{e}_\xi)_j$,

$$\boldsymbol{\lambda} = \boldsymbol{F}\boldsymbol{e}_\xi + \Delta\boldsymbol{\lambda} \qquad \Delta\boldsymbol{\lambda} = l\boldsymbol{A}_1 + l^2\boldsymbol{A}_2 + ... = o(l) \tag{A.23}$$

$$\boldsymbol{A}_1 = \frac{\partial^2 \boldsymbol{y}}{\partial x_j \partial x_k}\frac{e_j \bar{\xi}_k}{2} \qquad \boldsymbol{A}_2 = \frac{\partial^3 \boldsymbol{y}}{\partial x_j \partial x_k \partial x_l}\frac{e_j \bar{\xi}_k \bar{\xi}_l}{3!} \qquad ...$$

For the change of coordinates from $\boldsymbol{x}'$ to $\bar{\boldsymbol{\xi}}$ in the integral expressions, a normalized volume element is defined as $d\bar{V} = dV/l^n$. The normalized domain of integration is

denoted by $\bar{\Omega}$. Expanding the force with respect to $\boldsymbol{\lambda}$ yields

$$\begin{aligned}
\int_\Omega dV'\, \boldsymbol{f} &= \frac{E}{l}\int_\Omega \frac{dV'}{l^3}\, \bar{\boldsymbol{f}}(\boldsymbol{F}\boldsymbol{e}_\xi + \Delta\boldsymbol{\lambda}, \bar{\xi}) \\
&= \frac{E}{l}\int_{\bar{\Omega}} d\bar{V}_\xi\, \left[\bar{\boldsymbol{f}}(\boldsymbol{F}\boldsymbol{e}_\xi, \bar{\xi}) + \frac{\partial \bar{\boldsymbol{f}}}{\partial \lambda_j}(\boldsymbol{F}\boldsymbol{e}_\xi, \bar{\xi})\Delta\lambda_j + \frac{1}{2}\frac{\partial^2 \bar{\boldsymbol{f}}}{\partial\lambda_j\partial\lambda_k}(\boldsymbol{F}\boldsymbol{e}_\xi, \bar{\xi})\Delta\lambda_j\Delta\lambda_k + ...\right] \\
&= \frac{E}{l}\int_{\bar{\Omega}} d\bar{V}_\xi\, \left[\bar{\boldsymbol{f}} + l\frac{\partial \bar{\boldsymbol{f}}}{\partial \boldsymbol{\lambda}}\cdot\boldsymbol{A}_1 + l^2\left(\frac{\partial \bar{\boldsymbol{f}}}{\partial \boldsymbol{\lambda}}\cdot\boldsymbol{A}_2 + \frac{1}{2}\frac{\partial^2 \bar{\boldsymbol{f}}}{\partial\lambda_j\partial\lambda_k}A_{1,j}A_{1,k}\right) + ...\right] \\
&= \frac{1}{l}\,\boldsymbol{R}_{-1} + \boldsymbol{R}_0 + l\,\boldsymbol{R}_1 + l^2\,\boldsymbol{R}_2 + o(l^3)
\end{aligned}$$

with

$$\begin{aligned}
\boldsymbol{R}_{-1} &= \left[E\int_{\bar{\Omega}} d\bar{V}_\xi\, \bar{\boldsymbol{f}}(\boldsymbol{F}\boldsymbol{e}_\xi, \bar{\xi})\right] \\
\boldsymbol{R}_0 &= \left[\frac{E}{2}\int_{\bar{\Omega}} d\bar{V}_\xi\, \frac{\partial \bar{\boldsymbol{f}}}{\partial\lambda_s}(\boldsymbol{F}\boldsymbol{e}_\xi, \bar{\xi})e_j\bar{\xi}_k\right]\, \frac{\partial^2 y_s}{\partial x_j\partial x_k} \\
\boldsymbol{R}_1 &= \left[\frac{E}{6}\int_{\bar{\Omega}} d\bar{V}_\xi\, \frac{\partial \bar{\boldsymbol{f}}}{\partial\lambda_s}(\boldsymbol{F}\boldsymbol{e}_\xi, \bar{\xi})e_j\bar{\xi}_k\bar{\xi}_l\right]\, \frac{\partial^3 y_s}{\partial x_j\partial x_k\partial x_l} \\
&\quad + \left[\frac{E}{8}\int_{\bar{\Omega}} d\bar{V}_\xi\, \frac{\partial^2 \bar{\boldsymbol{f}}}{\partial\lambda_j\partial\lambda_k}(\boldsymbol{F}\boldsymbol{e}_\xi, \bar{\xi})e_m\bar{\xi}_n e_p\bar{\xi}_q\right]\frac{\partial^2 y_j}{\partial x_m\partial x_n}\frac{\partial^2 y_k}{\partial x_p\partial x_q} \\
&= B_{ijklm}(\boldsymbol{F})\frac{\partial^3 y_j}{\partial x_k\partial x_l\partial x_m} + B_{ijklmnp}(\boldsymbol{F})\frac{\partial^2 y_j}{\partial x_k\partial x_l}\frac{\partial^2 y_m}{\partial x_n\partial x_p} \\
&...
\end{aligned}$$

The expressions in brackets depend only on $\boldsymbol{F}$.

Note that $\boldsymbol{R}_{-1}$ and the tensor B_{ijklm} in $\boldsymbol{R}_1$ vanish if $\boldsymbol{x}$ is sufficiently far away from the boundary; this is a consequence of (2.12). In order to show that $\boldsymbol{R}_0 = \text{Div}\,\hat{\boldsymbol{\sigma}}_0(\boldsymbol{F})$, the definition of the first Piola-Kirchhoff stress (2.62) is combined with (3.2) for a gradient field $\boldsymbol{F} = \boldsymbol{F}(\boldsymbol{x}, t)$:

$$\begin{aligned}
\text{Div}\,\hat{\boldsymbol{\sigma}}_0(\boldsymbol{F}) &= \frac{E}{2}\,\text{Div}\,\left[\int_\Omega \frac{dV_\xi}{l^n}\, \bar{\boldsymbol{f}}\left(\boldsymbol{F}\boldsymbol{e}_\xi, \bar{\xi}\right)\otimes\frac{\boldsymbol{\xi}}{l}\right] \\
&= \frac{E}{2}\int_{\bar{\Omega}} d\bar{V}_\xi\, \frac{\partial \bar{\boldsymbol{f}}}{\partial\boldsymbol{\lambda}}(\boldsymbol{F}\boldsymbol{e}_\xi, \bar{\xi})\frac{\partial \boldsymbol{F}}{\partial x_k}\boldsymbol{e}_\xi\,\bar{\xi}_k \\
&= \left[\frac{E}{2}\int_{\bar{\Omega}} d\bar{V}_\xi\, \frac{\partial \bar{\boldsymbol{f}}}{\partial\boldsymbol{\lambda}}(\boldsymbol{F}\boldsymbol{e}_\xi, \bar{\xi})e_j\,\bar{\xi}_k\right]\frac{\partial^2 \boldsymbol{y}}{\partial x_j\partial x_k} = \boldsymbol{R}_0.
\end{aligned}$$

For approximation purposes, the series may be truncated. The approximation is good, if the terms that were left out are small. Consider the terms $l^m \boldsymbol{R}_m$ in the series. For a given value of the deformation gradient $\boldsymbol{F}$, they are small when the product of higher order gradients and length l is small. Therefore, ignoring terms of higher order than l^n requires usually that at least

$$\left\| \frac{\partial^m \boldsymbol{y}}{\partial x_j \partial x_k ... \partial x_p} \right\| << \frac{1}{l^{m-1}} \qquad \forall m > n$$

where $\|.\|$ denotes a tensor norm. Note that gradients of order less than n may still affect higher order terms due the non-linearities. Depending on the constitutive functions $B(\boldsymbol{F})$, they might have to be small, too.

A.12 Transition to Classical Elasticity

The results of the previous section imply that for $l \to 0$

$$\int_\Omega dV' \, \boldsymbol{f} \to \text{Div } \hat{\boldsymbol{\sigma}}_0(\boldsymbol{F}) \qquad \boldsymbol{x} \in \Omega \backslash \partial\Omega.$$

This equation holds on all regions of smooth deformations. *After* the transition to $l = 0$ is made, boundary conditions are only required on $\partial\Omega_b$. On $\partial\Omega_b \cap \partial\Omega_u$ the deformation may be prescribed. On $\partial\Omega_b \backslash \partial\Omega_u$, the sum of forces acting across the free boundaries is zero, therefore,

$$\hat{\boldsymbol{\sigma}}_0(\boldsymbol{F}(\boldsymbol{x}, t))\boldsymbol{n} = \boldsymbol{0} \qquad \boldsymbol{x} \in \partial\Omega_b \backslash \partial\Omega_b.$$

A.13 Transition to Integral Model with Strain

In this section, the linearized peridynamic equation of motion (2.77) is derived from the equation of motion of the non-local integral-type model, given by (3.10) and (3.11).

Let c_{ijkl}, C_{ij}, u_i and ε_{ij} represent the components of the forth order stiffness

kernel $\boldsymbol{c}(\boldsymbol{x}', \boldsymbol{x})$, the stiffness tensor $\boldsymbol{C}(\boldsymbol{x}', \boldsymbol{x})$, the displacement field $\boldsymbol{u}(\boldsymbol{x})$ and the strain tensor $\boldsymbol{\varepsilon}(\boldsymbol{x})$, respectively. Define $\boldsymbol{C}$ as

$$C_{il}(\boldsymbol{x}', \boldsymbol{x}) = -\frac{\partial^2 c_{ijkl}}{\partial x_j \partial x'_k}(\boldsymbol{x}', \boldsymbol{x}). \tag{A.24}$$

If $\boldsymbol{x}$ is sufficiently far away from the boundary and $\boldsymbol{c}$ and its derivatives go to zero fast enough for $|\boldsymbol{x}' - \boldsymbol{x}| \to \infty$, e.g., because $\boldsymbol{c}$ has a finite support, then the area integral

$$\int_{\partial\Omega} dA'_k \left[\frac{\partial c_{ijkl}}{\partial x_j}(\boldsymbol{x}', \boldsymbol{x}) \, [u_l(\boldsymbol{x}') - u_l(\boldsymbol{x})] \right]$$

is zero. Applying the Gauss theorem yields:

$$\begin{aligned}
0 &= \int_\Omega dV' \, \frac{\partial}{\partial x'_k} \left[\frac{\partial c_{ijkl}}{\partial x_j}(\boldsymbol{x}', \boldsymbol{x}) \, [u_l(\boldsymbol{x}') - u_l(\boldsymbol{x})] \right] \\
&= \int_\Omega dV' \, \left[\frac{\partial^2 c_{ijkl}}{\partial x'_k \partial x_j}(\boldsymbol{x}', \boldsymbol{x}) \right] [u_l(\boldsymbol{x}') - u_l(\boldsymbol{x})] + \int_\Omega dV' \, \frac{\partial c_{ijkl}}{\partial x_j}(\boldsymbol{x}', \boldsymbol{x}) \, \frac{\partial u_l}{\partial x'_k}(\boldsymbol{x}') \\
&= -\int_\Omega dV' \, C_{il}(\boldsymbol{x}', \boldsymbol{x}) [u_l(\boldsymbol{x}') - u_l(\boldsymbol{x})] + \frac{\partial}{\partial x_j} \int_\Omega dV' \, c_{ijkl}(\boldsymbol{x}', \boldsymbol{x}) \, \varepsilon_{kl}(\boldsymbol{x}').
\end{aligned}$$

Replacing the gradient of u_l by ε_{kl} was possible because of the symmetry of $\boldsymbol{C}(\boldsymbol{x}', \boldsymbol{x}) = \boldsymbol{C}(\boldsymbol{x}, \boldsymbol{x}')$. From this follows that

$$\mathrm{Div} \int_\Omega dV' \, \boldsymbol{c} \, \boldsymbol{\varepsilon} = \int_\Omega dV' \, \boldsymbol{C}\boldsymbol{r}$$

and if $\boldsymbol{c}_0 = \boldsymbol{0}$, then (3.10) implies (2.77) for inviscid materials.

Note that there was no requirement on the smoothness of the integrand, in particular on $\boldsymbol{u}$. In fact, the displacement field may be discontinuous. For the equations to remain valid, the strain field has to be interpreted as a generalized function of the type of a delta function distribution, and the Gauss theorem can be applied.

For two- and three-dimensional bodies, it remains to be shown for what $\boldsymbol{c}$, the tensor $\boldsymbol{C}$ assumes the form of a peridynamic stiffness tensor (2.78) that can be derived from an actual pair-wise force law. This shall be done for homogeneous and isotropic

materials, therefore, let

$$\boldsymbol{c} = \boldsymbol{c}(\xi) = \lambda(\xi)\mathbf{1} \otimes \mathbf{1} + 2\mu(\xi)\boldsymbol{I}_{\mathrm{sym}},$$

where $\boldsymbol{I}_{\mathrm{sym}}$ is the symmetrizer with $(\boldsymbol{I}_{\mathrm{sym}})_{ijkl} = \frac{1}{2}(\delta_{ik}\delta_{jl} + \delta_{il}\delta_{jk})$. Then, $\boldsymbol{C}$ reads

$$C_{il} = -\frac{\partial^2 c_{ijkl}(\xi)}{\partial x_j \partial x'_k} = \frac{\partial^2 c_{ijkl}(\xi)}{\partial \xi_j \partial \xi_k} = \frac{\partial^2 \lambda(\xi)}{\partial \xi_i \partial \xi_l} + \frac{\partial^2 \mu(\xi)}{\partial \xi_k \partial \xi_k} + \frac{\partial^2 \mu(\xi)}{\partial \xi_i \partial \xi_i}\delta_{il}$$

or in symbolic notation, with $\boldsymbol{\nabla} = \partial/\partial\boldsymbol{\xi}$,

$$\boldsymbol{C} = \boldsymbol{\nabla} \otimes \boldsymbol{\nabla}\lambda + \boldsymbol{\nabla} \otimes \boldsymbol{\nabla}\mu + \boldsymbol{\nabla} \cdot \boldsymbol{\nabla}\mu\mathbf{1}$$

Using the identities $\boldsymbol{\nabla}\xi = \boldsymbol{e}_\xi$ and $\boldsymbol{\nabla}\boldsymbol{e}_\xi = \frac{1}{\xi}\left[\mathbf{1} - \boldsymbol{e}_\xi \otimes \boldsymbol{e}_\xi\right]$, with $\boldsymbol{e}_\xi = \boldsymbol{\xi}/\xi$, finally, the stiffness tensor can be written as

$$\boldsymbol{C} = \left[\lambda'' + \mu'' - \frac{\lambda' + \mu'}{\xi}\right]\boldsymbol{e}_\xi \otimes \boldsymbol{e}_\xi + \left[\mu'' + \frac{\lambda' + n\mu'}{\xi}\right]\mathbf{1}, \tag{A.25}$$

where n denotes the dimensions of the body Ω. Comparison with (2.78) yields the pair-wise forces in the reference configuration

$$\hat{f}_0(\xi) = \xi\mu'' + \lambda' + n\mu'. \tag{A.26}$$

This seems to suggest that, as long as non-zero reference forces are admitted, any functions μ and λ are acceptable. However, the requirement that the reference configuration shall be free of stresses limits their choice. Using the definition of the first Piola-Kirchhoff stress (2.62) and setting it zero gives the requirement

$$\int_\Omega dV'\ \hat{f}_0(\xi)\boldsymbol{\xi} \otimes \boldsymbol{e}_\xi = \gamma\mathbf{1}\int_0^\infty d\xi\ \hat{f}_0(\xi)\xi^n = \mathbf{0},$$

where γ is a constant resulting from integration with respect to angles. Combing this

with (A.26) and integration by parts yields

$$\int_0^\infty d\xi \ \left[\xi^{n+1}\mu'' + \xi^n(\lambda' + n\mu')\right] = \int_0^\infty d\xi \ \xi^n(\lambda' - \mu') = 0, \tag{A.27}$$

where the fact was used that μ' is bounded for $\xi \to 0$. Expression (A.27) implies that if $\mu(\xi) = \lambda(\xi)$, then the reference configuration will be stress free and the choice of $\hat{f}_0$ is admissible. In this case, $\boldsymbol{C}$ simplifies to (3.13). Smoothness of $\lambda(\xi)$ was required to ensure the boundedness of $\boldsymbol{C}$ and thus $\frac{\partial \hat{f}}{\partial r}$ and $\hat{f}_0$.

A.14 Energies in Perturbation Analysis

For the derivation of the interface energies (5.23) and (5.25) and the bulk energy (5.26), the approximations of stiffness distributions in section 5.2 are used to simplify energy integrals. For the special solutions (5.21) and (5.24) the following expressions appear:

First, *stiffness values for the interface between interior region and boundary region.* The lower limit of the first integral (over the interior region) may be -1 or -2 without changing the stiffness value, assuming that the stiffness distribution decays sufficiently fast.

$$\begin{aligned}
C_{00}^{bu} &= \int_{-1}^{0} dx \int_0^1 \frac{dx'}{\lambda} C(\frac{x'-x}{\lambda}) = \lambda N_1 + o(\lambda^2) \\
C_{01}^{bu} &= \int_{-1}^{0} dx \int_0^1 \frac{dx'}{\lambda}\frac{x'}{\lambda} C(\frac{x'-x}{\lambda}) = \lambda N_2 + o(\lambda^2) \\
C_{02}^{bu} &= \int_{-1}^{0} dx \int_0^1 \frac{dx'}{\lambda}\frac{1}{2}\left(\frac{x'}{\lambda}\right)^2 C(\frac{x'-x}{\lambda}) = \lambda N_3 + o(\lambda^2) \\
C_{10}^{bu} &= \int_{-1}^{0} dx \int_0^1 \frac{dx'}{\lambda}\frac{x}{\lambda} C(\frac{x'-x}{\lambda}) = -\lambda N_2 + o(\lambda^2) \\
C_{20}^{bu} &= \int_{-1}^{0} dx \int_0^1 \frac{dx'}{\lambda}\frac{1}{2}\left(\frac{x'}{\lambda}\right)^2 C(\frac{x'-x}{\lambda}) = \lambda N_3 + o(\lambda^2) \\
C_{11}^{bu} &= \int_{-1}^{0} dx \int_0^1 \frac{dx'}{\lambda}\frac{x}{\lambda}\frac{x'}{\lambda} C(\frac{x'-x}{\lambda}) = -\lambda N_3 + o(\lambda^2).
\end{aligned}$$

Second, *stiffness values for interior regions.*

$$C^{bb}_{2;II} = \int_{-2}^{0} dx' \int_{-2}^{0} \frac{dx}{\lambda} \frac{1}{2} \left(\frac{x' - x}{\lambda} \right)^2 C(\frac{x' - x}{\lambda}) = 4N_2 - \lambda\, 6N_3 + o(\lambda^2).$$

Rearranging the terms appropriately yields the results (5.23), (5.25) and (5.26).

Appendix B

Definitions

The Dirac Delta Function Distribution. The Dirac delta function distribution is formally defined by its application to a test function $\boldsymbol{v}$ on the domain Ω,

$$\int_{\Omega} dV' \, \delta\left(\boldsymbol{x}' - \boldsymbol{x}\right) \boldsymbol{v}(\boldsymbol{x}') = \boldsymbol{v}(\boldsymbol{x}) \qquad \boldsymbol{x} \in \Omega.$$

Let L denote the physical dimension of length. As dV' has the dimension $[dV'] = L^n$, where n is the number of dimensions of Ω, δ must have the physical dimension of $[\delta] = 1/L^n$.

One-dimensional Fourier Transforms. The one-dimensional Fourier Transform of a function $u(x)$ and the Inverse Fourier Transform of a function $\bar{u}(k)$ are, respectively,

$$\bar{u}(k) = \mathcal{F}\{u\} = \int_{-\infty}^{+\infty} dx \; e^{-ikx} u(x)$$

and

$$u(x) = \mathcal{F}^{-1}\{\bar{u}\} = \frac{1}{2\pi} \int_{-\infty}^{+\infty} dk \; e^{ikx} \bar{u}(k).$$

Appendix C

Stiffness Distributions

This chapter lists normalized stiffness distributions $\bar{C}(\bar{\xi})$ for different dimensions and configurations. From them, the dimensional versions

$$C(\xi) = \frac{E}{l^{n+2}} \bar{C}(\xi/l)$$

can be easily constructed. n denotes the dimension of the reference configuration. E is the Young's Modulus of the three dimensional body. In addition, the horizon[1], the cutoff radius[2], and the non-dimensional stiffness moments are listed.

The functions $\bar{C}$ given here are such that the equations that relate a stiffness distribution and Young's Modulus are already satisfied. These relations are for three-dimensional bodies (2.71), for bodies in plane-strain (2.93), in anti-plane shear (2.95), in one-dimensional plane-strain (2.97) and in one-dimensional anti-plane shear (2.99).

In addition, the equations that relate the stiffness distribution and the internal length are satisfied. The internal length l is defined by (4.12) and imposes the restrictions listed in table 4.1.

[1] defined in section 4.5
[2] defined in section 5.3.1

3d	C	h_0/l	h_c/l	N_0	N_1	N_2	N_3	N_4
gaussian	$\frac{1944e^{-\frac{9\bar{\xi}^2}{5}}}{25\sqrt{5}\pi^{3/2}}$	∞	2.047	4.125	1.735	0.573	0.161	0.04
hat	$\frac{3888\sqrt{\frac{2}{5}}e^{-6\sqrt{\frac{2}{5}}\bar{\xi}}}{25\pi}$	∞	3.058	8.251	2.174	0.573	0.151	0.04
linear	$\frac{5184\sqrt{3}\left(1-\frac{2\sqrt{3}\bar{\xi}}{5}\right)}{625\pi}$	$\frac{5}{2\sqrt{3}}$	1.443	3.3	1.588	0.573	0.165	0.04
parabola	$\frac{1458\sqrt{\frac{2}{35}}\left(1-\frac{18\bar{\xi}^2}{35}\right)}{35\pi}$	$\frac{\sqrt{\frac{35}{2}}}{3}$	1.394	2.947	1.541	0.573	0.166	0.04

Table C.1: Normalized 3d Stiffness Distributions $\bar{C}(\bar{\xi}) = \frac{l^5}{E}C(\xi)$.

2d PSN	C	h_0/l	h_c/l	N_0	N_1	N_2	N_3	N_4
gaussian	$\frac{72e^{-\frac{3\bar{\xi}^2}{2}}}{5\pi}$	∞	2.104	3.317	1.528	0.553	0.17	0.046
hat	$\frac{216e^{-3\bar{\xi}}}{5\pi}$	∞	3.348	4.584	1.528	0.509	0.17	0.057
linear	$\frac{324\left(1-\frac{3\bar{\xi}}{2\sqrt{5}}\right)}{25\pi}$	$\frac{2\sqrt{5}}{3}$	1.491	3.075	1.528	0.569	0.17	0.042
parabola	$\frac{48\left(1-\frac{\bar{\xi}^2}{2}\right)}{5\pi}$	$\sqrt{2}$	1.414	2.881	1.528	0.576	0.17	0.041
gaussian(3d)	$\frac{1944\bar{\xi}\ \mathrm{erfc}\left[\frac{3\bar{\xi}}{\sqrt{5}}\right]}{25\sqrt{5\pi}}$	∞	1.948	2.725	1.528	0.568	0.17	0.044

Table C.2: Normalized 2d Stiffness Distributions $\bar{C}(\bar{\xi}) = \frac{l^4}{E}C(\xi)$ for plane strain.

2d APS	$\bar{C}$	h_0/l	h_c/l	N_0	N_1	N_2	N_3	N_4
gaussian	$\frac{72e^{-3\bar{\xi}^2}}{5\pi}$	∞	1.488	2.345	0.764	0.195	0.042	0.008
hat	$\frac{216e^{-3\sqrt{2}\bar{\xi}}}{5\pi}$	∞	2.368	3.241	0.764	0.18	0.042	0.01
linear	$\frac{324\left(1-\frac{3\bar{\xi}}{\sqrt{10}}\right)}{25\pi}$	$\frac{\sqrt{10}}{3}$	1.054	2.174	0.764	0.201	0.042	0.007
parabola	$\frac{48\left(1-\bar{\xi}^2\right)}{5\pi}$	1	1.	2.037	0.764	0.204	0.042	0.007
gaussian(3d)	$\frac{648}{25\pi}\left(e^{-\frac{9\bar{\xi}^2}{5}}-\frac{3\pi\bar{\xi}\mathrm{erfc}\left[\frac{3\bar{\xi}}{\sqrt{5}}\right]}{\sqrt{5\pi}}\right)$	∞	1.72	2.725	0.764	0.189	0.042	0.009

Table C.3: Normalized 2d Stiffness Distributions $\bar{C}(\bar{\xi}) = \frac{l^4}{E}C(\xi)$ for anti-plane shear.

1d PSN	C	h_0/l	h_c/l	N_0	N_1	N_2	N_3	N_4
gaussian	$\frac{24e^{-\bar{\xi}^2}}{5\sqrt{\pi}}$	∞	2.382	2.4	1.354	0.6	0.226	0.075
hat	$\frac{24e^{-2\bar{\xi}}}{5}$	∞	4.203	2.4	1.2	0.6	0.3	0.15
linear	$\frac{8}{5}\sqrt{3}\left(1-\frac{\bar{\xi}}{\sqrt{3}}\right)$	$\sqrt{3}$	1.732	2.4	1.386	0.6	0.208	0.06
parabola	$\frac{18}{5}\sqrt{\frac{2}{5}}\left(1-\frac{2\bar{\xi}^2}{5}\right)$	$\sqrt{\frac{5}{2}}$	1.581	2.4	1.423	0.6	0.198	0.054

Table C.4: Normalized 1d Stiffness Distributions $\bar{C}(\bar{\xi}) = \frac{l^3}{E}C(\xi)$ for plane strain

1d APS	C	h_0/l	h_c/l	N_0	N_1	N_2	N_3	N_4
gaussian	$\frac{24}{5}e^{-3\bar{\xi}^2}\sqrt{\frac{3}{\pi}}$	∞	1.375	2.4	0.782	0.2	0.043	0.008
hat	$\frac{24}{5}\sqrt{3}e^{-2\sqrt{3}\bar{\xi}}$	∞	2.427	2.4	0.693	0.2	0.058	0.017
linear	$\frac{24(1-\bar{\xi})}{5}$	1	1.	2.4	0.8	0.2	0.04	0.007
parabola	$\frac{18}{5}\sqrt{\frac{6}{5}}\left(1-\frac{6\bar{\xi}^2}{5}\right)$	$\sqrt{\frac{5}{6}}$	0.913	2.4	0.822	0.2	0.038	0.006

Table C.5: Normalized 1d Stiffness Distributions $\bar{C}(\bar{\xi}) = \frac{l^3}{E}C(\xi)$ for anti-plane shear.

1d	$\bar{C}$	h_0/l	h_c/l	N_0	N_1	N_2	N_3	N_4
gaussian	$\frac{4e^{-\bar{\xi}^2}}{\sqrt{\pi}}$	∞	2.382	2.	1.128	0.5	0.188	0.062
hat	$4e^{-2\bar{\xi}}$	∞	4.203	2.	1.	0.5	0.25	0.125
linear	$\frac{4\left(1-\frac{\bar{\xi}}{\sqrt{3}}\right)}{\sqrt{3}}$	$\sqrt{3}$	1.732	2.	1.155	0.5	0.173	0.05
parabola	$3\sqrt{\frac{2}{5}}\left(1-\frac{2\bar{\xi}^2}{5}\right)$	$\sqrt{\frac{5}{2}}$	1.581	2.	1.186	0.5	0.165	0.045

Table C.6: Normalized 1d Stiffness Distributions $\bar{C}(\bar{\xi}) = \frac{l^3}{E}C(\xi)$ for uniaxial extension.

Bibliography

[1] R. C. Abeyaratne, K. Bhattacharya, and J. K. Knowles. Strain-energy functions with multiple local minima: Modeling phase transformations using finite thermoelasticity. In Y. Fu and R. W. Ogden, editors, *Nonlinear Elasticity: Theory and Application*. Cambridge University Press, 2000.

[2] R. C. Abeyaratne and J. K. Knowles. On the stability of thermoelastic materials. *Int. J. Solids Structures*, 24:1021–1044, 1987.

[3] R. C. Abeyaratne and J. K. Knowles. On the driving traction acting on a surface of strain discontinuity in a continuum. *J. Mech. Phys. Solids*, 38:345–360, 1990.

[4] R. C. Abeyaratne and J. K. Knowles. On the stability of thermoelastic materials. *Journal of Elasticity*, 53:199–213, 1999.

[5] F. F. Abraham, J. Q. Broughton, N. Bernstein, and E. Kaxiras. Spanning the continuum to quantum length scales in a dynamic simulation of brittle fracture. *Europhysics Letters*, 44(6):783–787, 1998.

[6] M. P. Allen and D. J. Tildesley. *Computer Simulation of Liquids*. Clarendon Press, Oxford, 1987.

[7] T. L. Anderson. *Fracture Mechanics*. CRC Press, Boca Raton, New York, 2nd edition, 1995.

[8] Z. Banach. On a certain wave motion in the spatially nonlocal and nonlinear medium. *Int. J. Eng. Science*, 19:1047–1068, 1981.

[9] K. J. Bathe. *Finite Element Procedures*. Prentice-Hall, Englewood Cliffs, N.J., 1996.

[10] Z. P. Bažant. Imbricate continuum and its variational derivation. *J. Eng. Mechanics*, 110(12):1693–1712, 1984.

[11] Z. P. Bažant. Why continuum damage is nonlocal: Micromechanics arguments. *J. Eng. Mechanics*, 117(5):1070–1087, 1991.

[12] Z. P. Bažant and M. Jirašek. Nonlocal integral formulations of plasticity and damage: Survey of progress. *J. Eng. Mechanics*, 128(11):1119–1149, 2002.

[13] T. Belytschko, W. K. Liu, and B. Moran. *Nonlinear Finite Elements for Continua and Structures*. John Wiley, Chichester, New York, 2000.

[14] N. Bernstein and D. W. Hess. Lattice trapping barriers to brittle fracture. *Phys. Rev. Letters*, 91(2), 2003.

[15] M. Born and K. Huang. *Dynamical Theory of Crystal Lattices*. Clarendon Press, Oxford, 1954.

[16] J. Q. Broughton and F. F. Abraham. Concurrent coupling of length scales: Methodology and application. *Physical Review B*, 60(4):2391–2403, 1999.

[17] G. T. Camacho and Ortiz. Computational modeling of impact damage in brittle materials. *Int. J. Sol. Struct.*, 33:2899–2938, 1996.

[18] M. Charlotte and L. Truskinovsky. Linear elastic chain with hyper-pre-stress. *J. Mech. Phys. Solids*, 50:217–251, 2002.

[19] Y. Chen, J. D. Lee, and A. Eskandarian. Atomistic viewpoint of the applicability of microcontinuum theories. *Int. J. Sol. Struct.*, 41, 2004.

[20] J. Choi, D. Margetis, T. Squires, and M. Z. Bazant. Steady advection-diffusion around finite absorbers in two-dimensional potential flows. *J. Fluid. Mech.*, under consideration for publication; available at http://arxiv.org/abs/cond-mat/0403740eprint.

[21] B. D. Coleman and M. E. Gurtin. Thermodynamics with internal state variables. *J. Chem. Phys.*, 47:597–613, 1967.

[22] H. T. Davis. *The Theory of Linear Operators*. The Principia Press, Boomington, Indiana, 1936.

[23] M. S. Daw, S. M. Foiles, and M. I. Baskes. The embedded-atom method: a review of theory and applications. *Materials Science Reports*, 9:251–310, 1993.

[24] W. J. Drugan and J. R. Willis. A micromechanics-based nonlocal constitutive equation and estimates of representative volume element size for elastic composites. *J. Mech. Phys. Solids*, 44:497–524, 1996.

[25] D. G. Edelen. Nonlocal field theories. In A. C. Eringen, editor, *Continuum Physics IV*, New York, 1976. Academic Press.

[26] A. C. Eringen. Linear theory of nonlocal elasticity and dispersion of plane waves. *Int. J. Eng. Science*, 10:425–435, 1972.

[27] A. C. Eringen. On nonlocal plasticity. *Int. J. Eng. Science*, 19:1461–1474, 1981.

[28] A. C. Eringen. On differential equations of nonlocal elasticity and solutions of screw dislocations and surface waves. *J. Appl. Phys.*, 54:4703–4710, 1983.

[29] A. C. Eringen. Theory of nonlocal elasticity and some applications. *Res Mechanica*, 21:312–342, 1987.

[30] J. Fineberg and M. Marder. Instability in dynamic fracture. *Physics Reports*, 313:1–108, 1999.

[31] N. A. Fleck and J. W. Hutchinson. A phenomenological theory for strain gradient effects in plasticity. *J. Mech. Phys. Sol.*, 41:1825–1857, 1993.

[32] R. L. Fosdick and D. E. Mason. On a model of nonlocal continuum mechanics part ii: Structure, asymptotics and computations. *J. Elasticity*, 48:51–100, 1997.

[33] R. L. Fosdick and D. E. Mason. On a model of nonlocal continuum mechanics part i: Existence and regularity. *SIAM J. Appl. Math.*, 58(4):1278–1306, 1998.

[34] L. B. Freund. *Dynamic Fracture Mechanics*. Cambridge University Press, 1990.

[35] B. K. Gairola. The nonlocal continuum theory of lattice defects. In Rogula [59], pages 51–121.

[36] J. Gao and P. Klein. Numerical simulation of crack growth in an isotropic solid with randomized internal cohesive bonds. *J. Mech. Phys. Solids*, 46:187–218, 1998.

[37] I. M. Gelfand and S. V. Fomin. *Calculus of Variations*. Prentice-Hall, Englewood Cliffs, N.J., 1963.

[38] K. F. Graff. *Wave Motion in Elastic Solids*. Dover, 1996.

[39] M. E. Gurtin and E. C. Francis. Simple rate independent model for damage. *AIAA Journal of Spacecraft*, 18:285–286, 1981.

[40] D. Hilbert. *Grundzüge einer Theorie der allgemeinen Integralgleichungen*. Chelsea Publishing Company, New York, 1953.

[41] G. A. Holzapfel. *Nonlinear Solid Mechanics*. Wiley, Chichester, 2000.

[42] M. F. Horstemeyer and M. I. Baskes. Strain tensors at the atomic scale. *Mat. Res. Soc. Symp. Proc. 578*, pages 15–20, 2000.

[43] M. Jirašek. Objective modeling of strain localization. *Revue française de génie civil*, 6:1119–1132, 2002.

[44] M. Jirašek and S. Marfia. Nonlocal damage model based on displacement averaging. *Int. J. Numer. Meth. Engng.*, 60:1–24, 2004.

[45] D. Krajcinovic and J. Lemaitre, editors. *Continuum Damage Mechanics Theory and Applications*, Wien, 1987. Springer.

[46] E. Kröner. Interrelations between various branches of continuum mechanics. In E. Kröner, editor, *Mechanics of Generalized Continua*, pages 330–340, New York, 1968. Springer.

[47] E. Kröner. *Statistical Continuum Mechanics*. Springer, Wien, 1971.

[48] I. A. Kunin. *Elastic Media with Microstructure I: One-Dimensional Models*. Springer, Berlin, 1982.

[49] I. A. Kunin. *Elastic Media with Microstructure II: Three-Dimensional Models*. Springer, Berlin, 1983.

[50] Y. M. Leroy and A. Molinari. Spatial patterns and size effects in shear zones: A hyperelastic model with higher order gradients. *J. Mech. Phys. Solids*, 41:631–663, 1992.

[51] J. E. Marsden and T. J. Hughes. *Mathematical Foundations of Elasticity*. Dover, New York, 1994.

[52] R. E. Miller and E. B. Tadmor. The quasicontinuum method: Overview, applications and current directions. *J. Computer-Aided Mat. Design*, 9:203–239, 2002.

[53] R. S. Mindlin. Second gradient of strain and surface-tension in linear elasticity. *Int. J. Solids and Structures*, 1:417–438, 1965.

[54] W. Noll. A new mathematical theory of simple materials. *Archive for Rational Mechanics*, 48:1–50, 1972.

[55] R. C. Picu. On the functional form of non-local elasticity kernels. *J. Mech. Phys. Solids*, 50:1923–1939, 2002.

[56] G. Pijaudier-Cabot and Z. P. Bažant. Nonlocal damage theory. *J. Eng. Mechanics*, 113(10):1512–1533, 1991.

[57] X. Ren and L. Truskinovsky. Finite scale microstructures in nonlocal elasticity. *J. Elasticity*, 59:319–355, 2000.

[58] D. Rogula. Introduction to nonlocal theory of material media. In *Nonlocal Theory of Material Media* [59], pages 125–223.

[59] D. Rogula, editor. *Nonlocal Theory of Material Media*, Wien, 1982. Springer.

[60] G. Ruiz, M. Ortiz, and A. Pandolfi. Three-dimensional finite-element simulation of the dynamic brazilian tests on concrete cylinders. *Int. J. Num. Meth. Eng.*, 48:963–994, 2000.

[61] S. A. Silling. Reformulation of elasticity theory for discontinuities and long range forces. *J. Mech. Phys. Solids*, 48:175–209, 2000.

[62] S. A. Silling. Dynamic fracture modeling with a meshfree peridynamic code. In K. J. Bathe, editor, *Computational Fluid and Solid Mechanics*, pages 641–644, Amsterdam, 2003. Elsevier Science.

[63] S. A. Silling and F. Bobaru. Peridynamic modeling of membranes and fibers. *Int. J. Sol. Structures*, 40:395–409, 2005, available at www.sciencedirect.com.

[64] S. A. Silling, M. Zimmermann, and R. C. Abeyaratne. Deformation of a peridynamic bar. *J. Elasticity*, 73(1):173–190, 2003.

[65] J. C. Simo and T. J. Hughes. *Computational Inelasticity*. Springer, New York, 1998.

[66] E. B. Tadmor, M. Ortiz, and R. Phillips. Quasicontinuum analysis of defects in solids. *Phil. Mag. A*, 73:1529–1563, 1996.

[67] F. G. Tricomi. *Integral Equations*. Interscience Publishers, New York, 1957.

[68] C. A. Truesdell. *The Elements of Continuum Mechanics*. Springer, New York, 1967.

[69] C. A. Truesdell and W. Noll. The non-linear field theories of mechanics. In S. S. Antman, editor, *Handbuch der Physik, III/3*, Berlin, 1965. Springer.

[70] L. Truskinovsky and G. Zanzotto. Ericksen's bar revisited: Energy wiggles. *J. Mech. Phys. Solids*, 44(8):1371–1408, 1996.

[71] R. F. Wallis, editor. *Lattice Dynamics*. Pergamon Press, 1965.

[72] O. Weckner and R. C. Abeyaratne. The effect of long-range forces on the dynamics of a bar. *J. Mech. Phys. Solids*, accepted for publication, 2004.